

8.0 STEADY-STATE MODEL

The current section details the calibration of the steady-state model and presents the steady-state model results. This section also describes analyses of model sensitivity to various hydrologic parameters.

8.1 Calibration

This section describes the steady-state calibration targets and calibrated parameters including horizontal and vertical hydraulic conductivity, recharge, ET, stream conductance, and vertical conductance for younger sediments overlying the Queen City Formation.

8.1.1 Calibration Targets

Water-level measurements are needed as targets for steady-state calibration. However, where there is a well, water levels have often been affected by groundwater pumpage. As a result, valid targets for predevelopment conditions were limited, because wells were typically drilled for pumpage. Acceptable predevelopment targets included 18 Carrizo measurements and 91 Wilcox measurements (34 in the upper Wilcox and 57 in the middle Wilcox). A distinction was made between outcrop wells and wells located in the confined section. For wells in the outcrop, the water-level elevation was calculated based on the measured water-level depth using the grid-block averaged elevation from the model. For the confined section, the listed well elevation was used for calculating the water-level elevation. This was done to reduce potential errors induced by averaging ground-surface elevation over a 1-mile by 1-mile grid-block.

8.1.2 Horizontal and Vertical Hydraulic Conductivities

Section 6.4.1 described the determination of initial horizontal and vertical hydraulic conductivities for the model. Figures 8.1.1-8.1.4 show the final calibrated horizontal hydraulic conductivity (K_h) fields for Layer 3 (Carrizo), Layer 4 (upper Wilcox), Layer 5 (middle Wilcox), and Layer 6 (lower Wilcox). Figure 8.1.5 shows the vertical anisotropy ratio field for Layer 2 (Reklaw) for which a uniform horizontal hydraulic conductivity value of 1 ft/day was assumed. We used a hydraulic conductivity map for Layer 1 (Queen City) in the model, but no explicit calibration was performed for Layer 1. The spatial horizontal hydraulic conductivity distribution

for Layer 1, shown in Figure 4.3.8, is considered preliminary. Table 8.1.1 summarizes the calibrated hydraulic conductivity ranges and anisotropy ratios (K_h/K_v) for each layer.

The calibration process for the Northern Carrizo-Wilcox GAM was iterative. We developed an initial steady-state calibration through adjustment of recharge and hydraulic conductivity. Although the initial steady-state calibrated model met the calibration criteria, the subsequent transient model calibration indicated that the vertical hydraulic conductivities were too high. It became necessary to jointly calibrate the steady-state and transient models to achieve a consistent calibration to both steady-state and transient water-level data.

Overall, vertical hydraulic conductivities (K_v) were lowered based on the transient calibration. We then recalibrated the steady-state model through adjustment of recharge, ET (from groundwater), and hydraulic conductivities. Modifications to the initial estimates of horizontal hydraulic conductivity (Section 6.4.1), based on the steady-state calibration, involved increasing conductivities in areas where values were low to a minimum of 2 ft/day for Layer 3 and 1.5 ft/day for Layers 4, 5 and 6. On the other hand, transient calibration required limiting horizontal hydraulic conductivity in selected areas of the Carrizo, upper Wilcox, and middle Wilcox layers. This area encompassed part of Cherokee, Anderson, Henderson, Smith, Wood, Upshur, and Camp counties, where a uniform hydraulic conductivity value of 1 ft/day was assigned to Layers 4 and 5 (Wilcox), and a slightly higher value of 2 ft/day was assigned to Layer 3 (Carrizo). Also, the relatively high hydraulic conductivity area in the southern part of the Sabine Uplift, which was not supported by data, was reduced to values similar to those of surrounding data. For the Queen City (Layer 1), the minimum horizontal hydraulic conductivity value was set to 5 ft/day, mainly because of numerical instabilities along the outcrop edge of the Queen City, where it becomes relatively thin.

Table 8.1.1 shows the final calibrated anisotropy ratios for the steady-state model which were increased by a factor of 10 to 1000 from that of the initial steady-state calibration. Vertical hydraulic conductivity of the Reklaw was set to 1×10^{-5} ft/day and modified in two selected areas (Figure 8.1.5). In central Smith County and the adjacent northern part of Cherokee and Anderson counties, the vertical hydraulic conductivity of Layer 2 (Reklaw) was reduced to 1×10^{-6} ft/day based on transient calibration, to restrict downward flow from the shallow Queen City aquifer which has been induced by steep water-level declines in the Carrizo and upper

Wilcox in Smith County due to pumpage. On the other hand, vertical permeability in eastern Nacogdoches was increased to 1×10^{-4} ft/day based on the transient calibration to allow more cross-formational flow, because simulated water-level declines owing to pumpage exceeded observed declines in the Carrizo Aquifer.

There is no clear geologic or hydrologic information that can be used to support these spatial changes in vertical hydraulic conductivities of the Reklaw. The potential limitations of the steady-state model are discussed in Section 11.

8.1.3 Recharge and Groundwater Evapotranspiration

Recharge was input initially as an averaged distribution from the transient recharge results (Sections 6.3.4). However, this averaged recharge estimate was too high, resulting in numerical instabilities in the steady-state simulation. The low vertical hydraulic conductivities required for transient calibration required a reduction in recharge in the steady-state model. Recharge was selectively reduced by hydrogeologic unit and adjusted locally in case of numerical instabilities, until an acceptable calibration was achieved. The spatial distribution of calibrated recharge is shown in Figure 8.1.6.

Average groundwater ET was input, as provided by the SWAT results, and applied as ET maximum in the model (Section 6.3.4). The maximum rooting depths were taken from the SWAT results and input as the extinction depth (Figure 8.1.7). The ET surface was set to ground surface, so groundwater ET varied linearly starting from a maximum at ground surface and going down to the root depth. The potential ET from groundwater can and did exceed recharge in some circumstances; however, MODFLOW was unable to model this under steady-state conditions. For conditions where groundwater was near the surface and the ET rate exceeded the recharge rate, model convergence was difficult and model mass balances were not acceptable. In order to overcome this problem, we reduced the maximum ET rate (Figure 8.1.8) to 70 percent of the recharge rate on a cell by cell basis. This resulted in acceptable convergence and mass balances.

8.1.4 General-Head Boundaries and Stream Conductances

General-head boundaries (GHBs) were assigned to the confined part of the Queen City in the southern part of the model. The elevations of the GHBs were estimated from the surficial

water table (Section 6.3.2). The initial conductivities of the GHBs were estimated from reported vertical conductivities (Williamson et al., 1990) of the younger sediments overlying the Queen City. Heads in the Queen City formation (Layer 1) indicated limited sensitivity to the conductivity of the GHBs, and are more controlled by recharge in the outcrop and by streambed conductivities. Streambed conductivities were based on the hydraulic conductivities of the underlying formation. The overall conductance varies with the streambed width as specified in the EPA RF1 dataset (Section 6.3.3).

Table 8.1.1 Calibrated hydraulic conductivity ranges for the steady-state model.

	Horizontal Hydraulic Conductivity K_h (ft/d)	Vertical Hydraulic Conductivity K_v (ft/d)	Anisotropy Ratio (K_h/K_v)
Layer 1 (Queen City)	5 – 25	$5 \times 10^{-4} - 2.5 \times 10^{-2}$	1,000-10,000
Layer 2 (Reklaw)	1	$1 \times 10^{-6} - 1 \times 10^{-4}$	10,000 – 1,000,000.
Layer 3 (Carrizo)	2 – 40	$2 \times 10^{-2} - 4 \times 10^{-1}$	100
Layer 4 (upper Wilcox)	1 – 10	$1 \times 10^{-4} - 1 \times 10^{-3}$	10,000
Layer 5 (middle Wilcox)	1 – 10	$1 \times 10^{-4} - 1 \times 10^{-3}$	10,000
Layer 6 (lower Wilcox)	1.5 – 25	$1.5 \times 10^{-4} - 2.5 \times 10^{-3}$	10,000

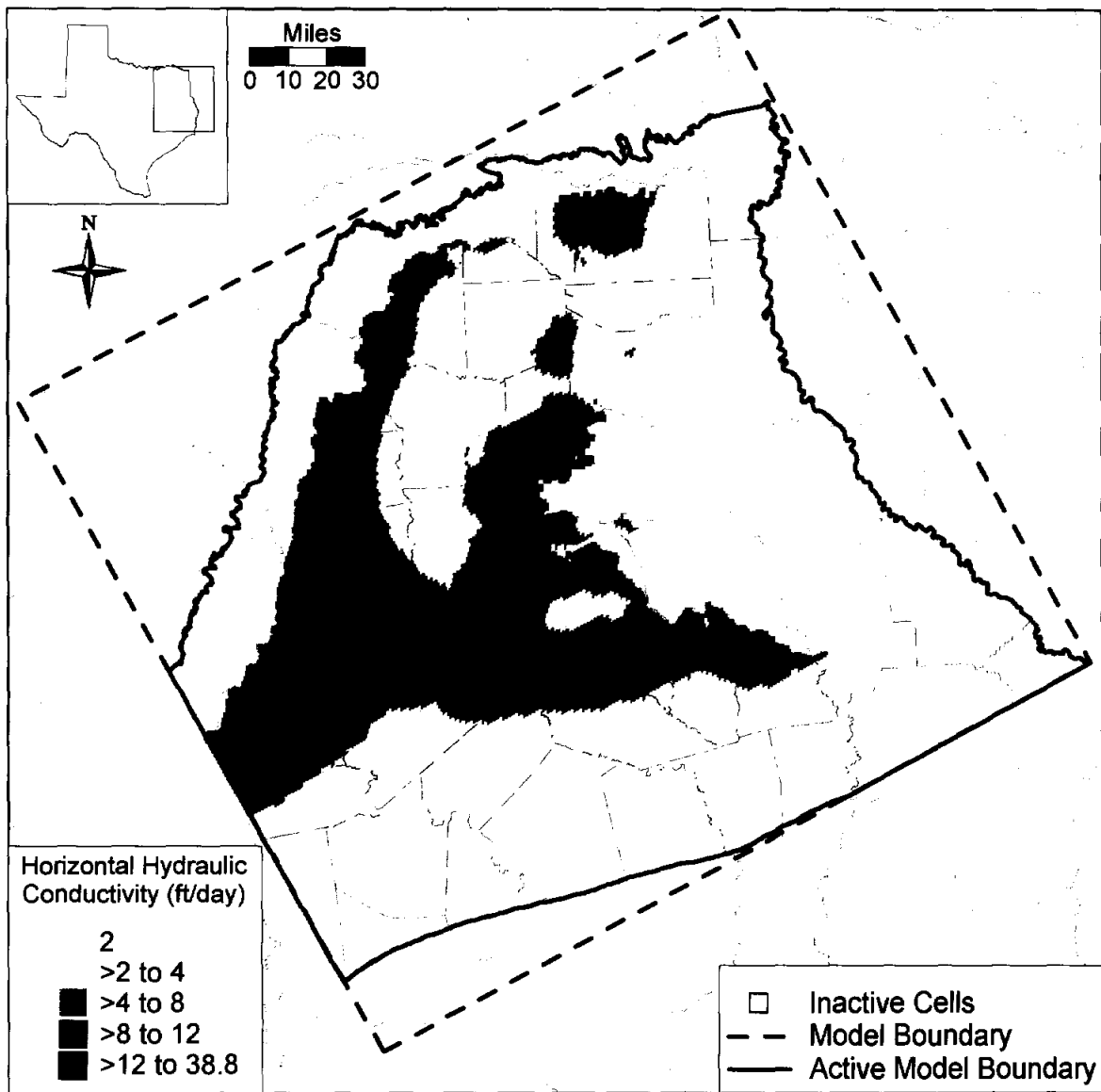


Figure 8.1.1 Calibrated horizontal hydraulic conductivity field for Layer 3 (Carrizo).

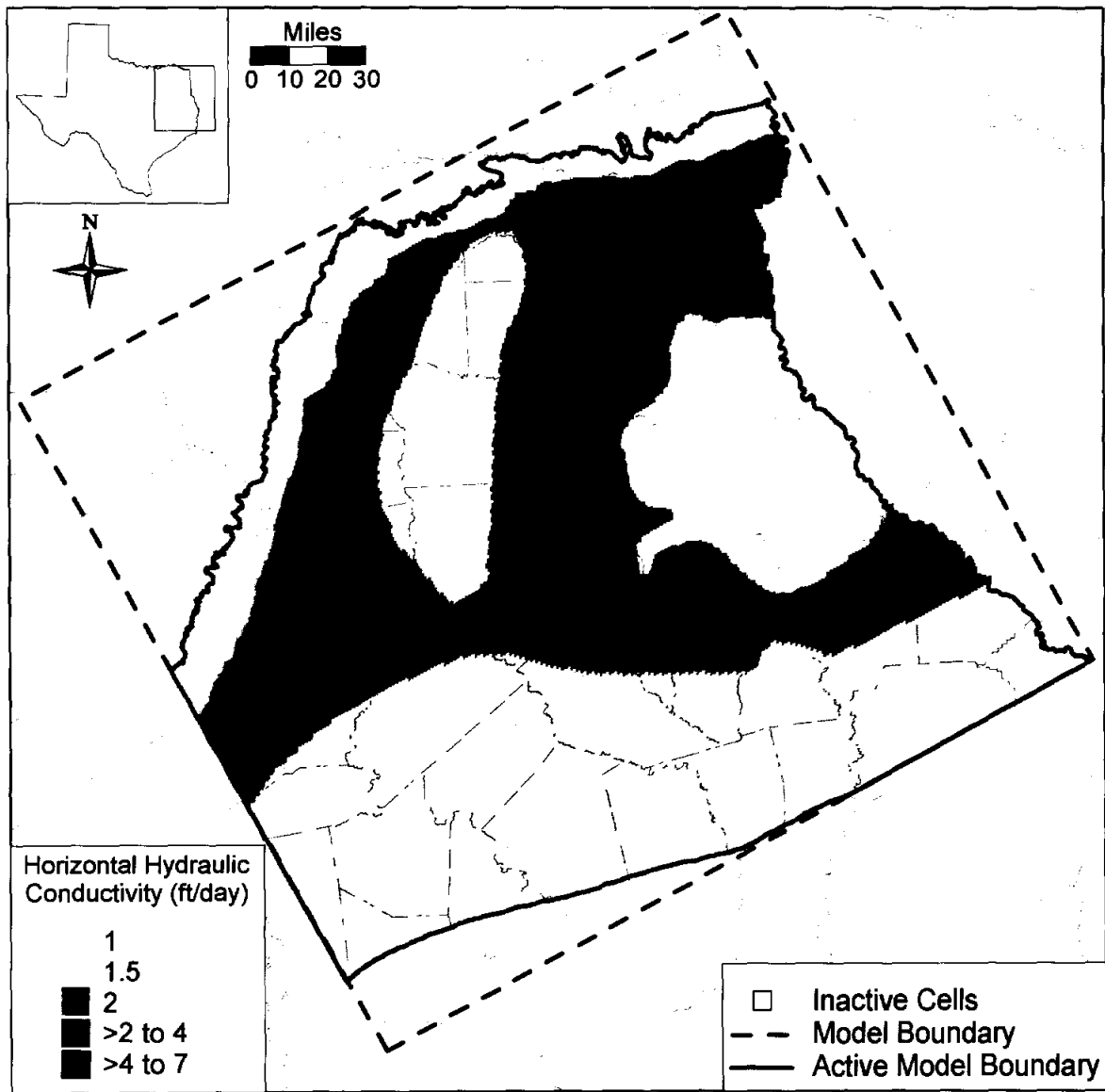


Figure 8.1.2 Calibrated horizontal hydraulic conductivity field for Layer 4 (upper Wilcox).

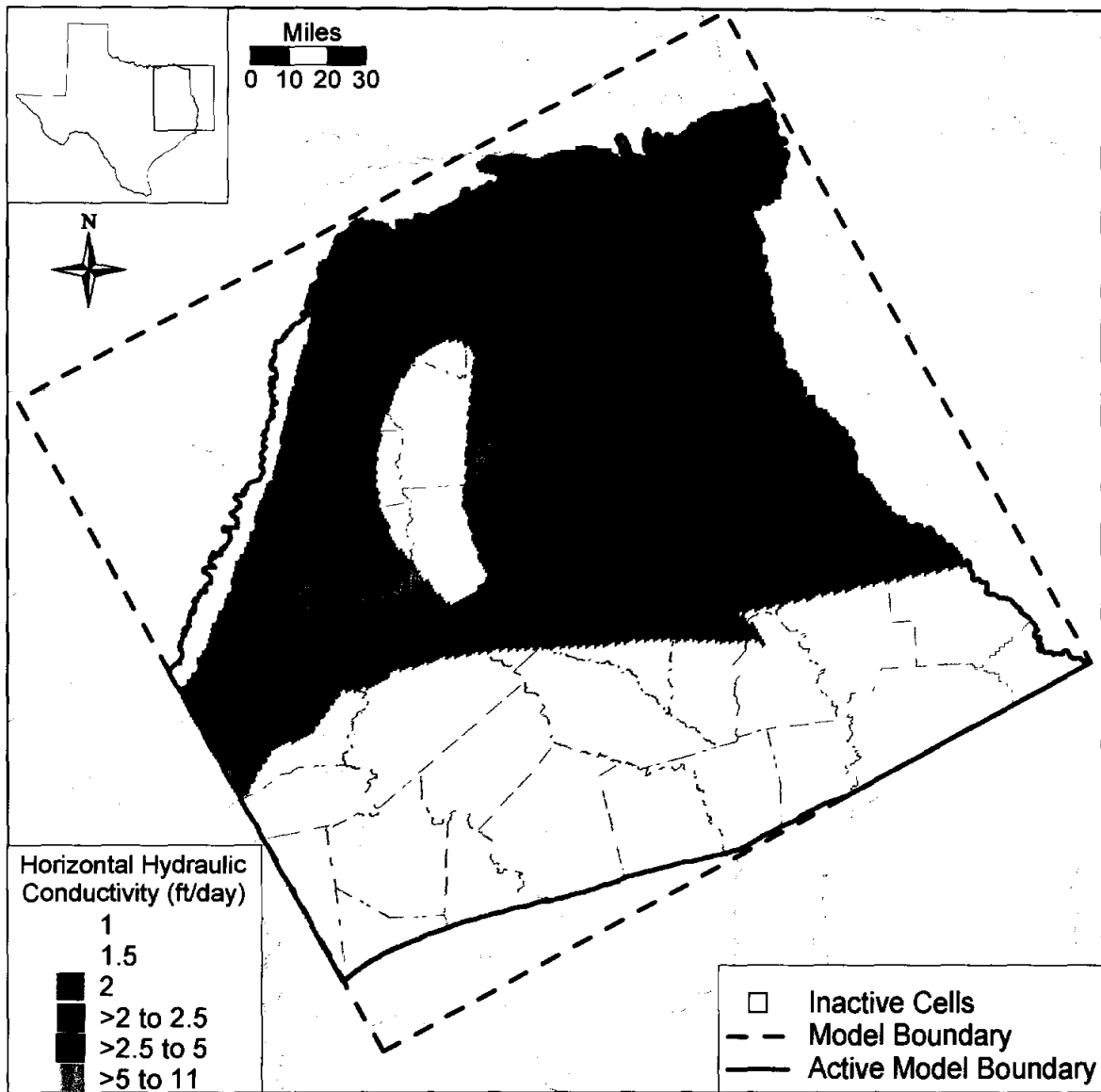


Figure 8.1.3 Calibrated horizontal hydraulic conductivity field for Layer 5 (middle Wilcox).

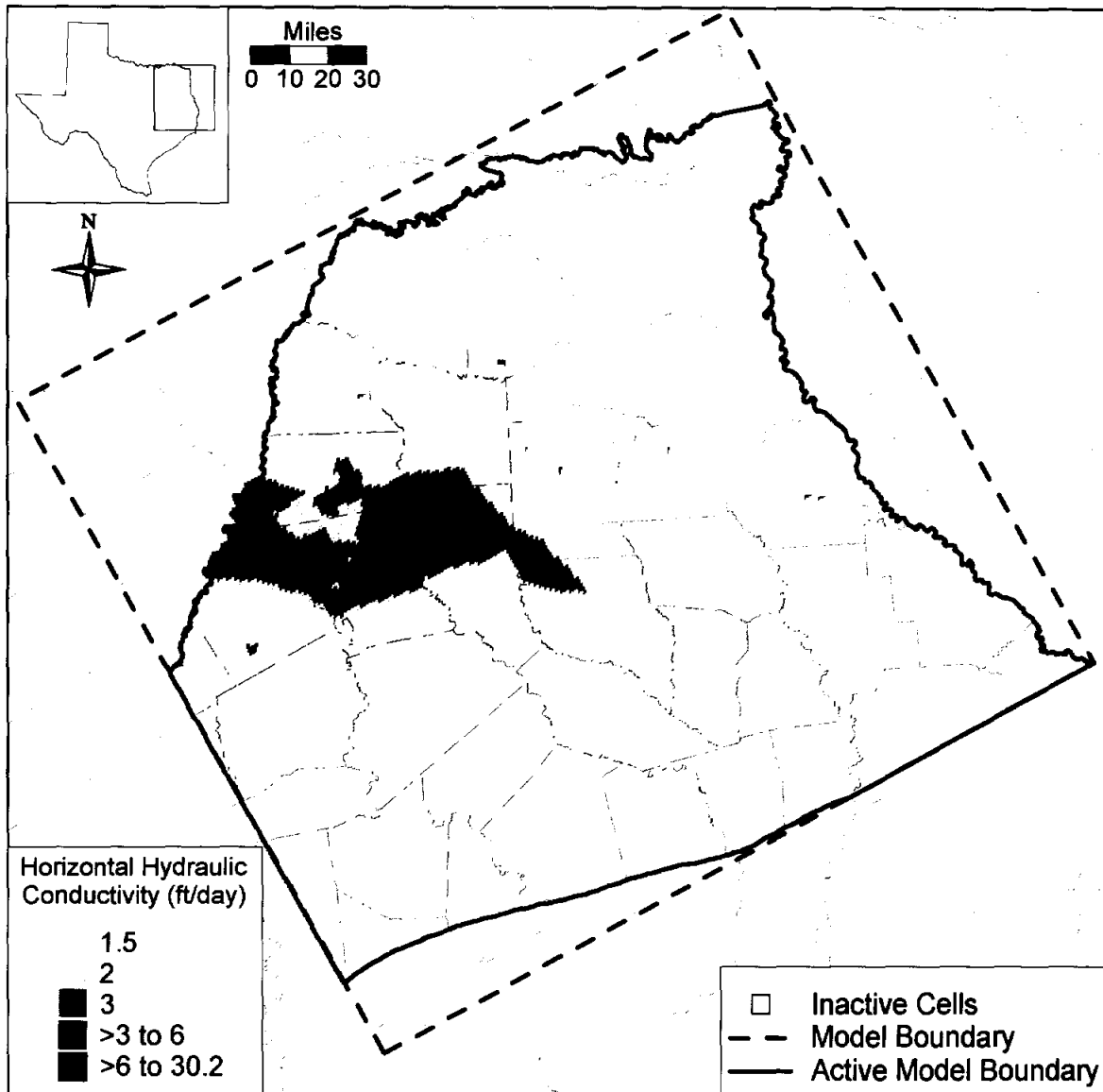


Figure 8.1.4 Calibrated horizontal hydraulic conductivity field for Layer 6 (lower Wilcox).

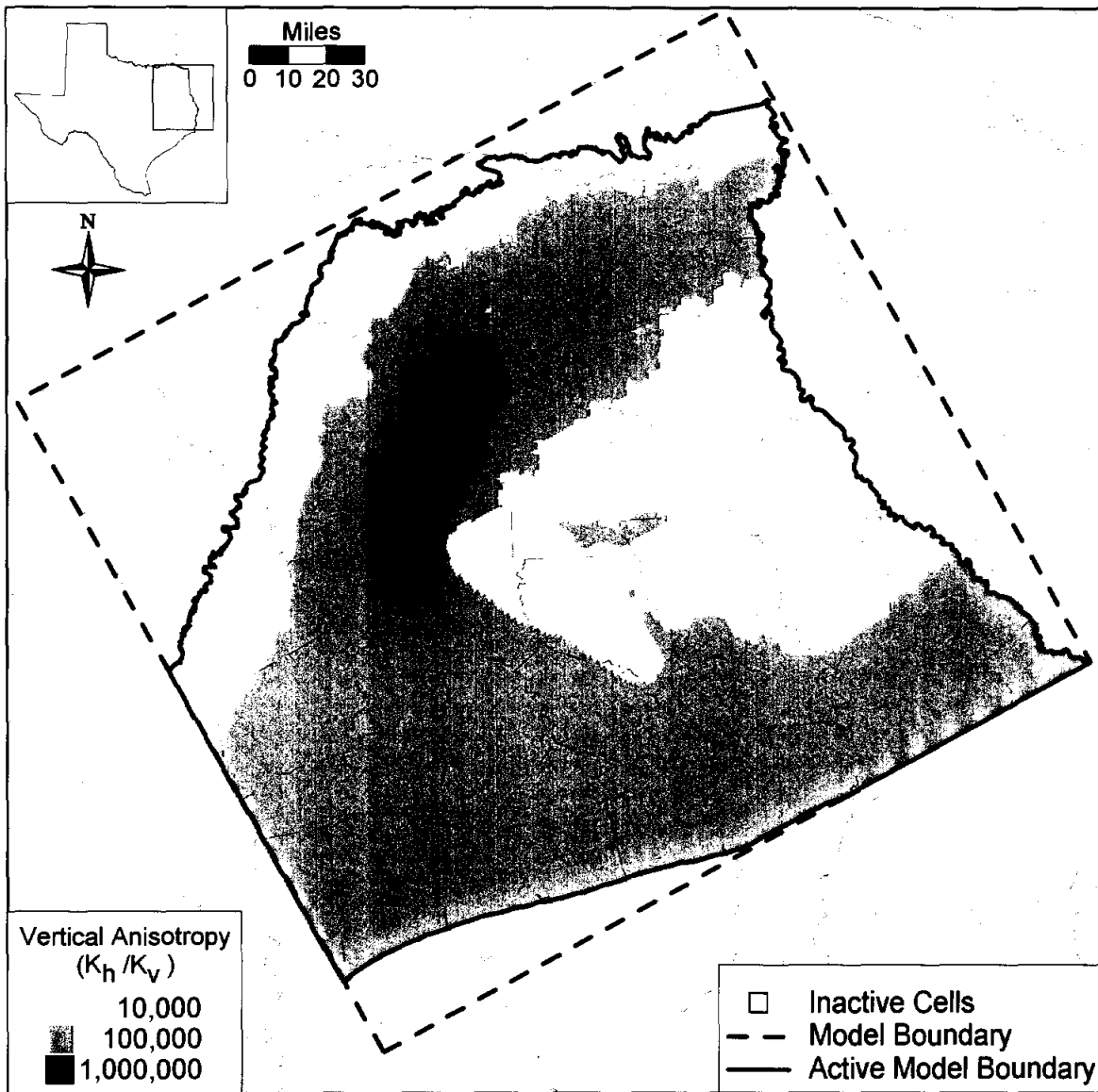


Figure 8.1.5 Calibrated vertical anisotropy (K_h/K_v) field for Layer 2 (Reklaw).

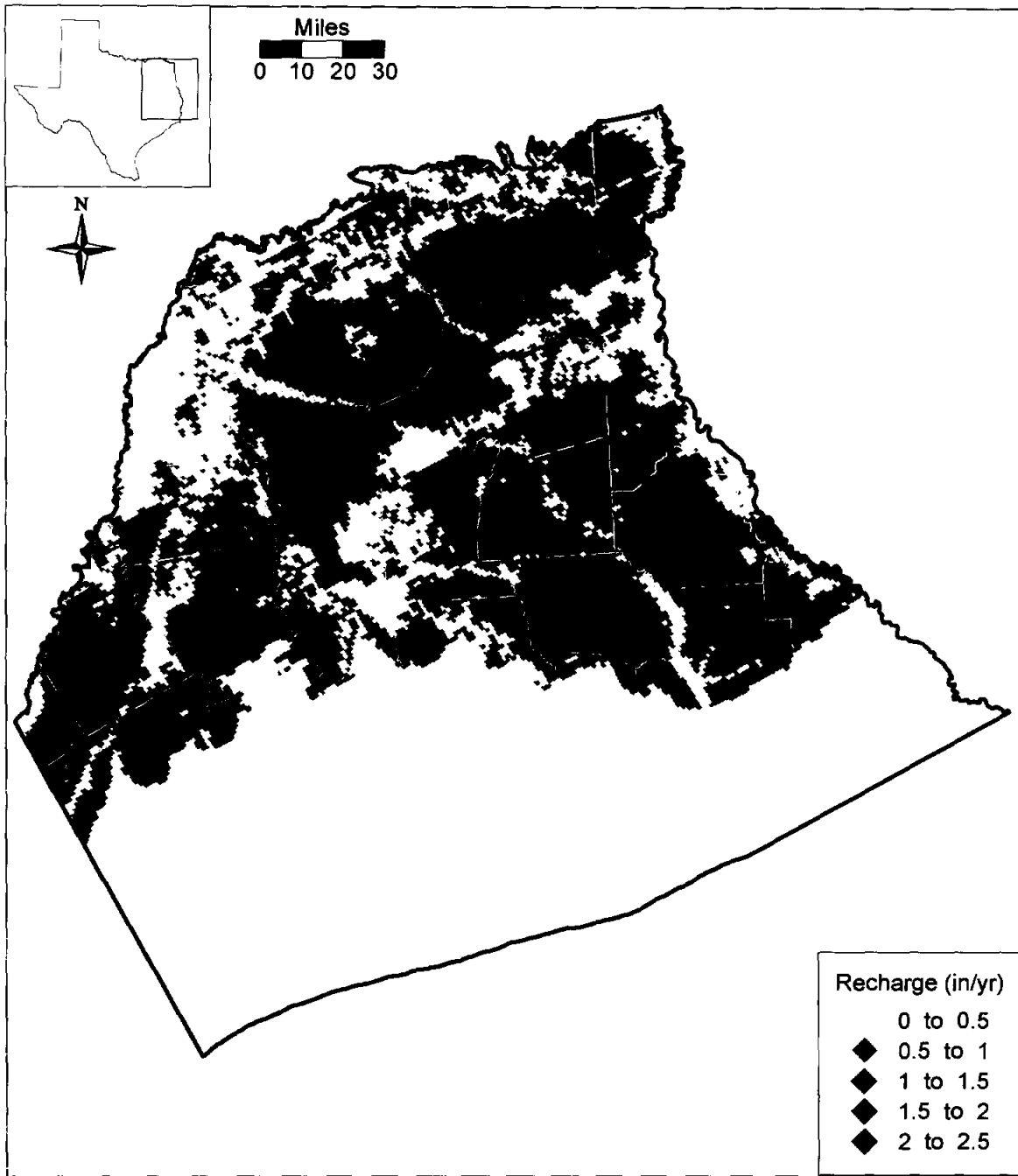


Figure 8.1.6 Calibrated recharge distribution for the steady-state model.

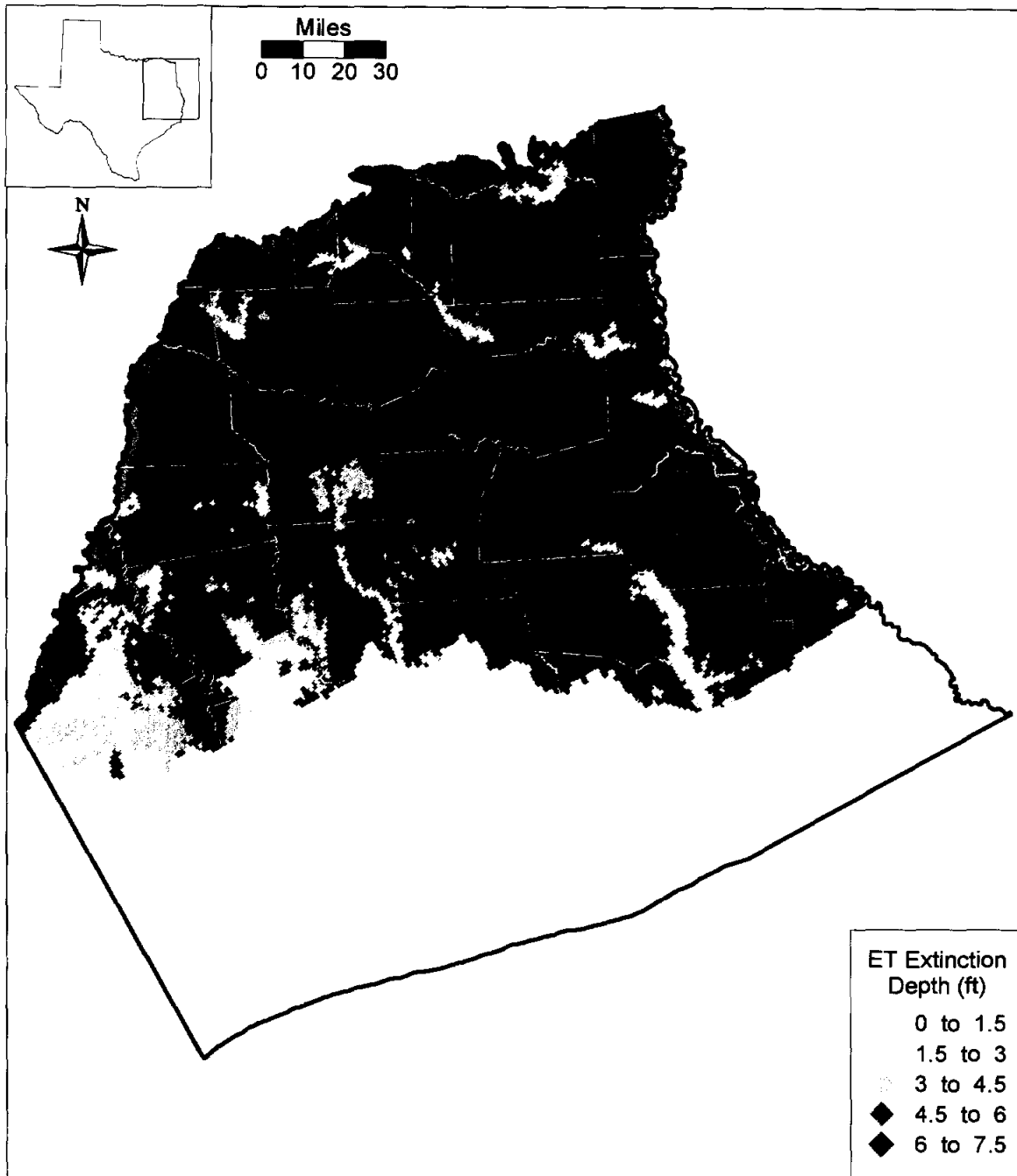


Figure 8.1.7 ET extinction depth distribution for the steady-state model.

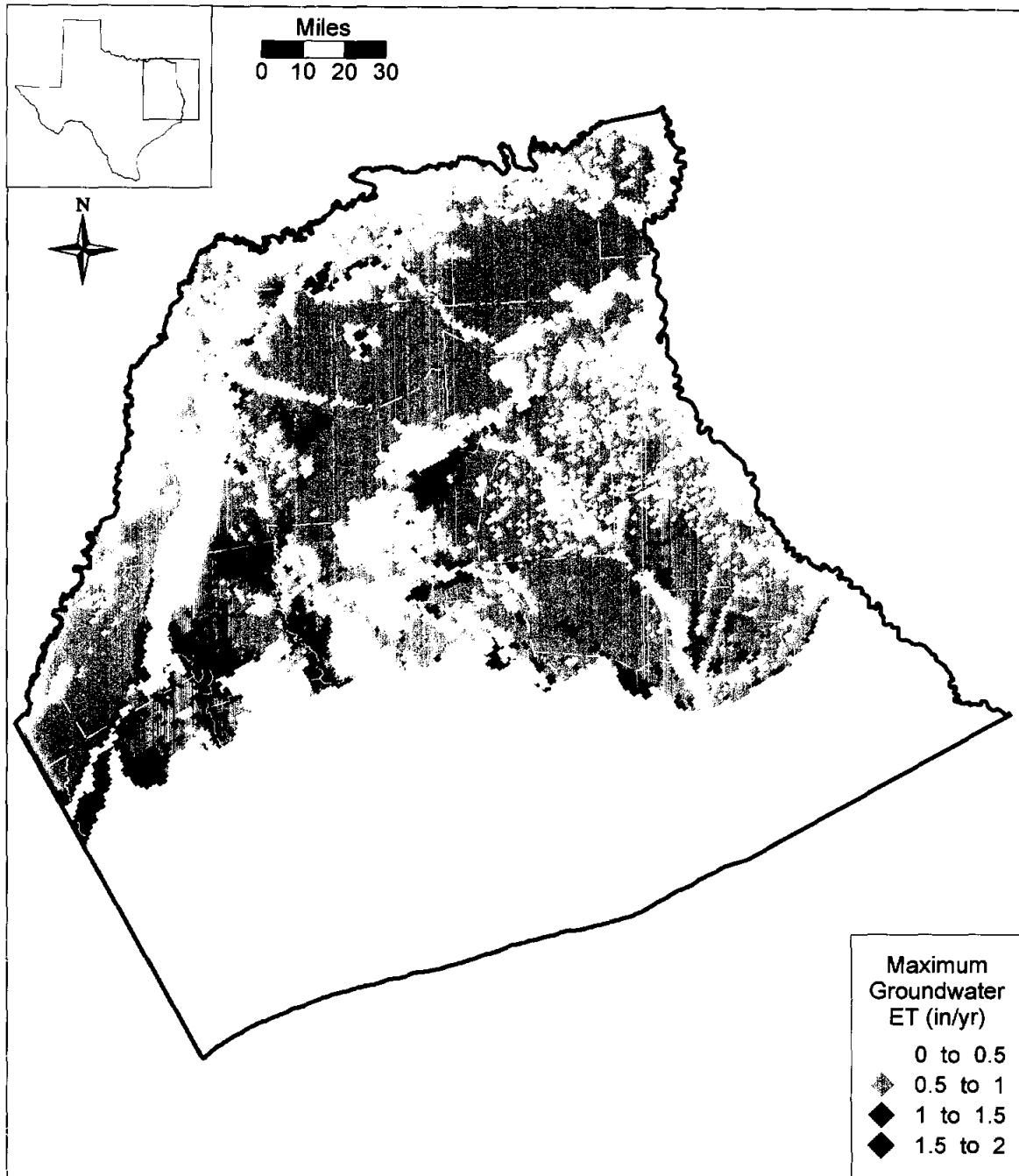


Figure 8.1.8 Calibrated maximum groundwater ET rate distribution for the steady-state model.

8.2 Simulation Results

Calibration of the steady-state model is not unique. Calibrated results can be obtained by numerous combinations of recharge and vertical and horizontal hydraulic conductivities. Overall, the steady-state model is most sensitive to recharge. This is to be expected, since recharge is the primary input source of water for the model.

8.2.1 Hydraulic Heads

Figures 8.2.1-8.2.5 show the head surface results from the calibrated steady-state model, together with the residuals for the target wells in the individual layers. The residuals were calculated from:

$$residual = head_{measured} - head_{simulated} \quad (8.2.1)$$

A positive residual indicates that the model has underpredicted the hydraulic head, while a negative residual indicates overprediction. The calibration statistics for the individual layers are summarized in Table 8.2.1, and the overall mass balance calculated by the steady-state model is given in Tables 8.2.2a and 8.2.2b.

Figure 8.2.1a shows the simulated hydraulic heads for Layer 1 (Queen City) and the corresponding residuals for the target well locations. As mentioned above, the Queen City aquifer was not explicitly calibrated during this GAM phase; however, hydraulic heads in the Queen City were considered important for controlling vertical flow across the Reklaw confining unit. The simulated hydraulic heads for Layer 1 in Figure 8.2.1 compare reasonably well with measured hydraulic heads, reproducing the water table as a reflection of the general topography in the Queen-City outcrop. No effort was made to refine the hydraulic parameters and improve the calibration for Layer 1. The calibration statistics shows an adjusted RMS of 13% for the Queen City, which is considered acceptable for bounding the vertical gradient across the Reklaw confining unit.

The calibration statistics for the Carrizo shows an adjusted RMS of 8% (Table 8.2.1) based on a relatively even distribution of the residuals throughout the confined and unconfined part of the aquifer (Figure 8.2.2a). The scatterplot of simulated and measured hydraulic heads indicates a uniform distribution around the unit-slope line (Figure 8.2.2b). The steady-state

hydraulic head surface shows an approximate west-east groundwater divide from van Zandt County through Smith County to Rusk County. North of this divide the hydraulic gradients in the confined portion of the Carrizo are to the east, indicating groundwater flow to the east toward the Red River in Louisiana. South of the divide, groundwater flow in the confined section is to the south and further downdip to the southeast. The overall head distribution and general flow pattern agrees reasonably well with that shown in Figure 4.4.3 (Fogg and Kreitler, 1982), considering that the simulated heads represent steady-state pre-development conditions and Fogg and Kreitler (1982) included pumpage effects on their constructed potentiometric surface for the entire Carrizo-Wilcox aquifer.

The calibration statistics for Layer 4 (upper Wilcox) indicates a relatively high adjusted RMS of 15%, even though the overall total RMS of 38.5 ft is not significantly greater than that of Layer 5 (Table 8.2.1). This is due to the relatively narrow hydraulic head range of 257 ft, compared to 418 ft for Layer 5. Figure 8.2.3a shows that the calibration data are located mostly in the outcrop in the Sabine Uplift, with some data points along the western outcrop, and with only a few data points in the confined section in Upshur and Rusk counties. The scatterplot of simulated and measured hydraulic heads shows this narrow head range (Figure 8.2.3b), resulting in the relatively large adjusted RMS. Given the potential uncertainty in well-location and associated uncertainty in well elevation and measured water-level elevation, an improvement in the fit was not attempted. Using the greater head range for the entire Wilcox aquifer would decrease the adjusted RMS to 9%. The overall groundwater flow pattern as inferred from the hydraulic head distribution (Figure 8.2.3a) corresponds largely to that of the Carrizo (Figure 8.2.2a).

The calibration statistics for Layer 5 (middle Wilcox) shows an adjusted RMS of 8% (Table 8.2.1). The simulated hydraulic head distribution together with the posted residual in the target wells is shown in Figure 8.2.4a. The residuals are generally low and uniformly distributed in the scatterplot (Figure 8.2.4b), except for a couple of data points in southern van Zandt County, indicating simulated hydraulic heads nearly 100 ft below measured heads of 574 ft. The recharge distribution used in this area is somewhat low compared to the surrounding areas in the outcrop of Layer 5 (Figure 8.1.6), and it is probable that by increasing recharge rates in this area, the difference could be reduced. On the other hand, potential uncertainties in the actual well location could cause a significant change in well elevation in this rather hilly outcrop area. That

is, the measured water levels could be significantly in error. Water-level measurements in a nearby well, used for transient calibration (well 3433801), indicated a water-level elevation of about 505 ft, which is significantly lower than the 574 ft reported for the two steady-state target wells. Furthermore, the water levels in nearby wells in the upper Wilcox and Carrizo agree well with simulated values, indicating little difference in hydraulic heads. As a result, no additional adjustment of recharge in this particular area was attempted to improve the fit. Overall, the adjusted RMS for Layer 5 was 8%, below that of the calibration criteria.

The simulated hydraulic head distribution for Layer 6 is shown in Figure 8.2.5. In the northern part of the area, the lower Wilcox pinches out and no simulated heads are shown. There were no calibration points identified in the lower Wilcox to provide a check of the simulated steady-state hydraulic heads in Layer 6. The simulated heads compare well with those in the overlying layer, showing somewhat higher hydraulic heads in the deeper confined section, which indicates upward flow from Layer 6, as one would expect.

Some cells went dry in the steady-state simulation. Out of 18,679 outcrop cells, 77 cells or less than one present were dry. These dry cells can be indicative of model instability or actual subsurface conditions. Because no obvious discontinuity exists in the outcrop water table, these cells likely are indicative of actual subsurface conditions (i.e., small cell thickness, low water table). The small number of dry cells does not have a significant impact on model results.

8.2.2 Streams

Figure 8.2.6 shows the gain/loss values for the stream reaches in the steady-state model. As would be expected, the larger stream segments are all gaining. Only the upper reaches of tributaries show losing segments. These losses are typically higher in shallow channels at higher overall elevations.

We compared the stream leakances to the stream gain/loss data compiled by Slade et al. (2002). Seven of the nine documented gain/loss studies that fall within the model area and include the Carrizo-Wilcox outcrop were compared to simulated stream leakances. The other two studies were conducted on minor streams that were not included as boundary conditions in the model due to their small size. The seven gain/loss studies used were conducted between 1942 and 1981 and covered reaches of the Sabine River, Little Cyprus Bayou, Bowles Creek, and Lake Fork Creek. Because the steady-state model simulates predevelopment conditions

based on average recharge, ET, and stream flows, stream gain/loss studies conducted under a particular set of conditions may or may not agree with the steady-state results. Figure 8.2.7 shows a cross-plot of the measured gain/loss values and those derived from the model. The data comparison shows a large scatter, though most of the data fall within the same quadrant.

Slade et al. (2002) note that the potential error in stream flow measurements is typically about 5 to 8 percent. Since this error is possible at both ends of a gain/loss subreach, the potential error in gain/loss can equal a significant fraction of the total flow in the subreach. Comparing the available gain/loss values discussed in the previous paragraph to mean stream flows from the EPA River Reach data set shows that almost all of the gain/loss values are less than 5 percent of the mean stream flow. This suggests that the gain/loss values are uncertain and can be used only qualitatively.

8.2.3 Water Budget

Tables 8.2.2a and 8.2.2b summarize the water budget for the model in terms of total volume and as a percentage of total inflow and outflow. The overall mass balance error for the steady-state simulation was 0.04 percent, well under the GAM requirement of one percent. The predominant input source is recharge, which accounts for 93% of the total inflow to the model. Water discharging from the model is mainly through the streams (68%), followed by ET (28%), and the GHBs (4%) in descending order. The total recharge averaged over the entire model region is 0.93 inches/yr.

As discussed above, the recharge for the steady-state model was reduced from the long-term average rate calibrated from the transient model. ET in the steady-state model also had to be reduced in certain location by limiting the ET rates to 70% of the recharge rate. This was done to avoid numerical difficulties in the steady-state MODFLOW simulation. The net recharge to the aquifer (i.e., recharge minus ET) for the steady-state simulation was 0.65 inches/yr. For comparison, the long-term average in the transient model was 0.93 inches/yr, based on the average recharge rate of 2.59 inches/yr. The likelihood of overall higher recharge rates during transient conditions because of water-level declines owing to pumpage was discussed in Section 5. Accordingly, the increased recharge during transient conditions would be equivalent to the rejected recharge during predevelopment conditions. However, the numerical problems encountered during the steady-state MODFLOW simulations required limiting ET to

about 70% of the recharge rate for a given cell. This problem may have some effect on the net recharge estimates for the steady-state model. In general, the estimated recharge rates are within the range reported in the various studies that are summarized in Table 4.5.1.

Table 8.2.1 Calibration statistics for the steady-state model.

Layer	ME (ft)	MAE (ft)	RMS (ft)	Range (ft)	RMS/Range
Layer 1 (Queen City)	-2.14	35.86	45.8	366	0.13
Layer 3 (Carrizo)	-6.10	20.99	25.9	308	0.08
Layer 4 (upper Wilcox)	10.12	32.20	38.5	257	0.15
Layer 5 (middle Wilcox)	12.62	24.56	33.9	418	0.08

ME = mean error

MAE = mean absolute error

RMS = root mean square error

Table 8.2.2a Water budget for the steady-state model. All rates reported in acre-ft/yr.

IN	Layer	GHBs	Recharge	Streams	Top	Bottom
	1	34517	448732	20668		11128
	2		33019	607	17033	13523
	3		65999	268	16198	8234
	4		165194	5292	20542	9816
	5		195020	10741	21359	6027
	6		17475	342	6929	
	Sum	34517	925439	37919	82060	48727
OUT	Layer	GHBs	ET	Streams	Top	Bottom
	1	35018	141058	321909		17033
	2		13264	23588	11128	16198
	3		26492	30132	13523	20542
	4		48854	122327	8234	21359
	5		45437	170685	9816	6929
	6		6017	12667	6027	
	Sum	35018	281123	681309	48727	82060

Table 8.2.2b Water budget for the steady-state model with values expressed as a percentage of inflow or outflow.

IN	Layer	GHBs	Recharge	Streams
	1	3	45	2
	2		3	0
	3		7	0
	4		17	1
	5		20	1
	6		2	0
	Sum	3	93	4
OUT	Layer	GHBs	ET	Streams
	1	4	14	32
	2		1	2
	3		3	3
	4		5	12
	5		5	17
	6		1	1
	Sum	4	28	68

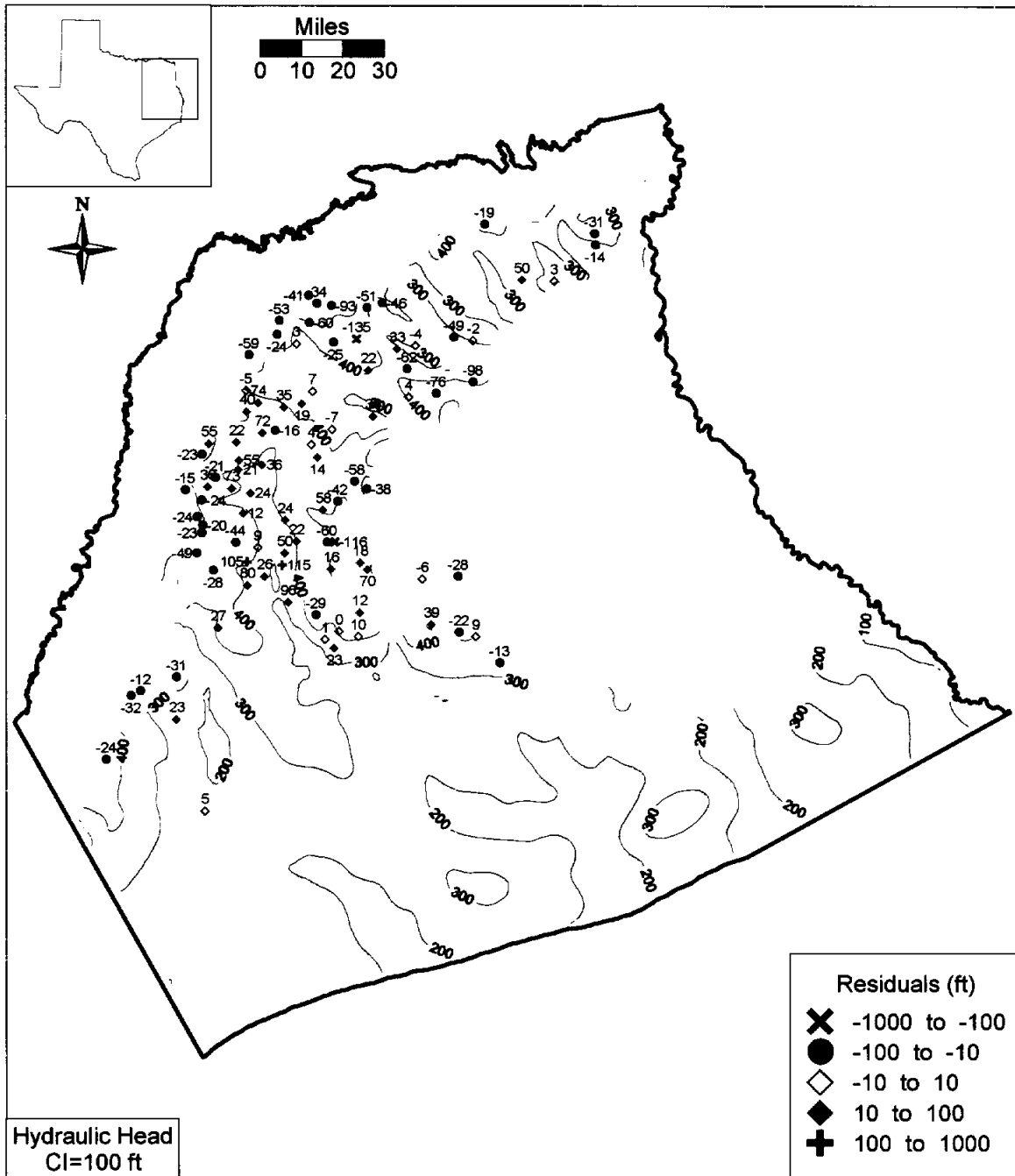


Figure 8.2.1a Simulated steady-state hydraulic heads and residuals for Layer 1 (Queen City).

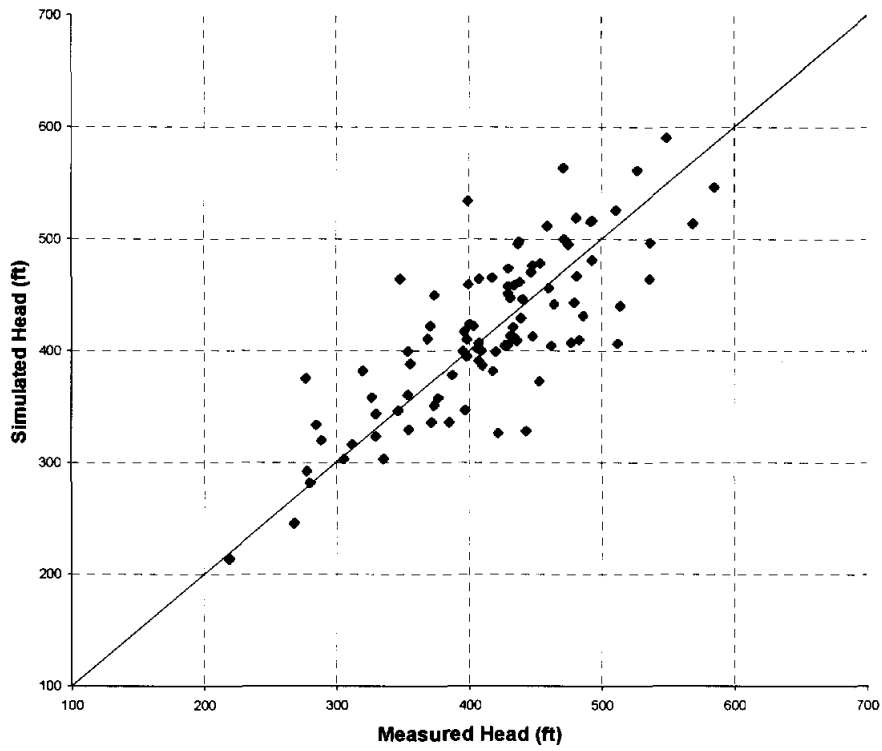


Figure 8.2.1b Scatterplot of simulated and measured hydraulic heads for Layer 1 (Queen City).

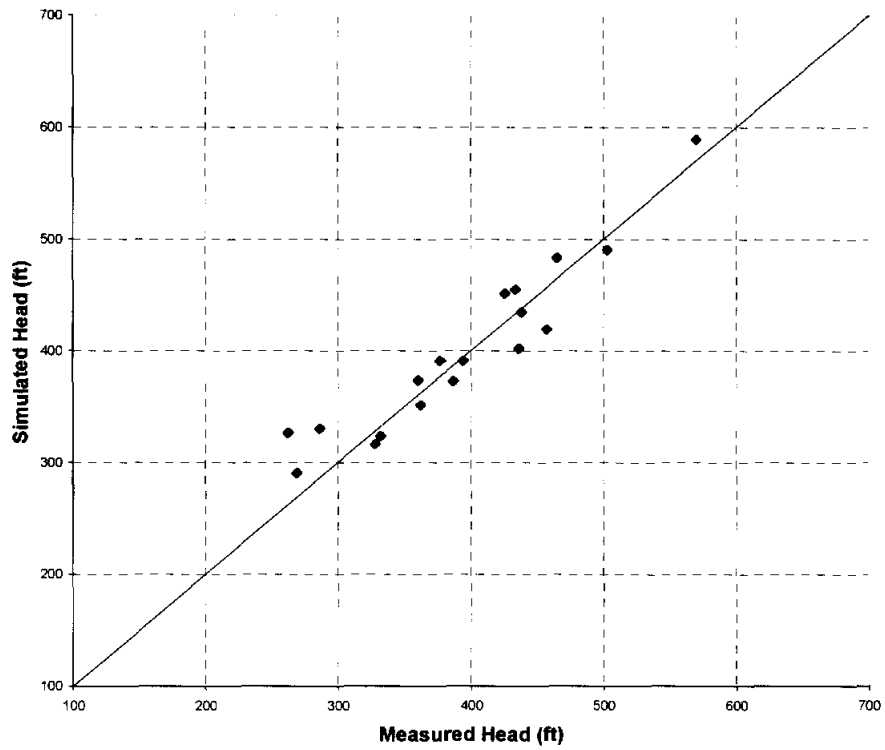


Figure 8.2.2b Scatterplot of simulated and measured hydraulic heads for Layer 3 (Carrizo).

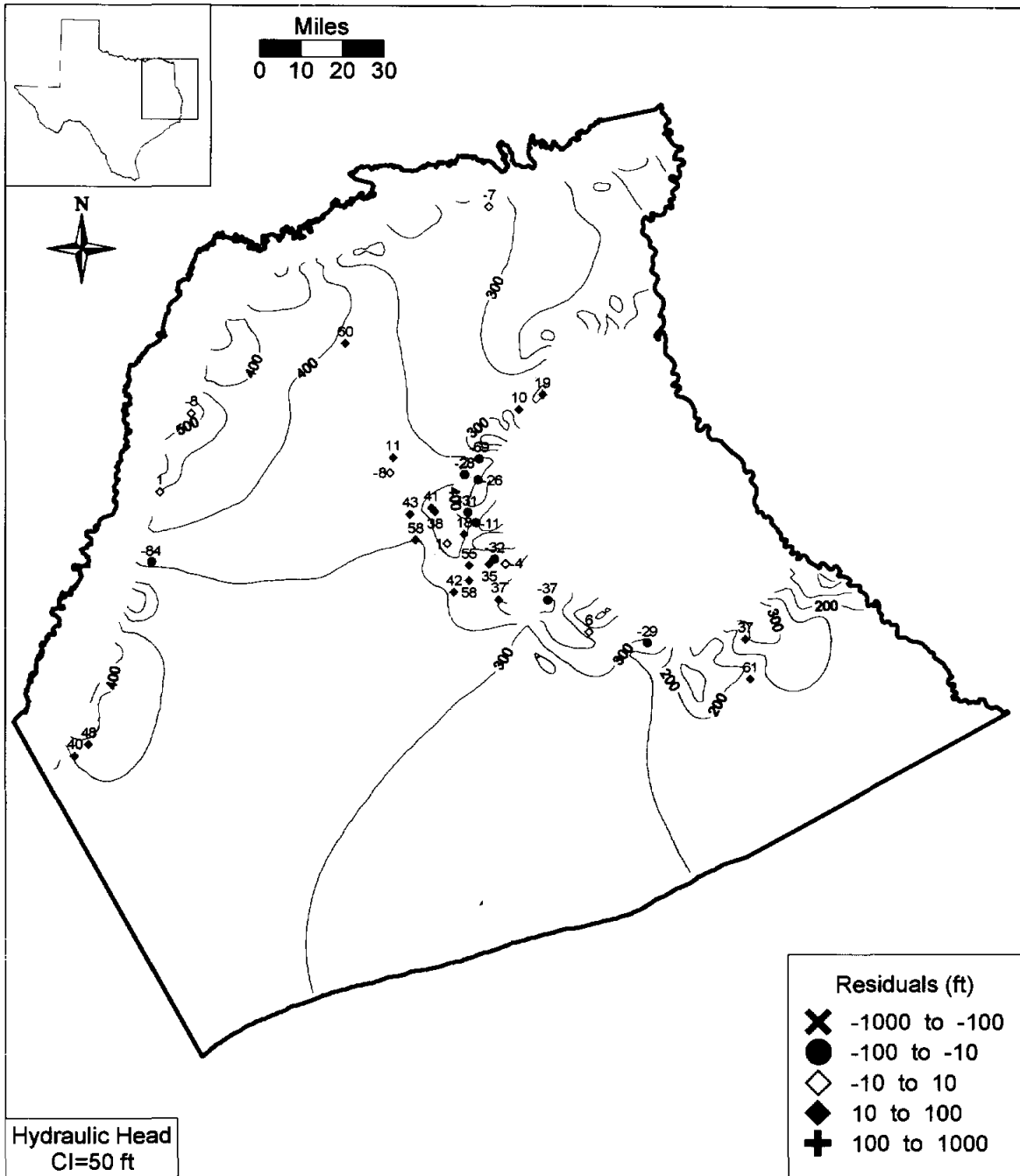


Figure 8.2.3a Simulated steady-state hydraulic heads and residuals for Layer 4 (upper Wilcox).

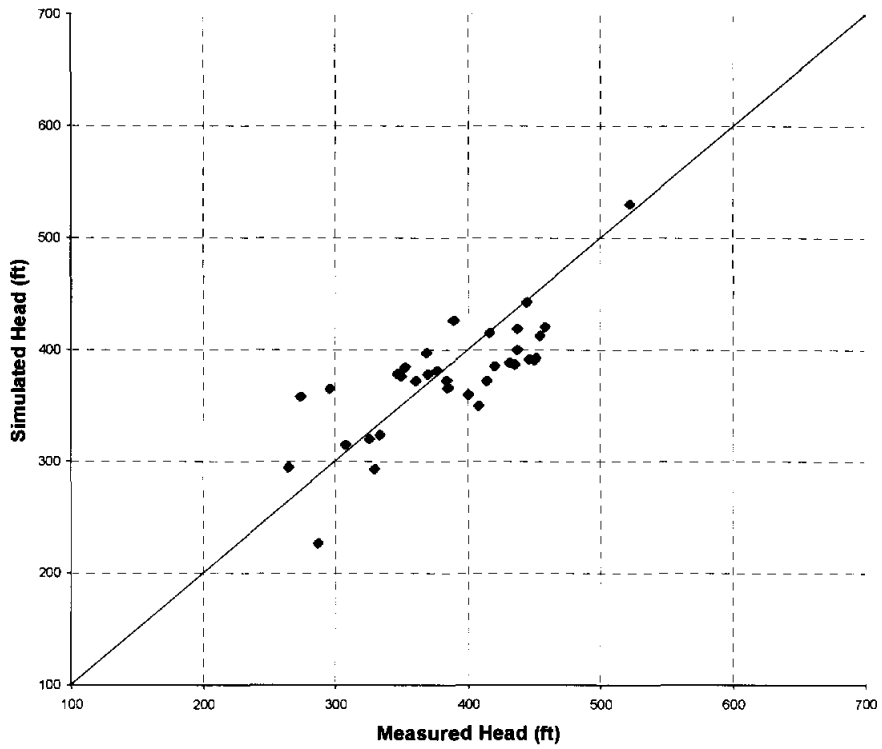


Figure 8.2.3b Scatterplot of simulated and measured hydraulic heads for Layer 4 (upper Wilcox).

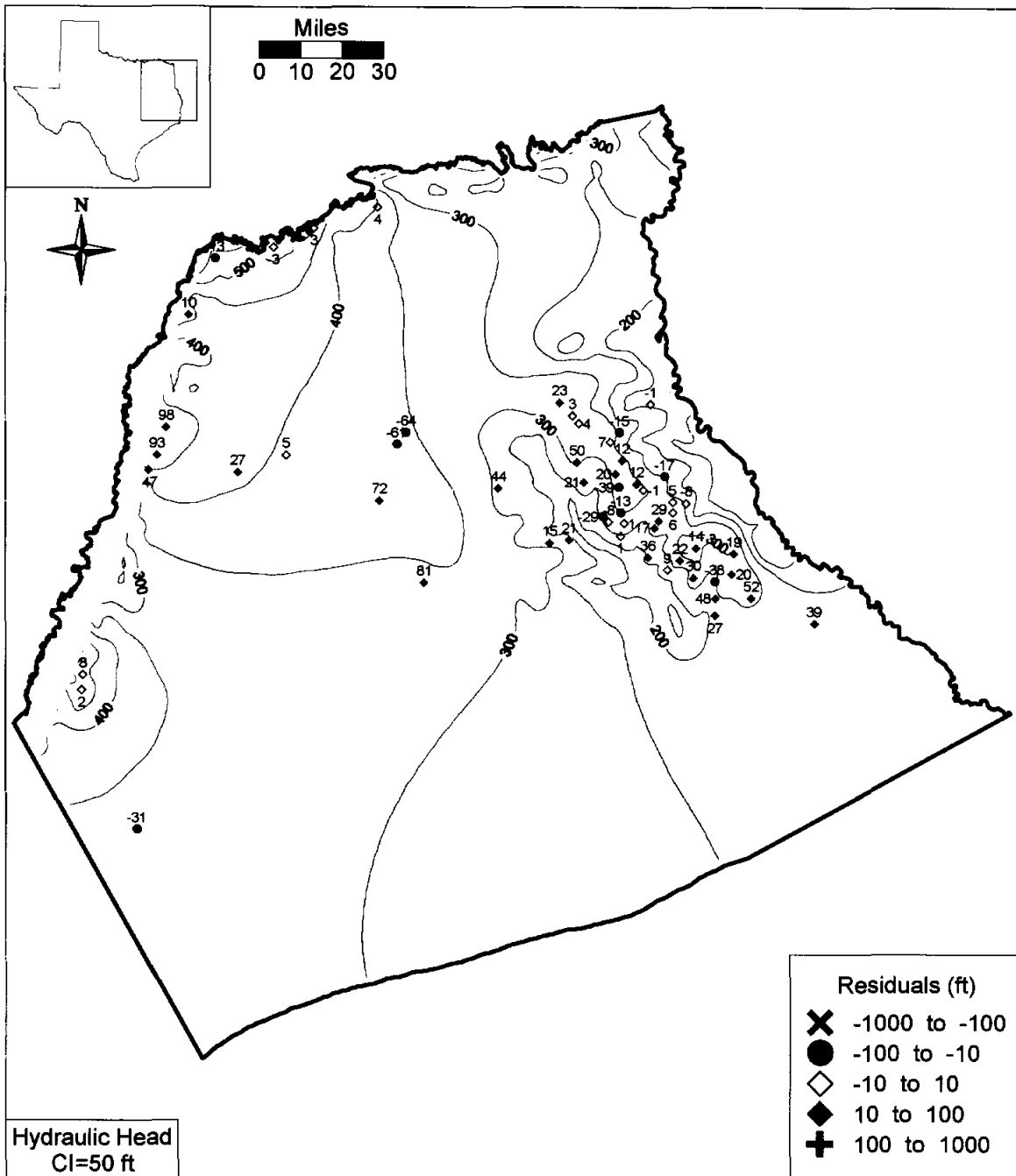


Figure 8.2.4a Simulated steady-state hydraulic heads and residuals for Layer 5 (middle Wilcox).

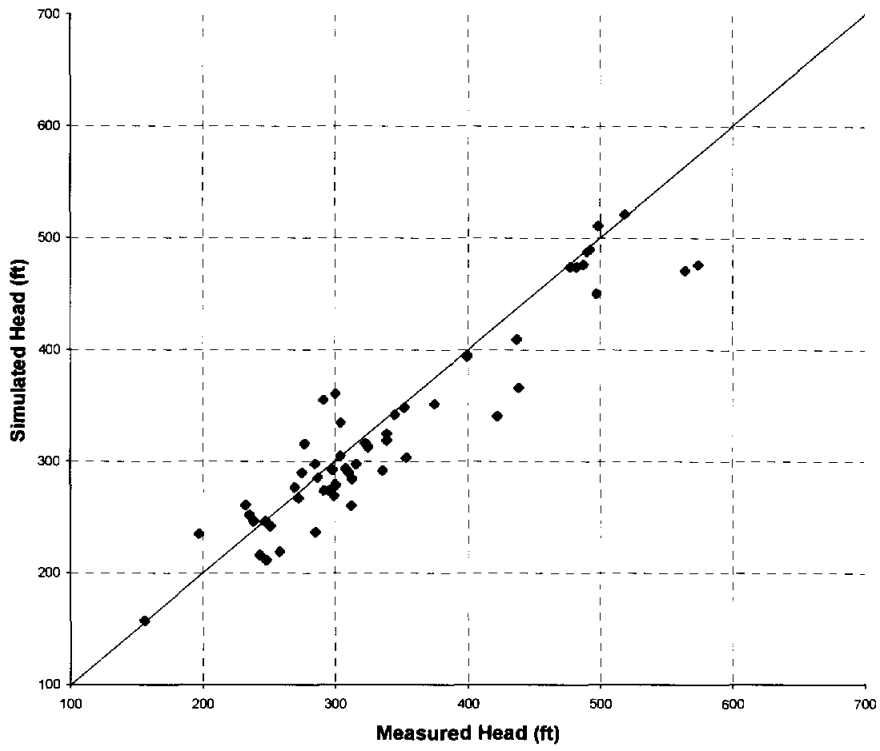


Figure 8.2.4b Scatterplot of simulated and measured hydraulic heads for Layer 5 (middle Wilcox).

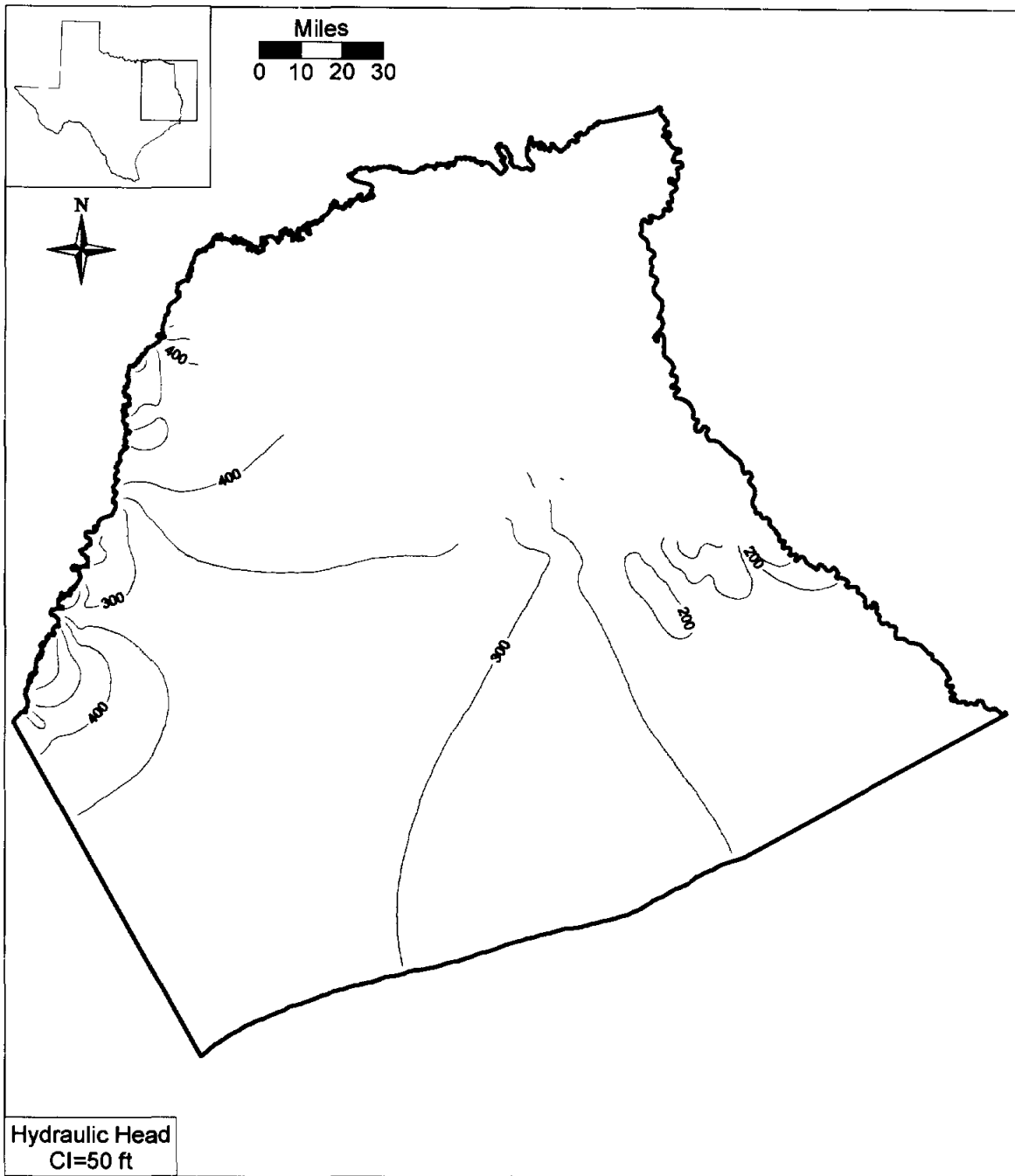


Figure 8.2.5 Simulated steady-state hydraulic heads for Layer 6 (lower Wilcox).

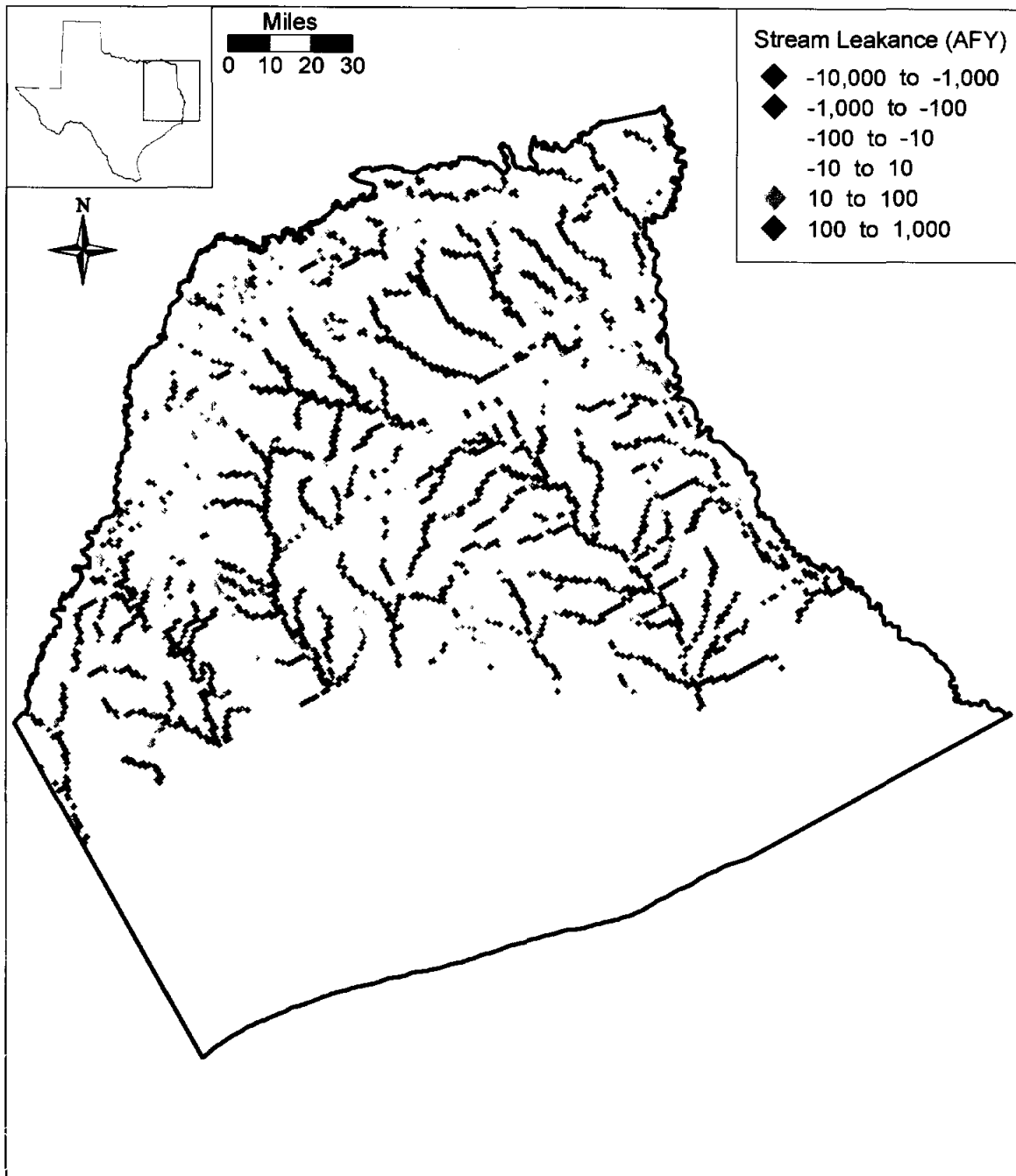


Figure 8.2.6 Steady-state model stream gain/loss (negative values denote gaining streams).

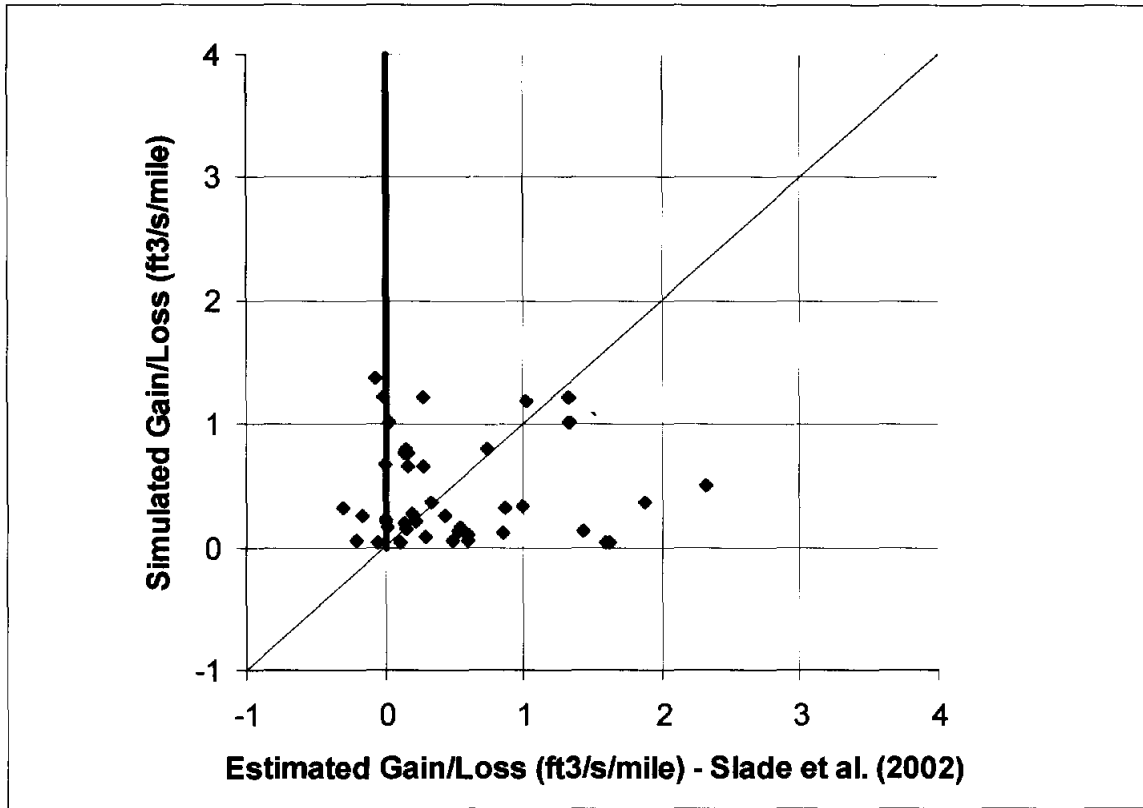


Figure 8.2.7 Simulated stream gain/loss compared to measurements compiled by Slade et al. (2002) for selected stream segments.

8.3 Sensitivity Analysis

A sensitivity analysis was performed on the calibrated steady-state model. A sensitivity analysis provides a means of formally describing the impact of varying specific parameters or groups of parameters on model outputs. In this sensitivity analysis, input parameters were systematically increased and decreased from their calibrated values while the change in head was recorded. Four simulations were completed for each parameter sensitivity, where the input parameters were varied either according to:

$$(\text{new parameter}) = (\text{old parameter}) * \text{factor} \quad (8.3.1)$$

or

$$(\text{new parameter}) = (\text{old parameter}) * 10^{(\text{factor} - 1)} \quad (8.3.2)$$

and the factors were 0.75, 0.9, 1.1, and 1.25. For parameters such as hydraulic conductivity, which are typically thought of as log-varying, equation (8.3.2) was used. Parameters such as recharge were varied linearly using equation (8.3.1). For the output variable, we calculated the mean difference (MD) between the base simulated head and the sensitivity simulated head:

$$MD = \frac{1}{n} \sum_{i=1}^n (h_{sens,i} - h_{cal,i}) \quad (8.3.3)$$

where

$h_{sens,i}$ = sensitivity simulation head at active gridblock i

$h_{cal,i}$ = calibrated simulation head at active gridblock i

n = number of active gridblocks

For the steady-state analysis, we completed seven parameter sensitivities:

1. Horizontal hydraulic conductivity of Layer 3 (K_h -Carrizo)
2. Horizontal hydraulic conductivity of Layers 4 - 6 (K_h -Wilcox)
3. Vertical hydraulic conductivity in Layer 2 (K_v -Reklaw) (leakance between Layers 2 and 3)
4. Vertical hydraulic conductivity in Layers 4-6 (K_v -Wilcox) (leakance between layers 3-4, 4-5, and 5-6)
5. Streambed conductance, model-wide (K -stream)
6. GHB conductance, model-wide (K -GHB)

7. Recharge, model-wide.

Equation 8.3.1 was used for sensitivity 7, and Equation 8.3.2 was used for the other sensitivities.

Figure 8.3.1 shows the results of the sensitivity analyses for the Carrizo (Layer 3) with *MDs* calculated from just the grid blocks where targets were available. In comparison, Figure 8.3.2 shows the corresponding sensitivity results with *MDs* calculated from all active cells in the layer. Note that the two figures indicate similar trends in sensitivities. The relative sensitivity differs somewhat between the two cases for *MDs* that were close to zero. However, the good agreement for the significant *MDs* indicates adequate target coverage. Because of the good agreement between sensitivities calculated using only target cells and those calculated using all active cells, only those sensitivities using all active cells are shown for the remaining sensitivities.

Figure 8.3.1 indicates that the change in head in the Carrizo for the steady-state model is most positively correlated with recharge. Similar *MD* trends are shown in Figures 8.3.3 and 8.3.4 indicating that hydraulic heads in Layer 1 (Queen City) and Layer 2 (Reklaw) are also strongly influenced by recharge. This is to be expected since Layer 1 crops out through most of the model and Layer 2 is in direct contact with Layer 1. Figure 8.3.5 indicates similar sensitivity to recharge for Layer 4 (upper Wilcox). In this case, the horizontal hydraulic conductivity of the Wilcox also shows high *MDs*, characterized by a negative correlation between hydraulic conductivity and head change in Layer 4. Similar sensitivity patterns are shown in Figures 8.3.6 and 8.3.7 for Layer 5 (middle Wilcox) and Layer 6 (lower Wilcox), respectively. Because of the relatively large outcrop area for the Wilcox, particularly in the Sabine Uplift, a decrease in the horizontal hydraulic conductivity of the Wilcox results in an increase in head, because of the more restricted flow of recharged groundwater.

The sensitivity of the vertical hydraulic conductivity of Layer 2 (Reklaw) on hydraulic heads in Layers 1 through 6 shows maximum *MDs* ranging between -2.5 and +3 ft (Figure 8.3.8). The plot indicates that the greatest impact is on Layer 3, followed by Layer 4, Layer 6, and Layer 5. The high impact on Layer 3 is expected because of its close proximity to Layer 2.

Sensitivity to streambed conductance is shown in Figure 8.3.9, indicating a negative correlation for all layers. Lower stream conductivities results in decreased discharge from the layers and concomitantly increased hydraulic heads. Layer 1 (Queen City) shows the lowest *MDs* despite the relatively large outcrop area, where the streams are in contact with the layer. This is probably an artifact caused by the relatively high minimum hydraulic conductivities assigned to the Layer 1 (Queen City). Even though the Carrizo is relatively thin, compared to the Wilcox layers, it shows relatively high *MDs*, suggesting that stream segments in the Queen City above the Reklaw confining unit affect vertical upward leakage from the Carrizo to discharge sites in stream valleys in the Queen City outcrop.

Sensitivity to recharge, shown in Figure 8.3.10, indicates similar trends for all layers, with Layer 4 (upper Wilcox) showing the greatest *MDs*. This can be explained by the relatively large outcrop area of the upper Wilcox, particularly on the Sabine uplift. Layer 1 (Queen City) shows the smallest *MDs* which may be due to the relatively high conductivities, which were artificially increased to avoid numerical problems. Note, for the Northern Carrizo-Wilcox GAM, the Queen City was included as a layer but was not explicitly calibrated. A separate GAM for the Queen City will be developed during the TWDB's next GAM phase.

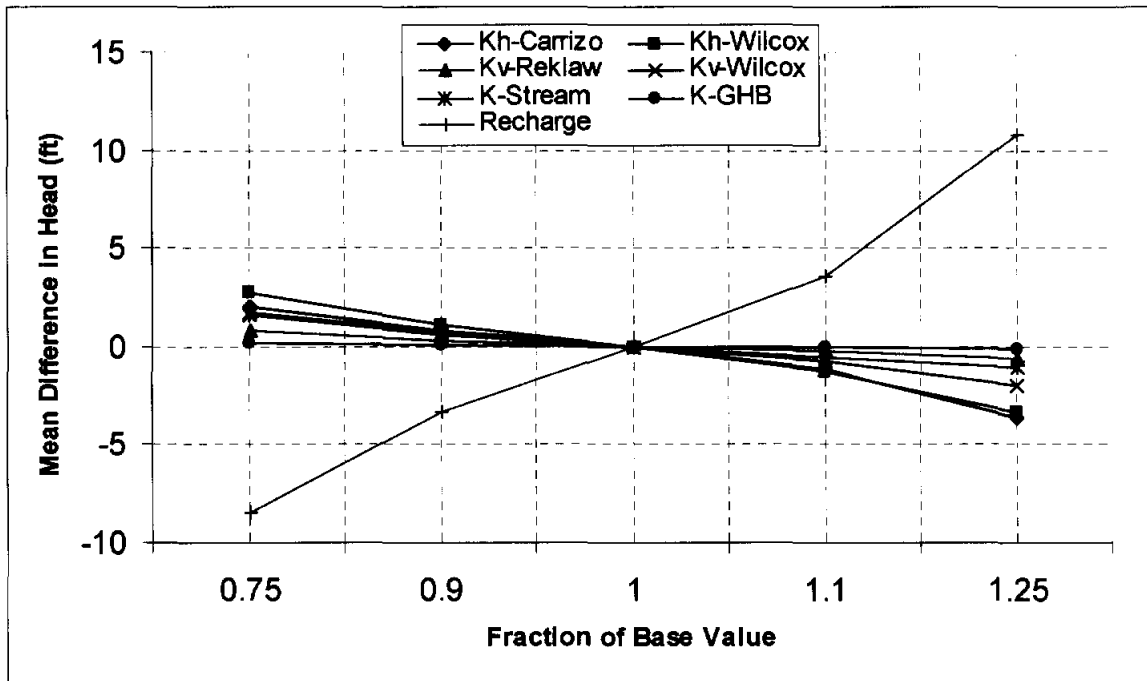


Figure 8.3.1 Steady-state sensitivity results for Layer 3 (Carrizo) using target locations.

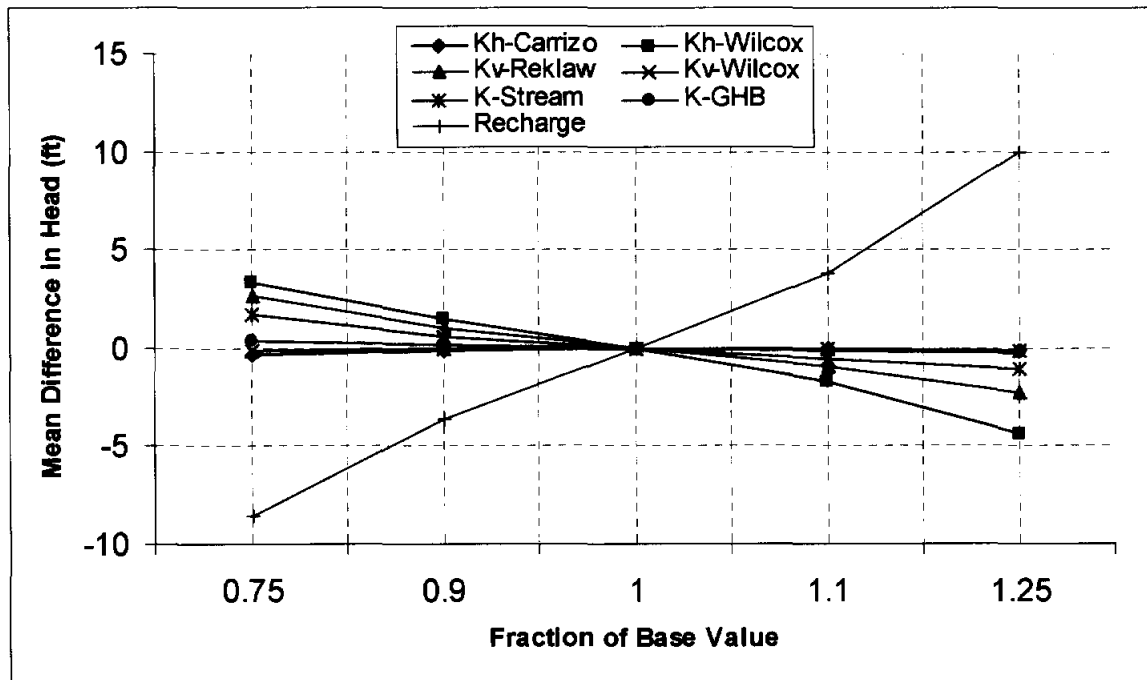


Figure 8.3.2 Steady-state sensitivity results for Layer 3 (Carrizo) using all active gridblocks.

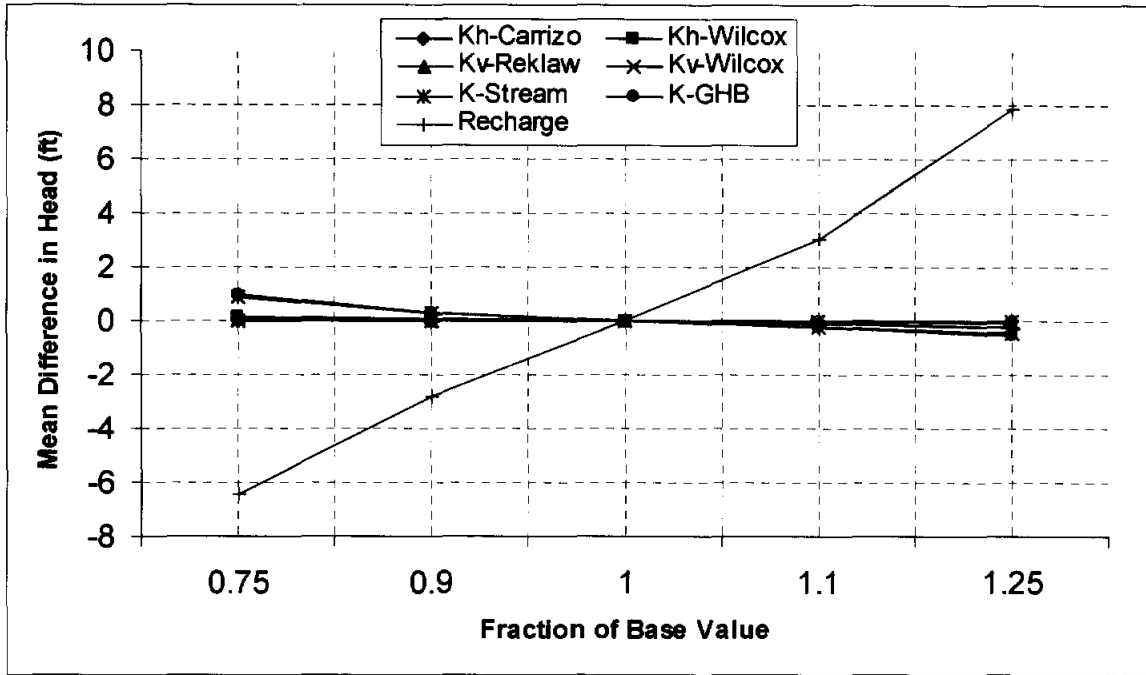


Figure 8.3.3 Steady-state sensitivity results for Layer 1 (Queen City) using all active gridblocks.

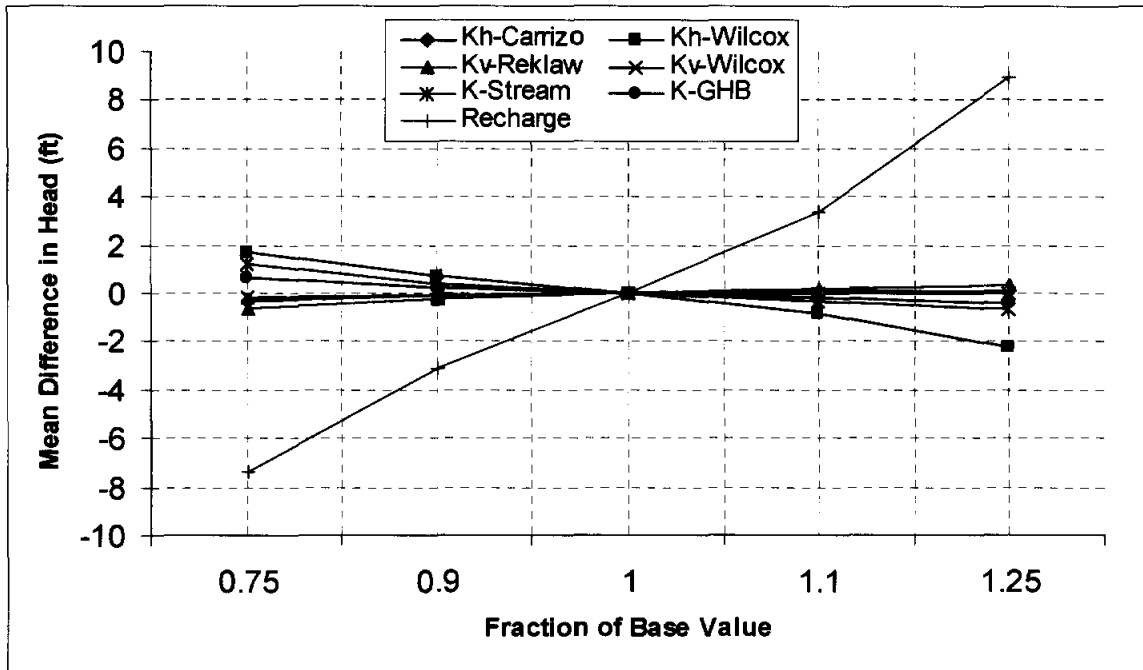


Figure 8.3.4 Steady-state sensitivity results for Layer 2 (Reklaw) using all active gridblocks.

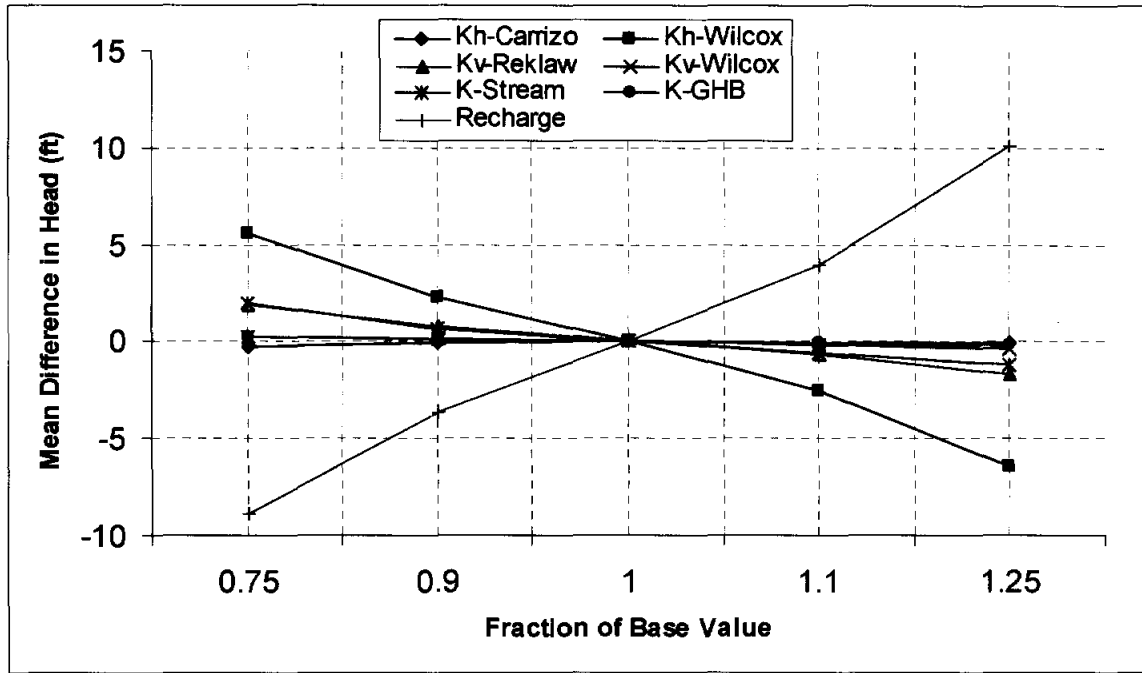


Figure 8.3.5 Steady-state sensitivity results for Layer 4 (upper Wilcox) using all active gridblocks.

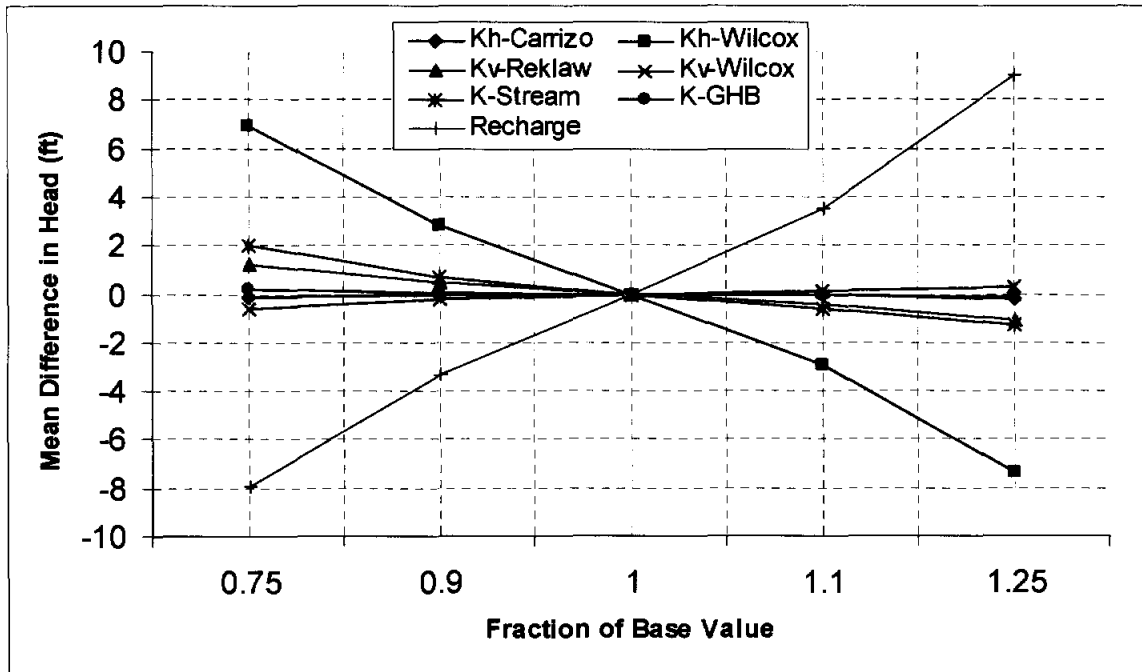


Figure 8.3.6 Steady-state sensitivity results for Layer 5 (middle Wilcox) using all active gridblocks.

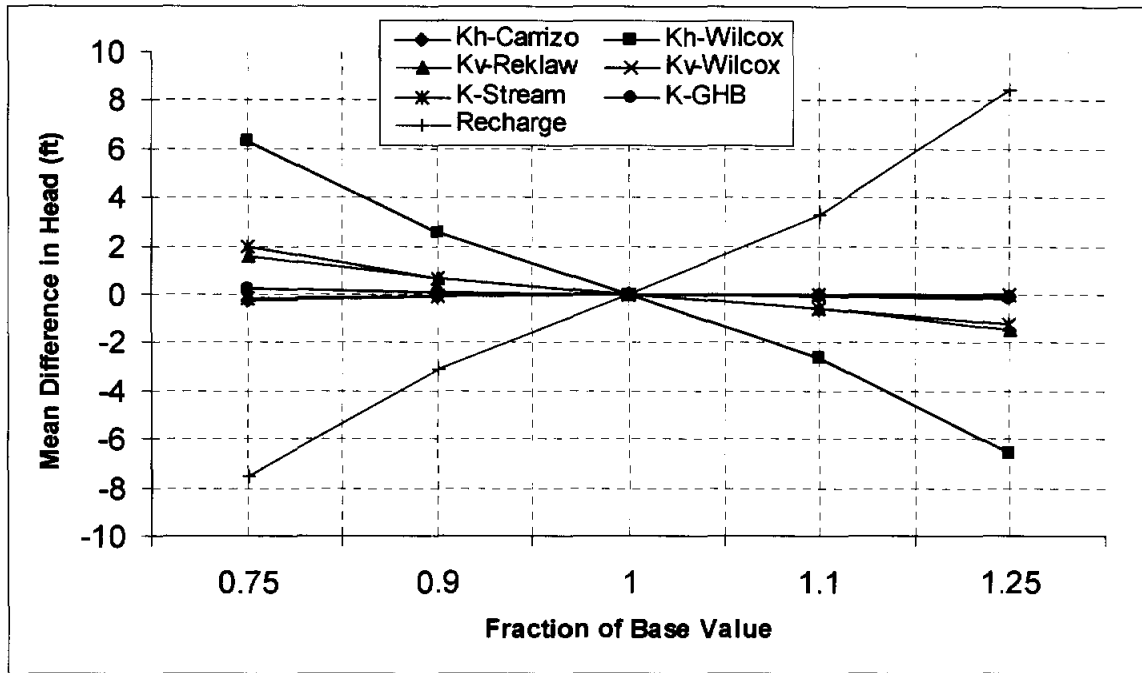


Figure 8.3.7 Steady-state sensitivity results for Layer 6 (lower Wilcox) using all active gridblocks.

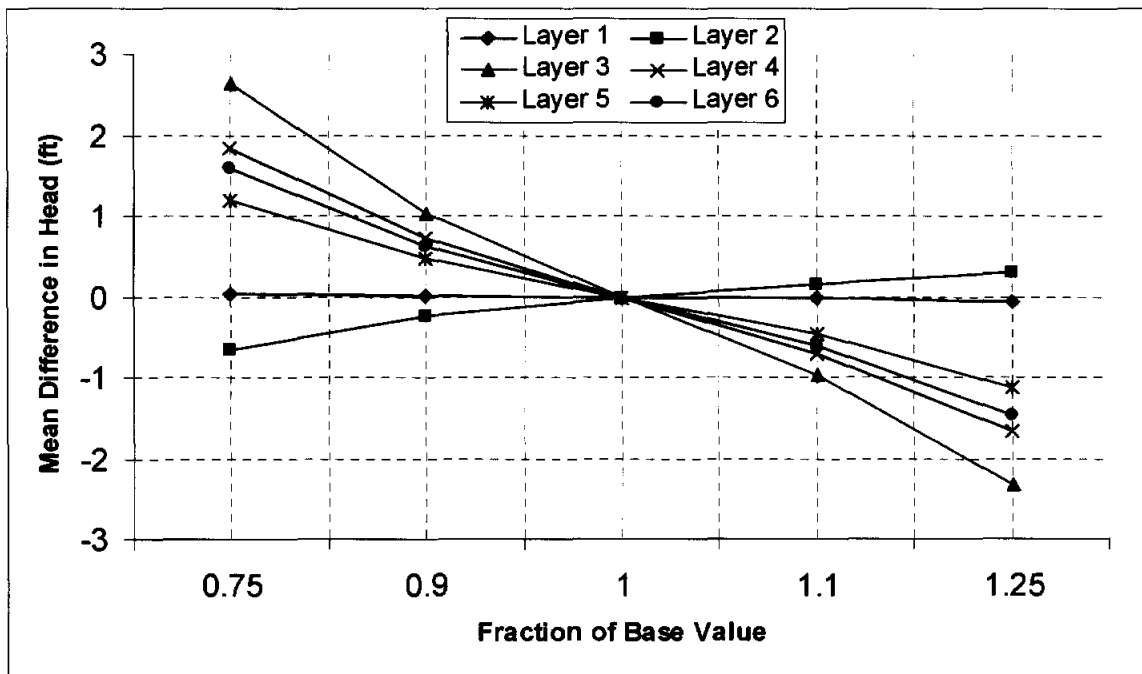


Figure 8.3.8 Steady-state sensitivity results where the vertical hydraulic conductivity of Layer 2 (Reklaw) is varied.

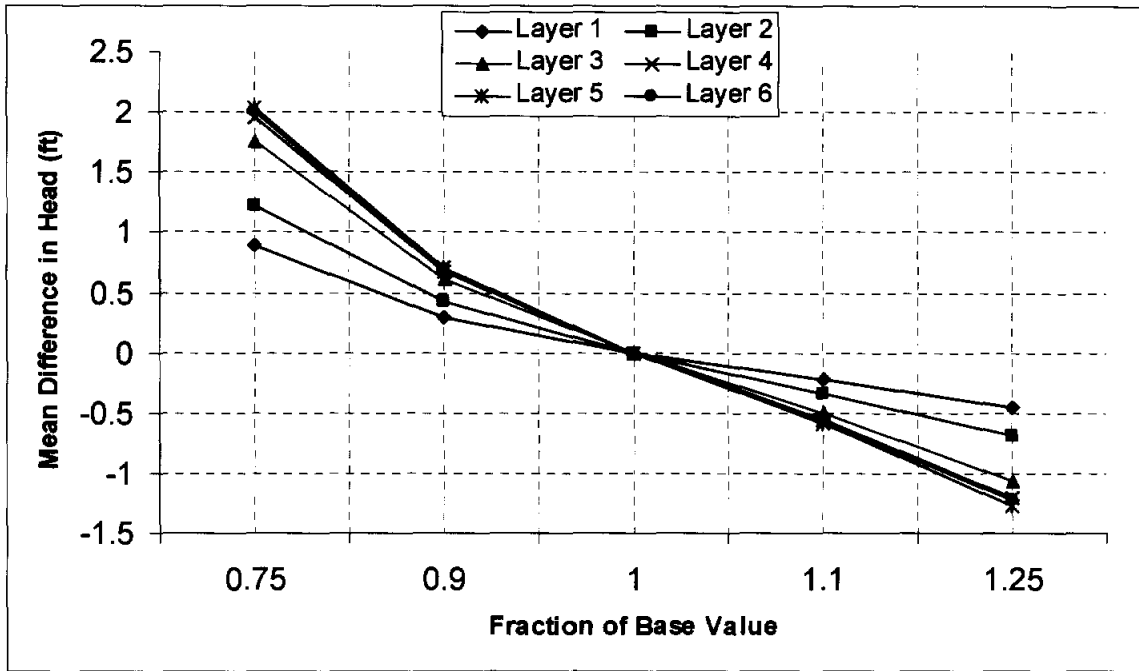


Figure 8.3.9 Steady-state sensitivity results where streambed conductivity is varied.

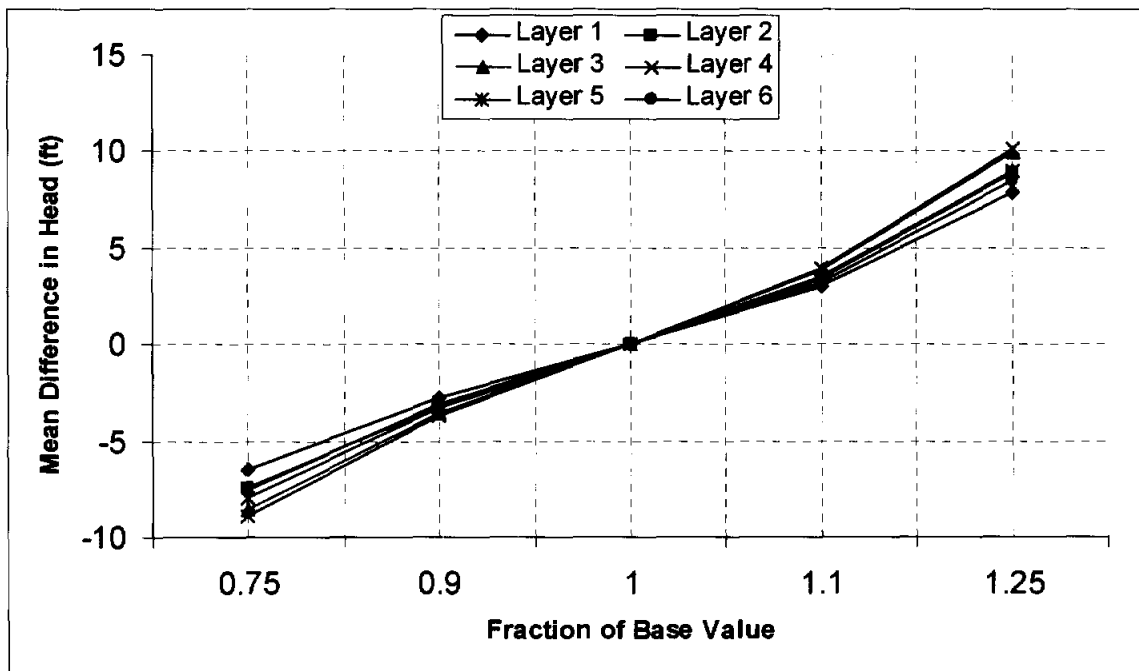


Figure 8.3.10 Steady-state sensitivity results where recharge is varied.

9.0 TRANSIENT MODEL

This section details the calibration and verification of the transient model and presents the transient model results. Section 9.1 describes the salient features of the calibration approach, and Section 9.2 presents the results of the transient calibration and verification together with the examination of residuals, hydrographs, and stream flow. A formal sensitivity analysis with the calibrated transient model can be found in Section 9.3.

9.1 Calibration

All properties or parameters common with the steady-state model were identical in the transient model. Section 8.1 contains the discussion of hydraulic properties in the steady-state model. A discussion of important inputs and new properties (such as storativity) follows. Figure 9.1.1 shows the distribution of calibration targets (head measurements) used for the transient model calibration.

The transient model played an important part in setting vertical anisotropy ratios for the model. We had initially set the anisotropy ratios of Layers 3, and 4 through 6, representing the Carrizo and Wilcox, respectively, to values on the order of 10 to 100; further, the maximum anisotropy for Layer 2 (Reklaw) was 4000. However, during initial transient calibration we found that water was passing between formations so easily that drawdowns could not be maintained at the estimated pumping rates. Water was moving into the Carrizo from storage in the Wilcox and Reklaw layers (or from storage in the Queen City through the Reklaw) due to the cross-formational flow resulting from the initialized drawdown cones, especially in Smith and Nacogdoches counties. We significantly increased the anisotropy ratios (decreased vertical hydraulic conductivity) in Layers 2, 4, 5 and 6 to near the extreme of previous/published values. This increase in anisotropy mitigated the “rebound” effect considerably. The final vertical hydraulic conductivities resulting from the calibrated anisotropy ratios (Table 8.1.1) are within published limits for these formation materials, but are closer to the “pure” material vertical hydraulic conductivity values than we would have anticipated for a regional scale model.

Note that for Smith and surrounding counties, the vertical permeability of the Reklaw (Layer 2) had to be decreased from 1×10^{-5} to 1×10^{-6} ft/day and the horizontal permeability of the Carrizo (Layer 3) and Wilcox (Layers 4 and 5) was limited to a maximum of 2 ft/d and 1 ft/d,

respectively (see Section 8.1.2). Such a reduction was needed even after reallocating 80% of the estimated pumpage from the Queen City to the Carrizo Layer to reproduce the observed drawdown. In contrast, the vertical hydraulic conductivity of Layer 2 had to be increased in Nacogdoches County from 1×10^{-5} to 1×10^{-4} ft/day so that the model did not overpredict the observed drawdown in Nacogdoches and Angelina counties.

Primary and secondary storage (also called storativity and specific yield) are properties in a transient model that are not present in a steady-state model. For specific storage, we used the geometric mean value of 4.5×10^{-6} 1/ft in all layers, based on field data compiled for the Carrizo-Wilcox aquifer by Mace et al. (2000a). This specific storage was then multiplied by layer thickness to provide the storativity at each grid cell. As a result, the variation in storativity corresponds to the variation in thickness of the different layers. Storativity has some effect on amplitude of head variation due to pumping. However, we did not find overall hydrograph trends to be sensitive to storativity, and, therefore, did not make areal changes in storativity during calibration or distinguish between specific storage of sand and mud in the Wilcox.

Because we lacked good targets for stream leakance, we set the streambed conductivity in a first approximation to the same value as the hydraulic conductivity in that particular cell. The streams exchange significant volumes of water with the aquifer, so they are important in the outcrop area. However, in the transient model, the hydrology of the outcrop has little effect on downdip regions during the simulation period, as hydraulic heads in the deeper confined section were mostly unaffected by streams or by recharge.

There are a total of 40 reservoirs in the model area, which played a significant role in the calibration. Initially, the conductivity of the reservoir bed was set to the hydraulic conductivity value of the corresponding layer; however, the value had to be reduced by two orders of magnitude, so that the amount of water passing between the reservoirs and the aquifer was within a reasonable range.

Similar to the steady-state calibration, recharge was critical for the calibration, primarily for hydraulic heads in the outcrop areas, whereas recharge was less sensitive for heads in the confined sections. The initial seasonally varying recharge distribution was reduced to about 33% of the initial SWAT estimates to get acceptable hydraulic heads in the outcrop. The recharge rates at 50% of the SWAT estimates generally yielded heads that were high, whereas recharge

rates at 15% of the SWAT estimates resulted in average recharge rates that were less than ET, and, hence, unacceptable.

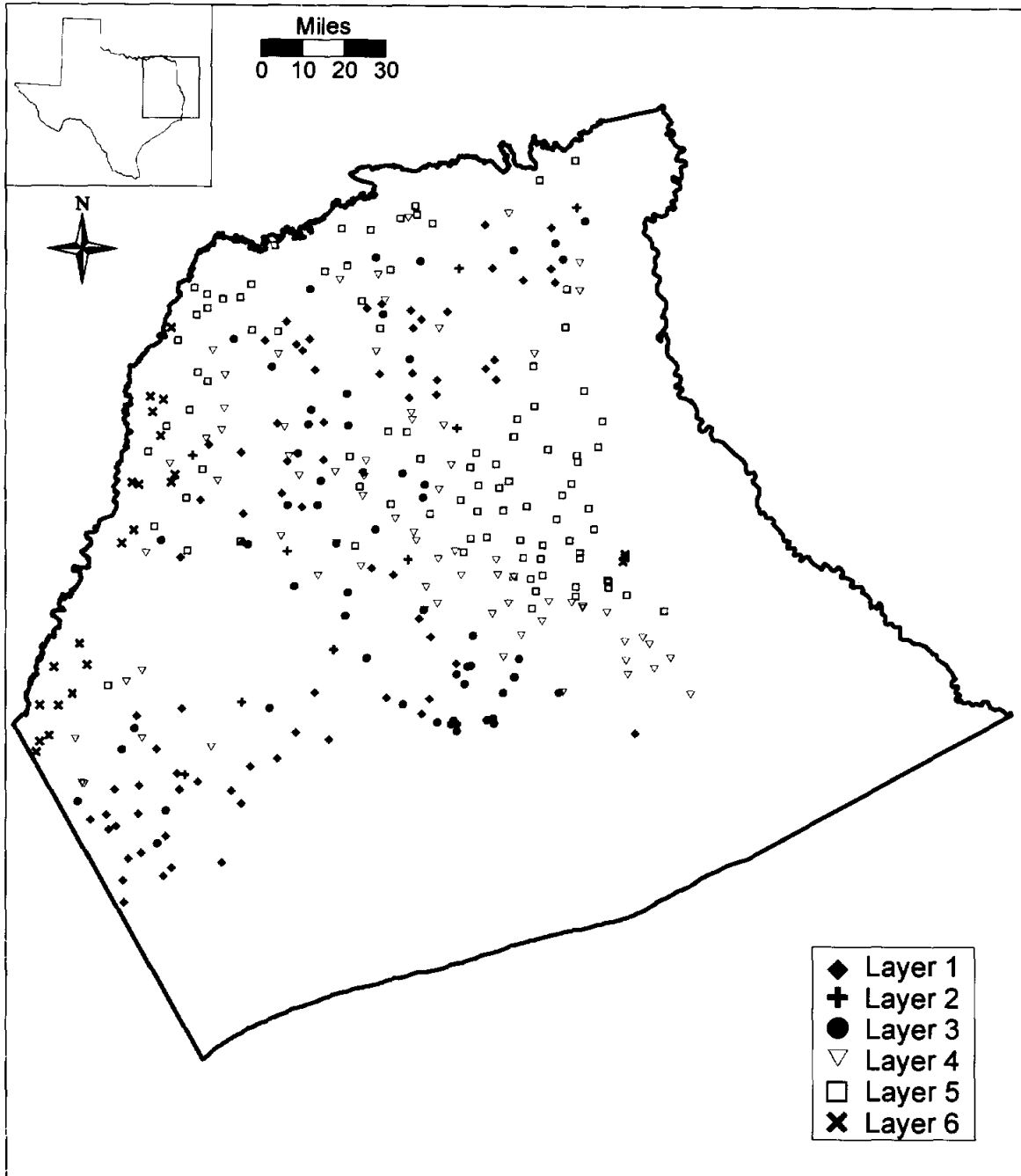


Figure 9.1.1 Target well locations for the different layers used in the transient calibration.

9.2 Simulation Results

Results for the transient model are presented in this section. Simulated hydraulic heads are compared to measured values, and stream leakances and water budgets are discussed.

9.2.1 Hydraulic Heads

The transient modeling is divided into a calibration period (1980 – 1989) and a verification period (1990 – 1999). Results of the calibration period are described first, followed by the performance of the verification period. Table 9.2.1 lists the mean error (ME), mean absolute error (MAE), root mean square error (RMS), range, and RMS/range for all aquifer layers for the calibration and verification periods. Figure 9.2.1 shows the simulated hydraulic-head distribution for Layer 1 (Queen City) at the end of the transient calibration period (December 1989). There was no hydraulic head contour map produced for the Queen City for 1989 as was done for the Carrizo-Wilcox aquifer layers, which are documented in Section 4.4. As mentioned in Section 8 for the steady-state results, the hydraulic head distribution in the Queen City was not explicitly calibrated. Nevertheless, the Queen City was considered relevant for controlling potential vertical flow between the confined Carrizo-Wilcox and the shallow water table aquifer in the study area. The simulated hydraulic heads reflect the overall topography in the Queen City outcrop and simulated heads compared reasonably well with target heads as indicated by the overall calibration statistics (Table 9.2.1).

Figure 9.2.2 shows the simulated and measured hydraulic heads for Layer 3 (Carrizo) at the end of the calibration period (December 1989). The measured head contours correspond to those discussed in Section 4.4 (Figure 4.4.10a), which were based on water-level measurements taken at various times over a five year period between 1987 and 1992. That is, the measured head contour may have significant seasonal variability included and an exact “fit” cannot be expected. Overall, the simulated and measured hydraulic head contours show a good agreement, reproducing the major cones of depression in Nacogdoches and Angelina counties, as well as in Smith County (Figure 9.2.2).

Figures 9.2.3 to 9.2.5 show the simulated and measured hydraulic heads for Layer 4 (upper Wilcox), Layer 5 (middle Wilcox), and Layer 6 (lower Wilcox) at the end of the calibration period (December 1989). Similar to Layer 3, the cones of depression in Layer 4 (upper Wilcox) in Nacogdoches County and in Smith County are reproduced reasonably well.

For the middle and lower Wilcox, there were no specific water-level measurements in Nacogdoches or Angelina counties, but a cone of depression was inferred owing to the close proximity of the pumpage from the overlying layers. In the outcrop and shallow confined section, the simulated head contours agree more closely with the measured heads (Figure 9.2.4). A similar pattern is indicated in Figure 9.2.5 for Layer 6 (lower Wilcox).

Figures 9.2.6 through 9.2.9 show the residuals at the different target well locations for Layers 3, 4, 5, and 6, respectively, at the end of the calibration period (December 1989). A positive residual indicates that the model has underpredicted the hydraulic head, while a negative residual indicates overprediction. The magnitude and spatial distribution of residuals at the target well locations for Layer 3 (Carrizo) indicate a maximum head difference of 151 ft in Smith County (Figure 9.2.6). In general, however, the differences are less than 40 ft. The residuals for Layer 4 (upper Wilcox) (Figure 9.2.7) are generally lower than those in Layer 3 (Figure 9.2.6). Target well locations for Layer 5 (middle Wilcox) are primarily in the Sabine Uplift and the western outcrop area, indicate a relatively even distribution of positive and negative residuals (Figure 9.2.8). For Layer 6 (lower Wilcox), the target wells are mainly in the western outcrop area (Figure 9.2.9).

The goodness-of-fit of the simulated and measured hydraulic heads is presented as scatterplots for Layers 1, 3, 4, 5, and 6 at the end of the calibration period (December 1989) in Figure 9.2.10. The data show mostly uniform scatter around the unit-slope line, indicating no particular trend in the simulated results. A similar distribution is shown for the comparison of the simulated and measured heads at the target wells for Layers 1, 3, 4, 5, and 6 at the end of the verification period (December 1999) in Figure 9.2.11. In general, the goodness-of-fit at the end of the verification period decreases somewhat compared to the calibration period. This is indicated in the calibration statistics in Table 9.2.1, where the adjusted RMS increased slightly for Layers 5 and 6. Overall, the adjusted RMS is significantly below 10%.

The hydraulic head contours based on the simulated heads at the end of the verification period (December 1999) and water-level contours that were discussed in Section 4.4 are shown in Figures 9.2.12 through 9.2.15 for Layers 3, 4, 5, and 6, respectively. Similar to the comparison at the end of the calibration period, the head contours show reasonably good agreement for Layer 3 (Carrizo) and Layer 4 (upper Wilcox), reproducing the cone of depression

in Nacogdoches and Angelina counties and in Smith County. For Layer 5 (middle Wilcox) and Layer 6 (lower Wilcox), the simulated heads in the deeper confined section are generally higher than the kriged head contours.

In the following discussion, selected hydrographs of simulated and measured heads are presented describing the general model response in the different layers. Table 9.2.2 lists the calibration statistics for these hydrographs. All hydrographs in this section are shown on a 100-ft vertical scale for consistency, unless the data range exceeds 100 ft. Figures 9.2.16a – c show hydrographs from Layer 3 (Carrizo). Hydrographs from the northern part indicate relatively little change in water levels through time (Figure 9.2.16a) with simulated water levels falling both above and below the measured heads and trending slightly upward or downward. Similar patterns are shown for hydrographs in the central part of the Carrizo (Figure 9.2.16b). Simulated heads tend to be lower than measured heads and reproduced the overall trend, particularly the observed drawdown in Smith County. Hydrographs in the southern part indicated effects of pumpage, particularly in Nacogdoches and in Angelina counties (Figure 9.2.16c). Simulated heads in wells 37-27-506 (Nacogdoches County) and in 37-36-501 (Angelina County) are noticeably lower than measured heads, whereas simulated heads in well 37-35-703 are significantly higher than measured heads at the end of the verification period (December 1999). As mentioned above, vertical hydraulic conductivity for Layer 2 (Reklaw) was increased from 1×10^{-5} ft/d to 1×10^{-4} ft/d in Nacogdoches County to allow for more vertical leakage to offset the head decline owing to pumpage.

Hydrographs from Layer 4 (upper Wilcox) are shown in Figures 9.2.17a – d. Simulated heads in the northern part (Figure 9.2.17a) show reasonably good agreement in Wood County and Van Zandt County, whereas the observed water-level decline could not be reproduced in Upshur County. The simulated heads in Cass County are lower than the measured heads, but reproduce the general trend. Hydrographs from the central part indicate relatively good agreement, reproducing the water-level declines in western Smith County and northern Cherokee County (Figure 9.2.17b). In eastern Smith County, however, the simulated heads did not reproduce the downward trend of measured water levels. Simulated heads in Rusk, Gregg, and Harrison counties showed relatively good agreement, though the simulated heads in Harrison County show an upward trend. The hydrograph of well 34-46-511 in Smith County indicates relatively large variability in both measured and simulated heads that indicate significant short-

term water-level declines owing to pumpage (Figure 9.2.17b). Vertical permeability of Layer 2 (Reklaw) was decreased from 1×10^{-5} ft/day to 1×10^{-6} ft/day in the central area in order to maintain the cone of depression observed in Smith and Cherokee counties. Hydrographs from the southern part (Figure 9.2.17c) show relatively small water-level changes and generally good agreement, except in central Nacogdoches County. The simulated heads in well 37-20-902 trend upward, whereas measured water levels show a significant decline. Hydrographs from the western part (Figure 9.2.17d) show both positive and negative offsets in the simulated heads but reproduce the overall trends.

Hydrographs for Layer 5 (middle Wilcox) are shown in Figures 9.2.18a – c. Simulated heads in the northern part indicated a relatively good fit for Morris, Rains, Wood, and Harrison counties (Figure 9.2.18a). Simulated heads in Cass County are higher than the measured heads, but reproduce the general trend, whereas simulated heads in Upshur County trend in an opposite direction from the measured water-level trends. Similar hydrograph patterns are evident in the central part (Figure 9.2.18b), with higher simulated heads in Smith and central Rusk counties, and a flat to upward trend in Shelby County. Simulated heads in the western part indicate significant offsets both positive and negative within the same county (Figure 9.2.18c).

Hydrographs for Layer 6 (lower Wilcox) are shown in Figure 9.2.19. Simulated heads trend upward in Henderson, Limestone, and Freestone counties, whereas measured water levels show a slight decline. The hydrographs in Rains and Van Zandt counties agree reasonably well, whereas Shelby County simulated heads are higher than measured heads. The simulated upward trend in hydraulic heads corresponds to the overall higher heads in the lower Wilcox in the southern part of the model as indicated in the hydraulic head contours in Figure 9.2.15.

The simulated head increase in the southwestern part of Layer 6 (lower Wilcox) suggests potentially too high recharge rates in the outcrop or low hydraulic conductivity in this area. A long-term average recharge distribution over the 25-year transient simulation period is shown in Figure 9.2.20. These SWAT recharge estimates indicate significantly higher recharge rates in the Carrizo-Wilcox outcrop in the southwestern part (e.g., Freestone County) compared to the outcrop area farther north (e.g., Van Zandt County). SWAT recharge estimates are largely controlled by soil type and vegetation cover that are based on the STATSGO soil maps. Any error in these input data can result in errors in the recharge estimates.

9.2.2 Stream Leakance

Figures 9.2.21 and 9.2.22 show the simulated stream leakance indicating the gains and losses along the major streams in the area at two different times, representing relatively dry and wet conditions. The stream leakance during May 1989 indicates predominantly losing stream segments during relatively wet conditions when stream stages are highest (Figure 9.2.21), whereas the plotted stream leakance during November 1989 indicates gaining stream segments (Figure 9.2.22). The different flow conditions are indicated in the individual streamflow gauges. Figure 9.2.23 shows simulated and measured stream flows for specific gauging stations on the Trinity, Neches, and Sabine rivers for the transient simulation period (1980 – 2000). Simulated stream flows follow the seasonal pattern and are typically below the measured flow rates. This is expected because the model does not simulate surface runoff.

We also compared the stream leakances to the stream gain/loss study by Slade et al. (2002). They documented stream flow measurements along a couple of segments of the Sabine River and at one of its tributaries (Lake Fork Creek) over the transient simulation period. Figure 9.2.24 shows a cross-plot of the measured gain/loss and those derived from the model. The data comparison shows a large scatter, though most of the data fall within the same quadrant. Relatively large variability in measured streamflows are indicated by the measured data at the different gaging stations along the river that were measured on the same day. In comparison, simulated stream flows show more gradual changes along the river.

Slade et al. (2002) note that the potential error in stream flow measurements is typically about 5 to 8 percent. Since this error is possible at both ends of a gain/loss subreach, the potential error in gain/loss can equal a significant fraction of the total flow in the subreach. Comparing the available gain/loss values to mean stream flows from the EPA River Reach data set shows that almost all of the gain/loss values are less than 5 percent of the mean stream flow. This suggests that the gain/loss values are uncertain and can be used only qualitatively.

9.2.3 Water Budget

Table 9.2.3 shows the water budget for the transient model totaled for years 1980, 1988 (drought year for the calibration period), 1989 and 1999. The overall mass balance error for the transient simulation was 0.09 percent, well under the GAM requirement of one percent. In the model, the greatest influx of water consistently occurs from recharge, and the greatest outflow of

water is through streams and groundwater ET. Overall outflow from pumpage increased from 117,000 ac-ft/yr in 1980 to 148,000 ac-ft/yr in 1999. Groundwater ET rates show relatively large changes from hot summers (e.g., 1980) to more temperate summers (e.g., 1990). The seasonal variations in totals for stream recharge/discharge, diffuse recharge, groundwater ET, and pumpage over the transient simulation period (1980 – 1999) are summarized in Figure 9.2.25. Peak pumpage during the summer months continuously increased over the years, and total ET exceeds recharge during the summer months.

Table 9.2.1 Calibration statistics for the transient model.

Calibration period (1980-1989)					
	Layer 1	Layer 3	Layer 4	Layer 5	Layer 6
ME	-22.49	4.55	0.53	1.24	-10.03
MAE	31.05	26.10	18.86	23.43	20.28
RMS	40.87	35.14	26.57	31.74	24.70
Range	433	743	491	523	310
RMS/Range	0.094	0.047	0.054	0.061	0.080
Verification period (1990-1999)					
	Layer 1	Layer 3	Layer 4	Layer 5	Layer 6
ME	-20.48	-4.64	-9.67	-5.57	-18.93
MAE	31.40	31.43	23.74	28.71	26.67
RMS	41.08	42.10	34.37	38.44	31.01
Range	459	821	660	523	300
RMS/Range	0.090	0.051	0.052	0.073	0.103

ME = mean error

MAE = mean absolute error

RMS = root mean square error

Table 9.2.2 Calibration statistics for the hydrographs shown in Figures 9.2.16a – 9.2.19.

Well	Layer	Count	ME (ft)	MAE (ft)	RMS (ft)	Figure Number
1658904	3	20	5.57	6.61	8.84	9.2.16a
1663402	3	21	-6.16	8.60	9.80	9.2.16a
3412803	3	19	16.27	16.27	16.45	9.2.16a
3518401	3	18	-23.47	23.47	24.60	9.2.16a
3453604	3	14	0.39	26.45	34.02	9.2.16b
3457301	3	20	21.94	21.94	22.26	9.2.16b
3463503	3	14	-1.38	4.38	5.34	9.2.16b
3464302	3	19	11.49	11.49	11.85	9.2.16b
3550501	3	18	12.10	12.10	12.17	9.2.16b
3719301	3	19	3.47	3.90	4.78	9.2.16c
3727506	3	20	54.17	58.32	61.92	9.2.16c
3735703	3	17	-87.01	87.01	107.99	9.2.16c
3736501	3	14	39.39	39.39	74.66	9.2.16c
3940601	3	19	-32.55	32.55	32.62	9.2.16c
1663902	4	9	27.35	27.35	27.38	9.2.17a
3421302	4	17	10.80	10.80	13.67	9.2.17a
3442108	4	21	4.38	4.38	4.94	9.2.17a
3501803	4	18	-35.02	35.07	40.24	9.2.17a
3446511	4	17	11.71	21.62	27.56	9.2.17b
3448802	4	15	-25.09	25.09	25.81	9.2.17b
3522401	4	17	-8.35	8.35	9.85	9.2.17b
3526706	4	18	-6.50	6.68	9.49	9.2.17b
3549801	4	17	2.34	4.13	4.61	9.2.17b
3806603	4	16	1.23	40.66	54.09	9.2.17b
3617502	4	20	-7.20	7.20	7.31	9.2.17c
3625504	4	17	1.60	2.22	2.59	9.2.17c
3704301	4	17	-6.48	6.48	7.01	9.2.17c
3710302	4	11	-1.07	1.48	1.94	9.2.17c
3714501	4	20	2.20	2.20	2.41	9.2.17c
3720902	4	13	19.68	20.08	24.34	9.2.17c
3932205	4	19	-8.34	10.81	12.60	9.2.17d
3938902	4	23	-14.62	15.04	15.24	9.2.17d
3940906	4	20	-13.60	13.60	14.30	9.2.17d
1650207	5	18	3.72	5.05	6.00	9.2.18a
3403101	5	12	9.28	9.28	9.43	9.2.18a
3413401	5	18	-4.29	5.62	6.46	9.2.18a
3507801	5	18	-46.80	46.80	47.41	9.2.18a
3509403	5	19	-48.70	48.70	51.32	9.2.18a
3531602	5	19	-4.59	4.59	5.56	9.2.18a
3448803	5	13	-33.32	33.32	34.13	9.2.18b
3464403	5	10	4.56	9.13	11.61	9.2.18b
3544103	5	11	0.52	4.99	5.78	9.2.18b
3550801	5	22	-91.32	91.32	94.33	9.2.18b
3553902	5	17	-4.15	4.66	6.32	9.2.18b
3706401	5	20	-11.03	11.09	13.38	9.2.18b

Table 9.2.2 (continued)

Well	Layer	Count	ME (ft)	MAE (ft)	RMS (ft)	Figure Number
3426605	5	11	-30.21	30.21	33.47	9.2.18c
3434101	5	18	44.69	44.69	45.27	9.2.18c
3449810	5	15	45.66	45.66	45.68	9.2.18c
3450306	5	18	-60.04	60.04	60.81	9.2.18c
3410202	6	6	3.18	3.18	3.21	9.2.19
3433302	6	18	7.28	10.22	12.09	9.2.19
3442403	6	17	-18.47	18.87	21.35	9.2.19
3708801	5	15	-10.89	10.89	10.92	9.2.19
3923101	6	15	-37.79	37.79	41.35	9.2.19
3929801	6	23	-9.05	9.05	11.04	9.2.19

Table 9.2.3 Water budget for transient model. All rates reported in acre-ft/yr.

Year	Layer	GHBs	Reservoirs	Wells	ET	Top	Bottom	Recharge	Streams	Storage
1980	1	29,653	-42,758	-6,959	-452,559	0	-30,614	847,222	-410,536	66,529
	2	0	-1,485	-526	-208,546	30,614	-39,195	205,313	-422,217	436,044
	3	0	-2,066	-42,808	-120,840	39,195	-35,608	135,122	-78,963	105,965
	4	0	128,011	-34,789	-237,959	35,608	-29,049	395,803	-248,242	-9,382
	5	0	32,984	-26,829	-178,205	29,049	-14,449	508,713	-181,172	-170,106
	6	0	3,928	-5,257	-36,912	14,449	0	41,101	-36,687	19,378
	Sum	29,653	118,613	-117,169	-1,235,020	148,915	-148,915	2,133,274	-1,377,818	448,429
1988*	1	24,516	-63,754	-8,891	-492,581	0	-30,230	860,053	-477,642	188,513
	2	0	-474	-653	-196,440	30,230	-39,849	188,680	-135,772	154,280
	3	0	-1,550	-46,075	-118,868	39,849	-33,494	91,755	-46,330	114,709
	4	0	-58,974	-42,851	-227,104	33,494	-24,196	309,932	-217,521	227,215
	5	0	-107,645	-37,556	-157,848	24,196	-11,673	453,461	-343,416	180,466
	6	0	2,289	-6,616	-25,541	11,673	0	25,473	-17,468	10,189
	Sum	24,516	-230,109	-142,642	-1,218,383	139,441	-139,441	1,929,354	-1,238,149	875,373
1989	1	24,259	-20,561	-9,386	-176,442	0	-30,289	1,014,412	-316,591	-485,426
	2	0	-1,295	-667	-61,568	30,289	-40,638	267,297	-92,189	-101,228
	3	0	-2,715	-49,773	-43,235	40,638	-34,551	148,618	-36,114	-22,874
	4	0	-30,151	-45,465	-62,292	34,551	-23,327	480,413	-85,660	-268,077
	5	0	-47,297	-31,641	-71,423	23,327	-11,164	587,913	-30,078	-419,660
	6	0	128,949	-6,134	-10,415	11,164	0	48,274	-4,242	-167,597
	Sum	24,259	26,931	-143,066	-425,375	139,969	-139,969	2,546,927	-564,874	-1,464,862
1999	1	21,848	-33,720	-11,772	-385,815	0	-30,673	694,847	-556,026	301,132
	2	0	-515	-775	-121,227	30,673	-42,263	171,875	-117,977	80,206
	3	0	-4,021	-51,789	-55,999	42,263	-30,706	89,235	-45,898	56,908
	4	0	-87,738	-37,766	-108,712	30,706	-22,093	331,665	-192,157	86,089
	5	0	-92,453	-38,875	-104,099	22,093	-9,300	438,221	-317,435	101,827
	6	0	-14,165	-6,847	-17,520	9,300	0	33,520	-24,286	19,998
	Sum	21,848	-232,612	-147,825	-793,372	135,035	-135,035	1,759,363	-1,253,780	646,160

*Drought year for calibration period

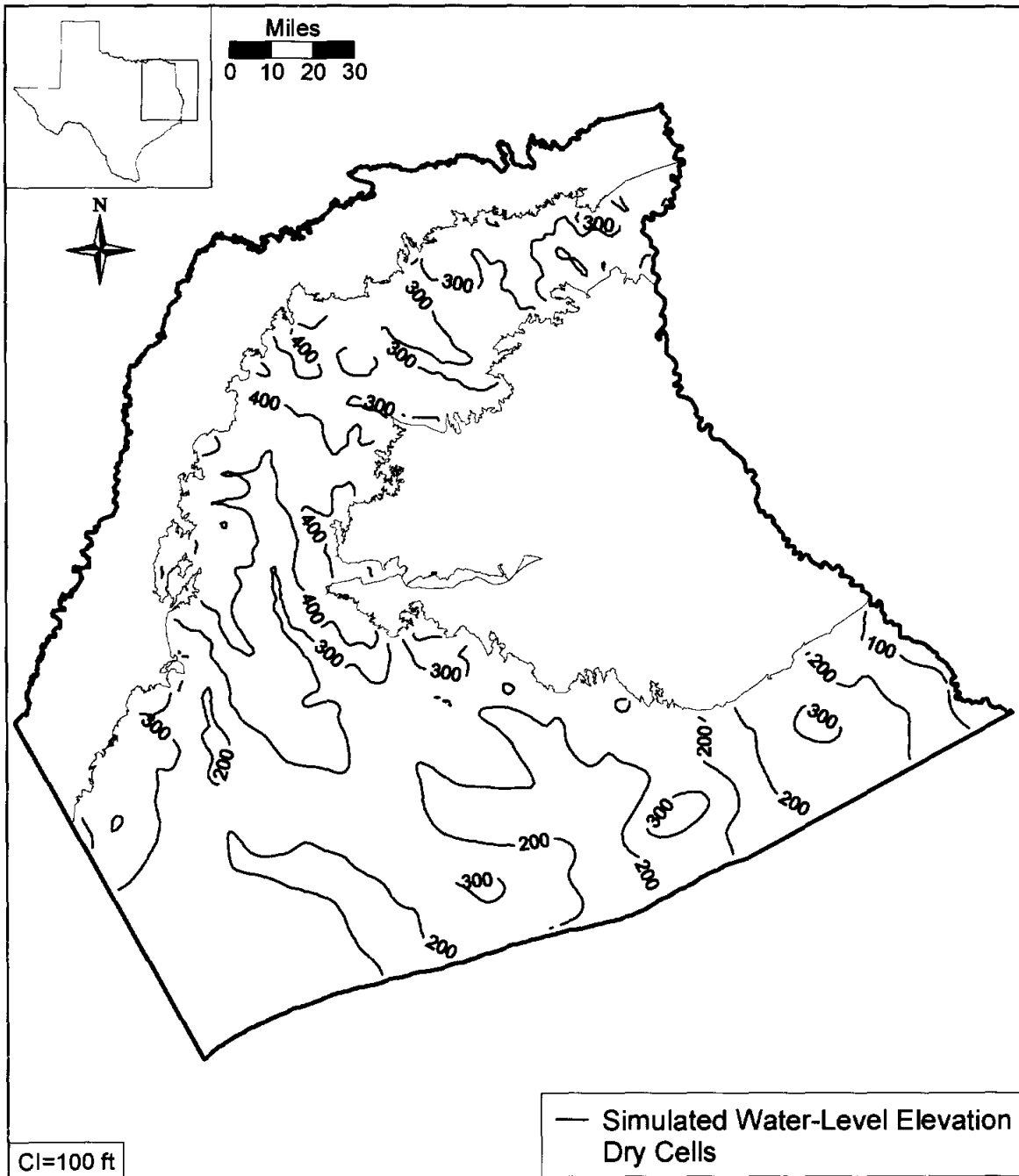


Figure 9.2.1 Simulated hydraulic head distribution for Layer 1 (Queen City) at the end of the transient model calibration (December 1989).

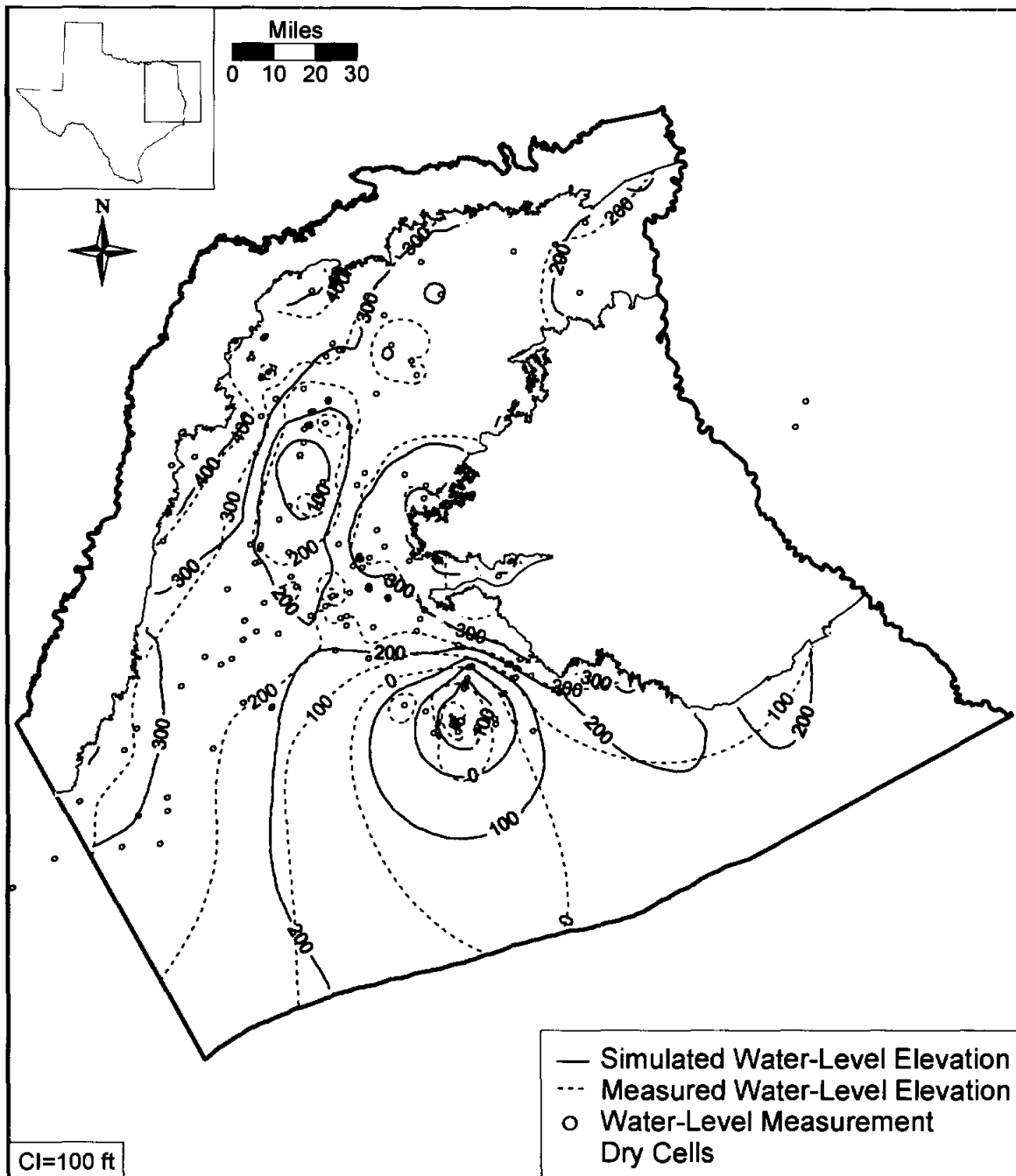


Figure 9.2.2 Simulated and measured hydraulic head distribution for Layer 3 (Carrizo) at the end of the transient model calibration (December 1989).

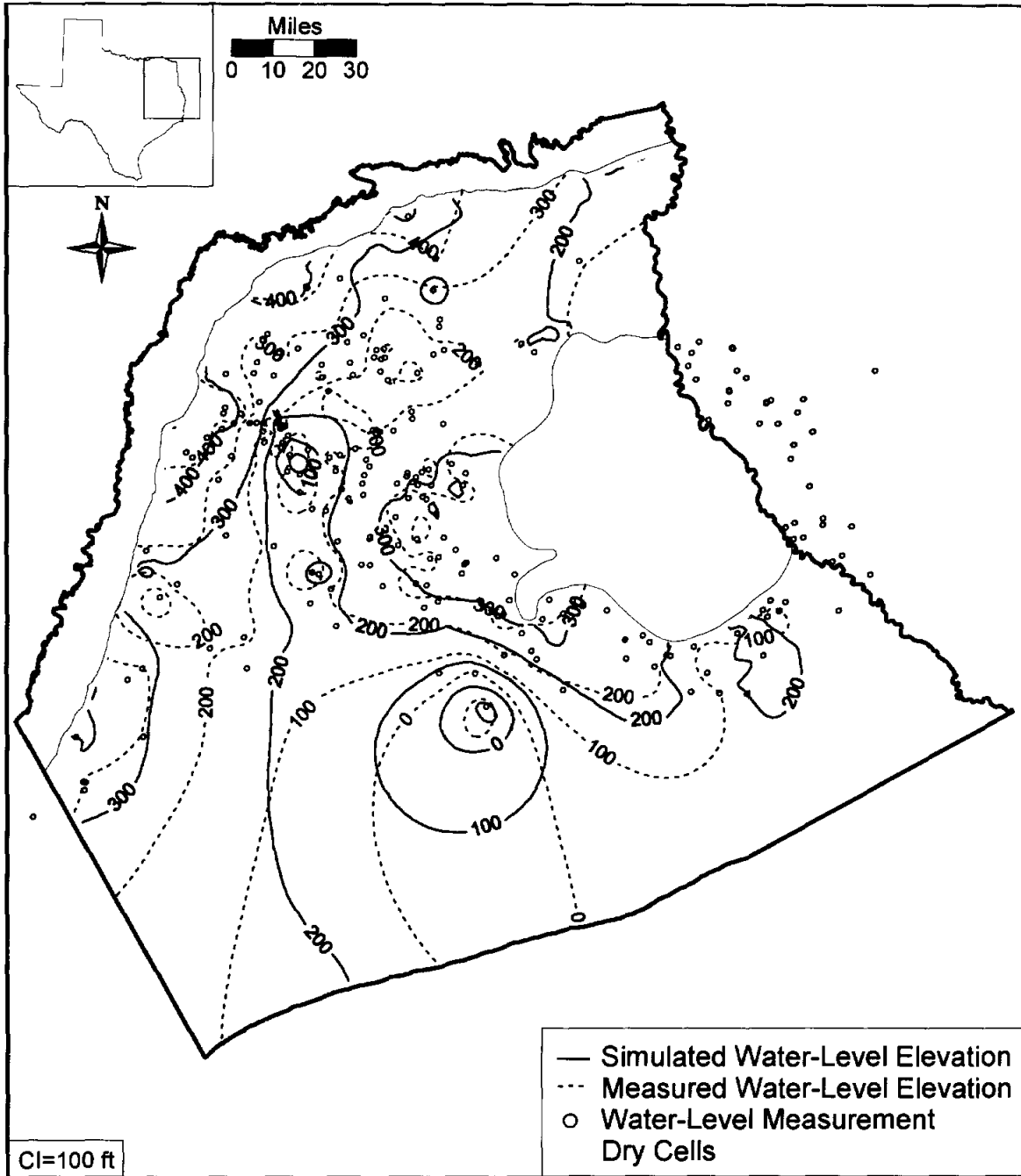


Figure 9.2.3 Simulated and measured hydraulic head distribution for Layer 4 (upper Wilcox) at the end of the transient model calibration (December 1989).

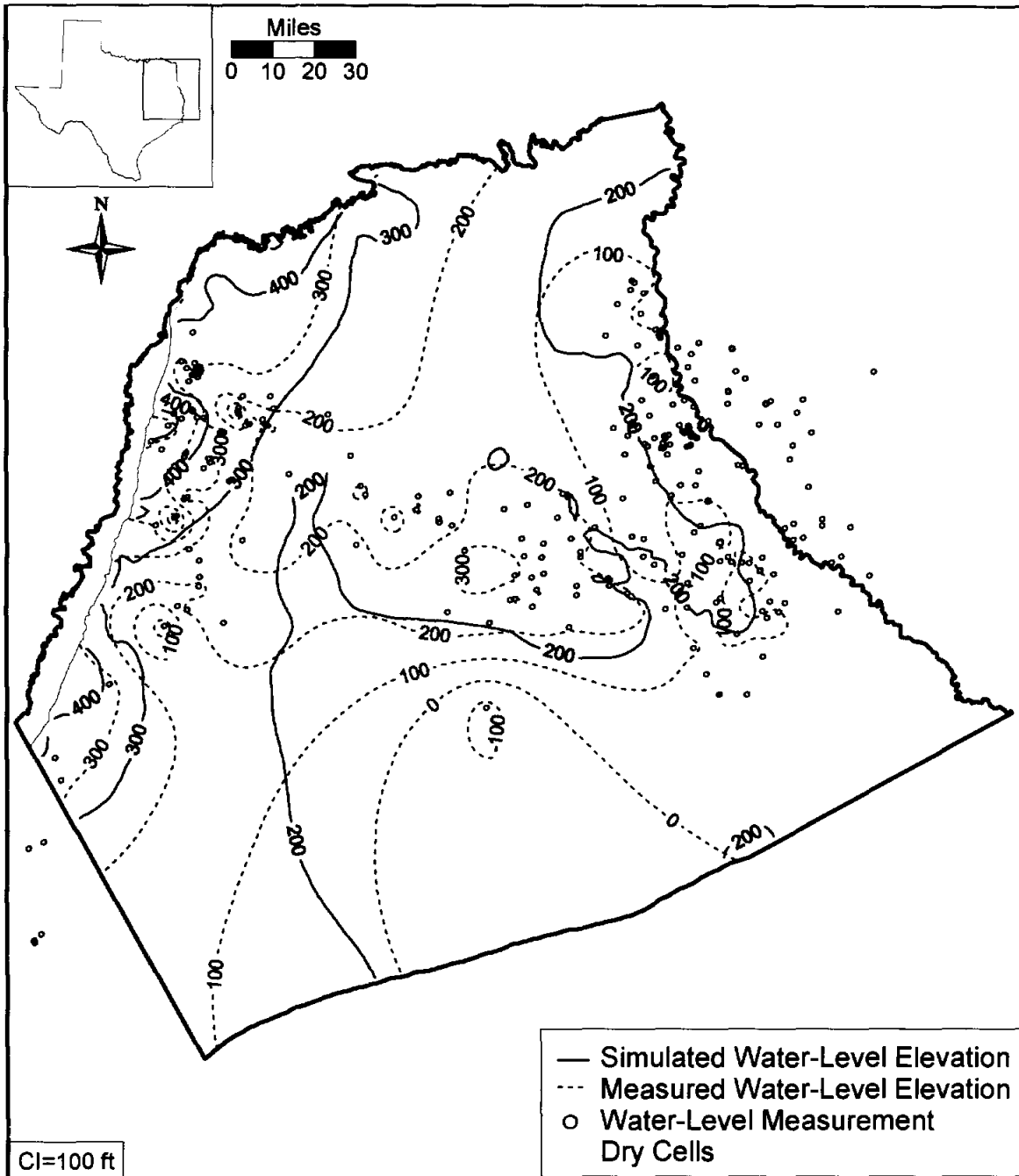


Figure 9.2.4 Simulated and measured hydraulic head distribution for Layer 5 (middle Wilcox) at the end of the transient model calibration (December 1989).

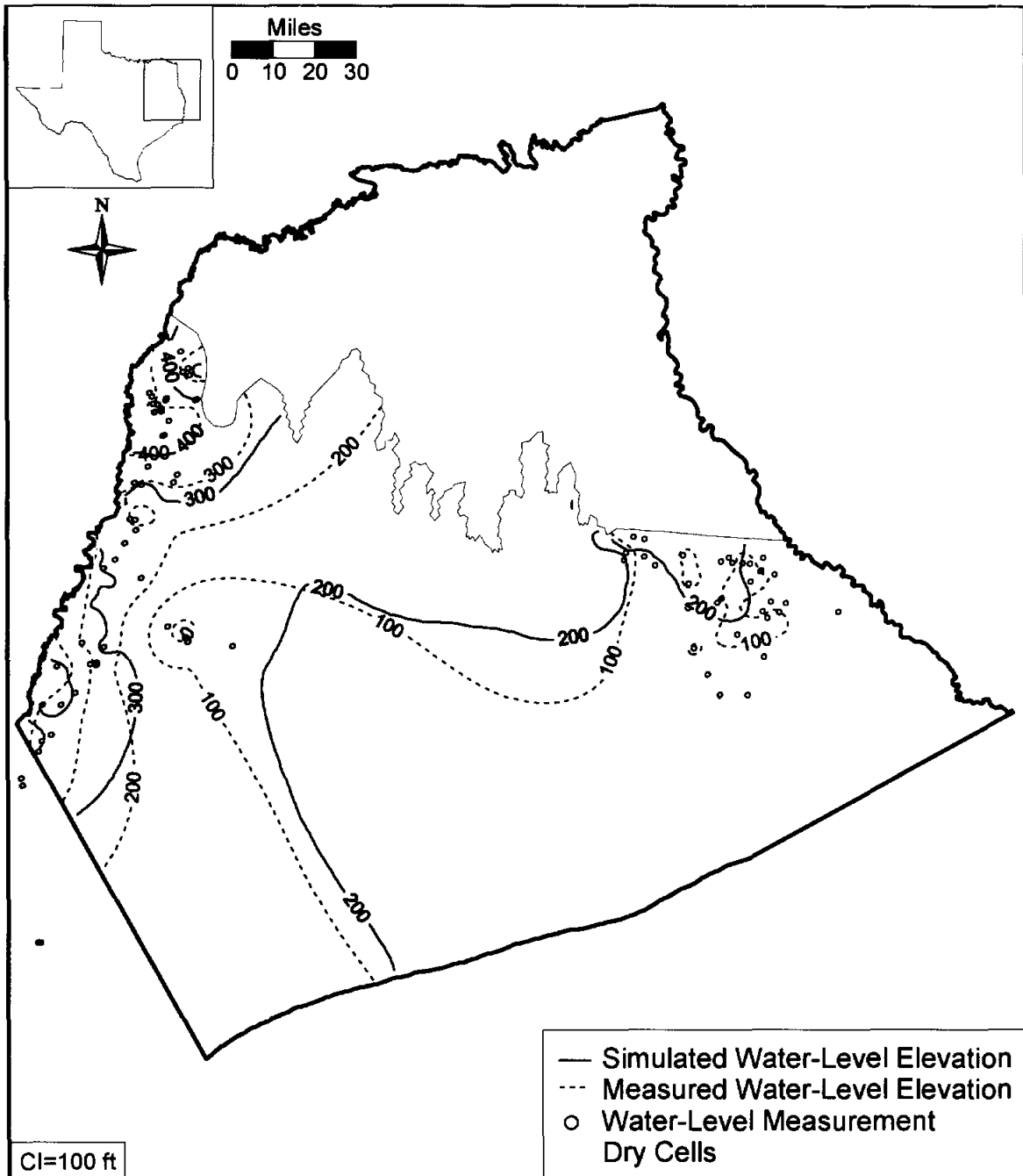
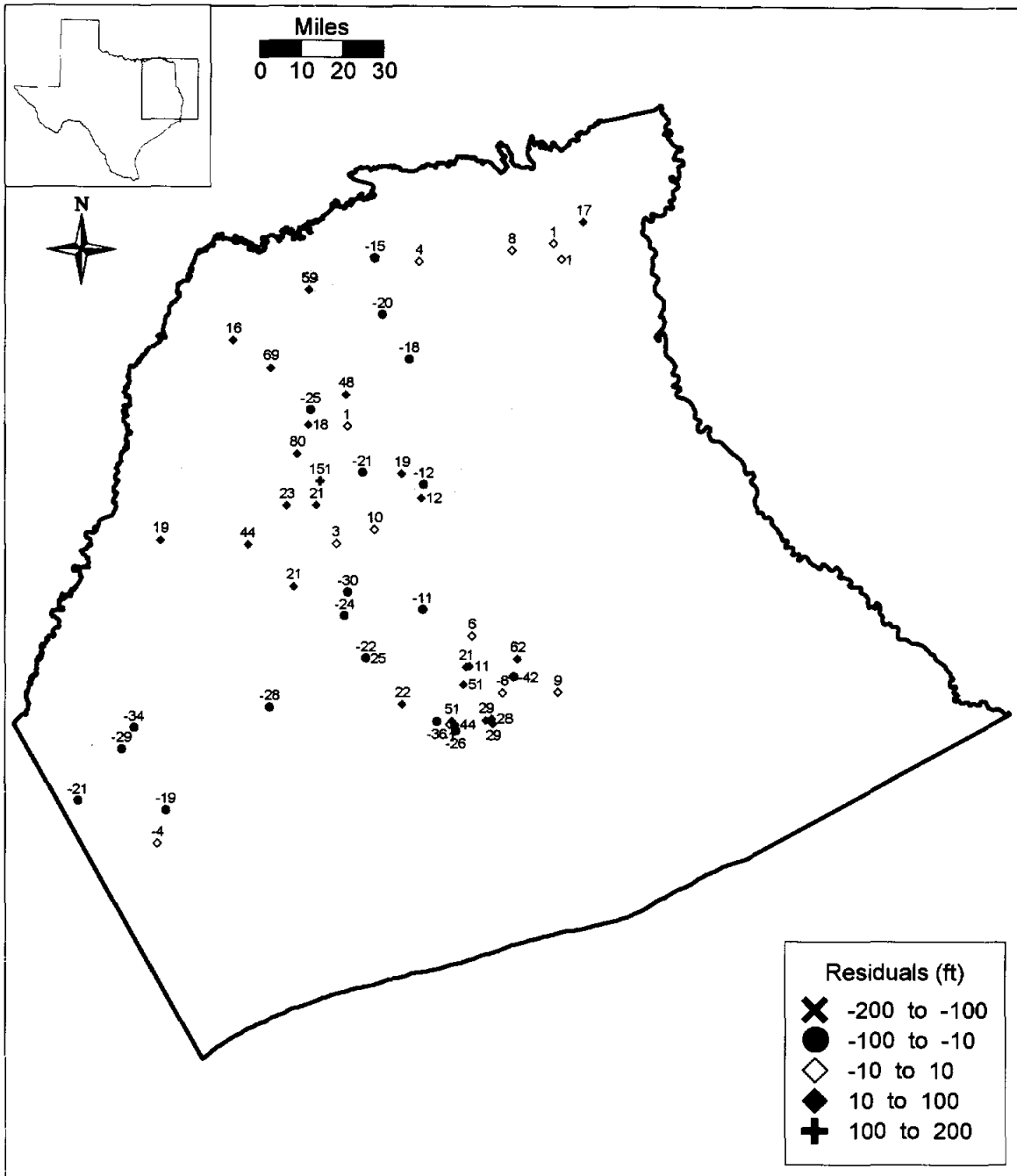


Figure 9.2.5 Simulated and measured hydraulic head distribution for Layer 6 (lower Wilcox) at the end of the transient model calibration (December 1989).



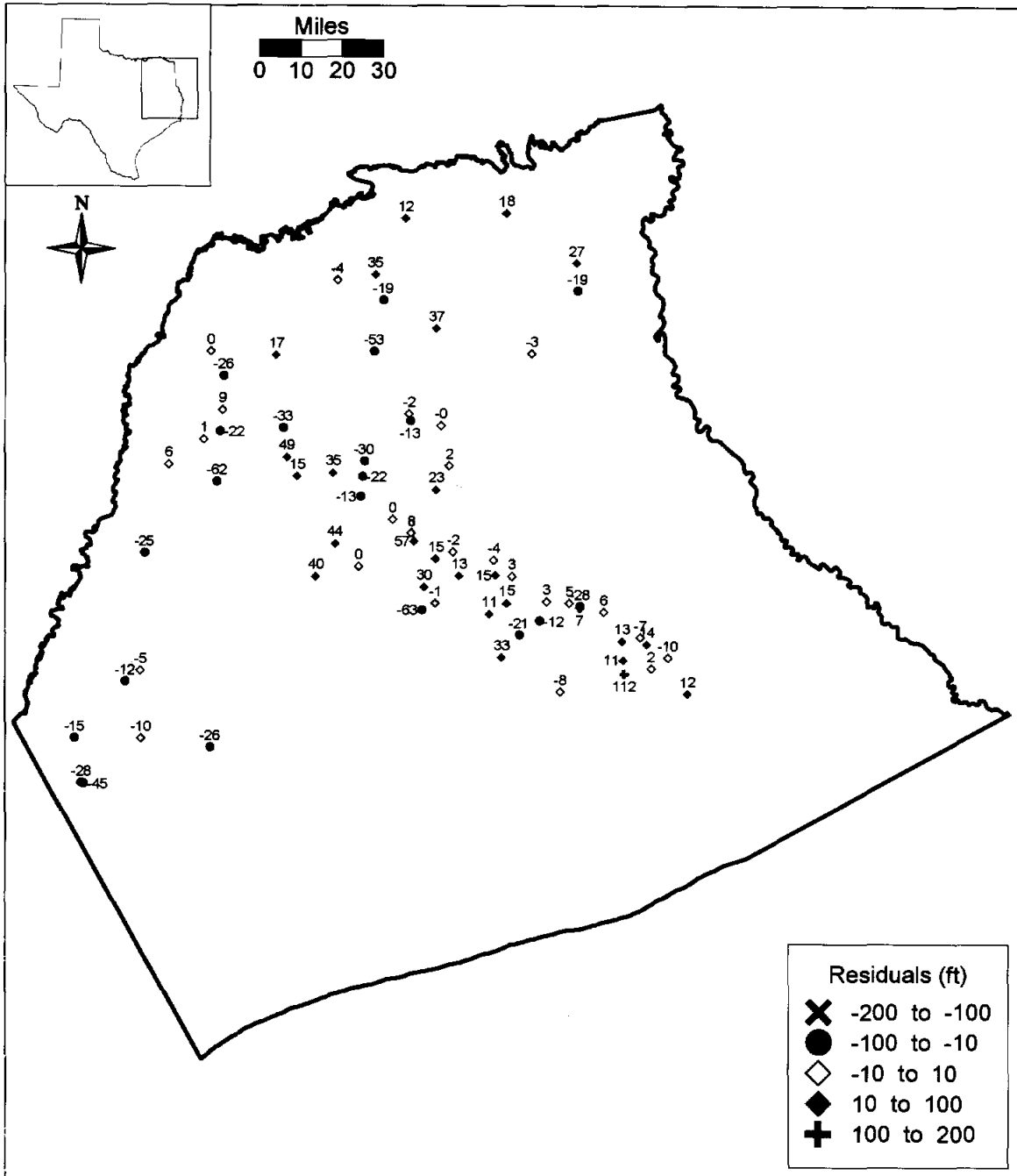


Figure 9.2.7 Residuals at target wells for Layer 4 (upper Wilcox) at the end of the transient model calibration (December 1989).

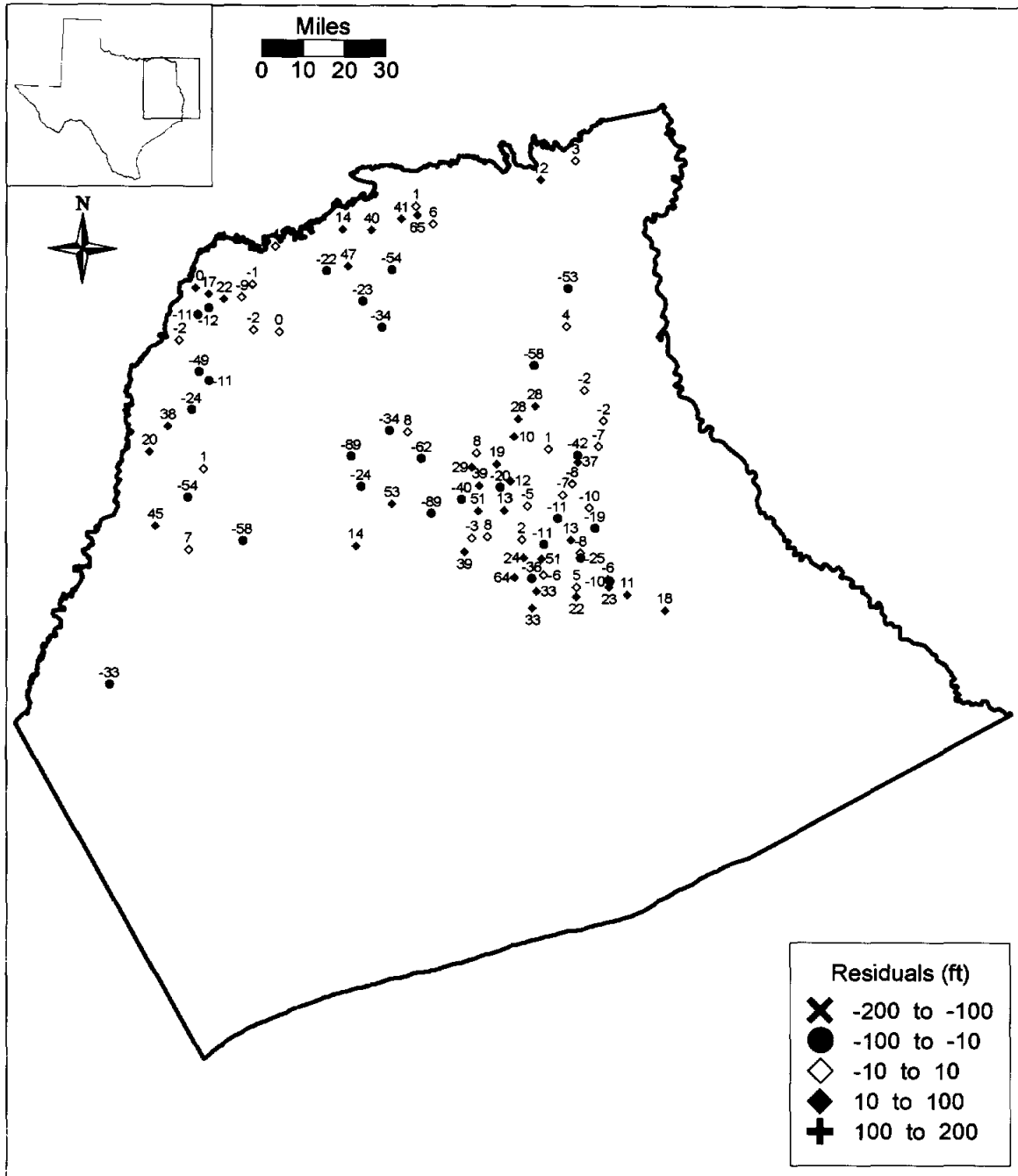


Figure 9.2.8 Residuals at target wells for Layer 5 (middle Wilcox) at the end of the transient model calibration (December 1989).

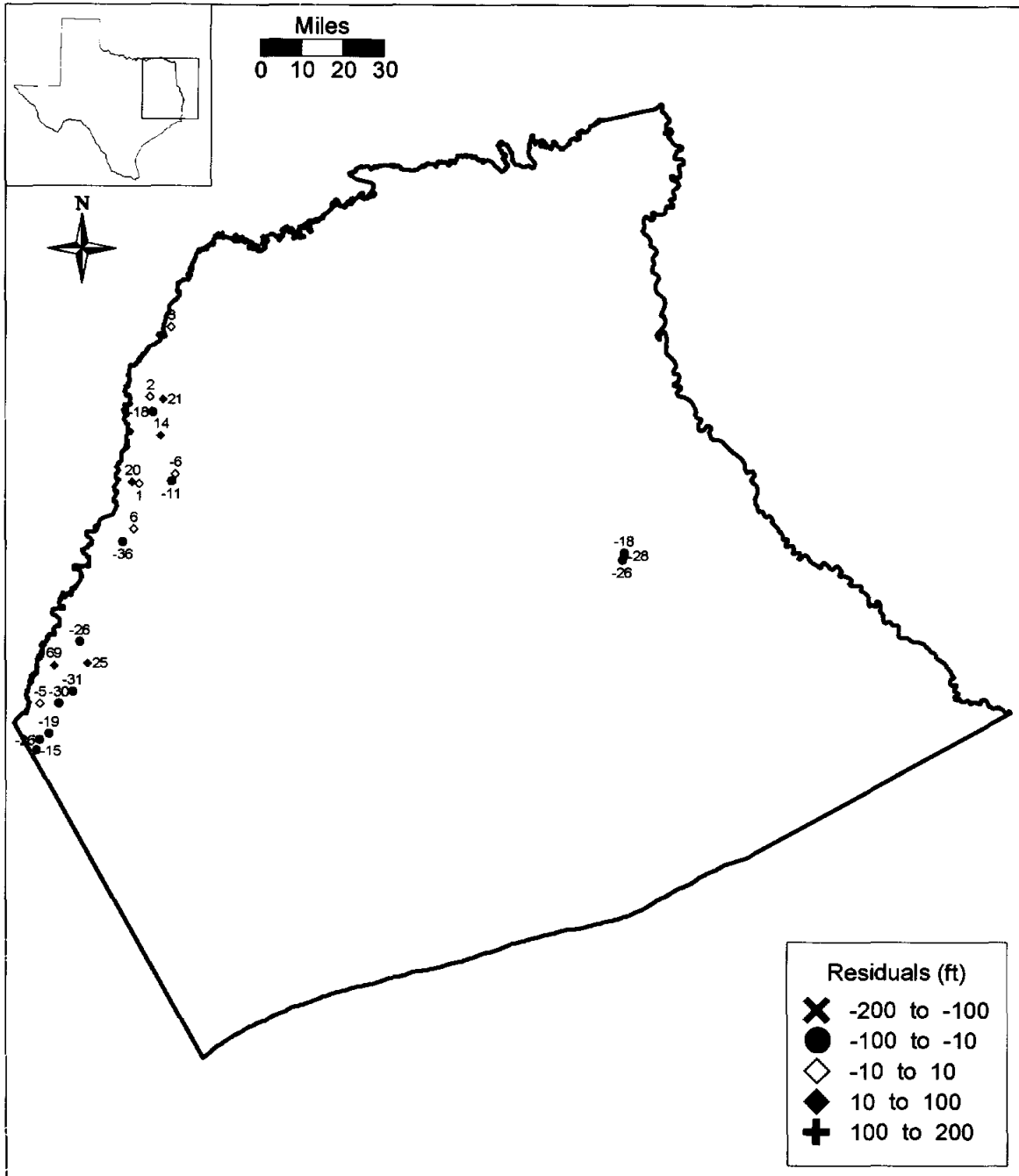


Figure 9.2.9 Residuals at target wells for Layer 6 (lower Wilcox) at the end of the transient model calibration (December 1989).

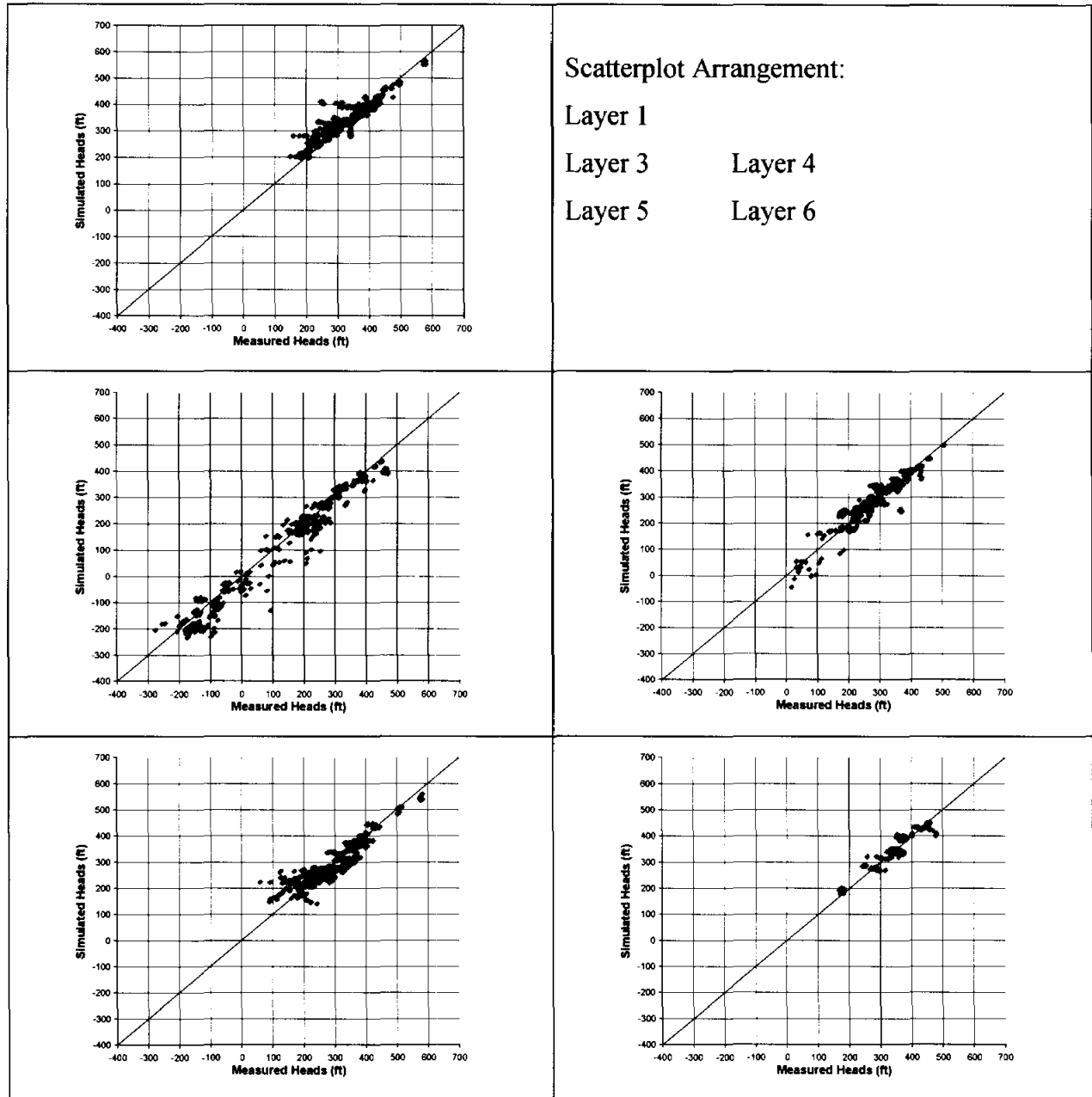


Figure 9.2.10 Scatterplots of simulated and measured hydraulic heads for the different layers at the end of the transient model calibration (December 1989).

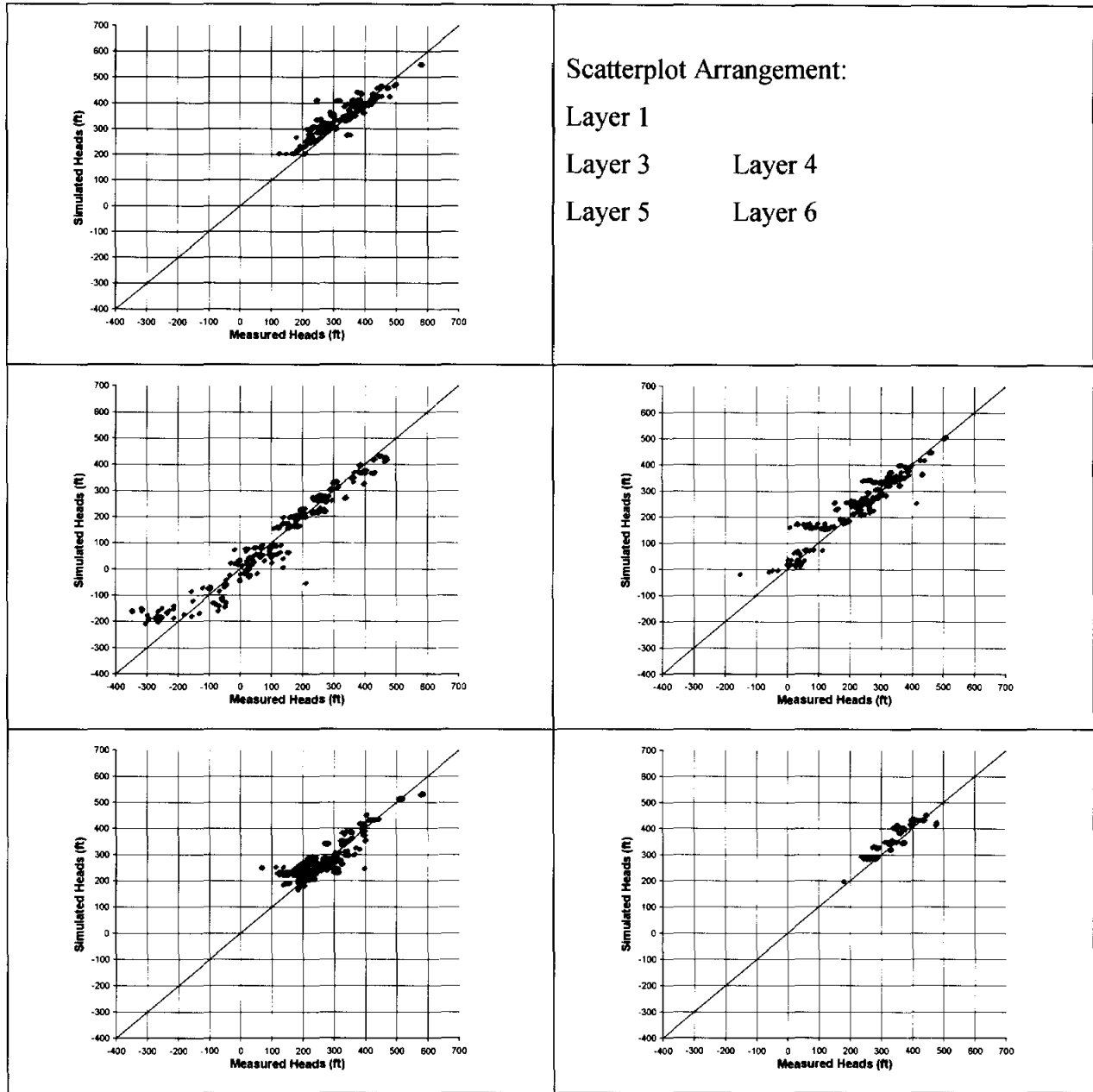


Figure 9.2.11 Scatterplots of simulated and measured hydraulic heads for the different layers at the end of the transient model verification (December 1999).

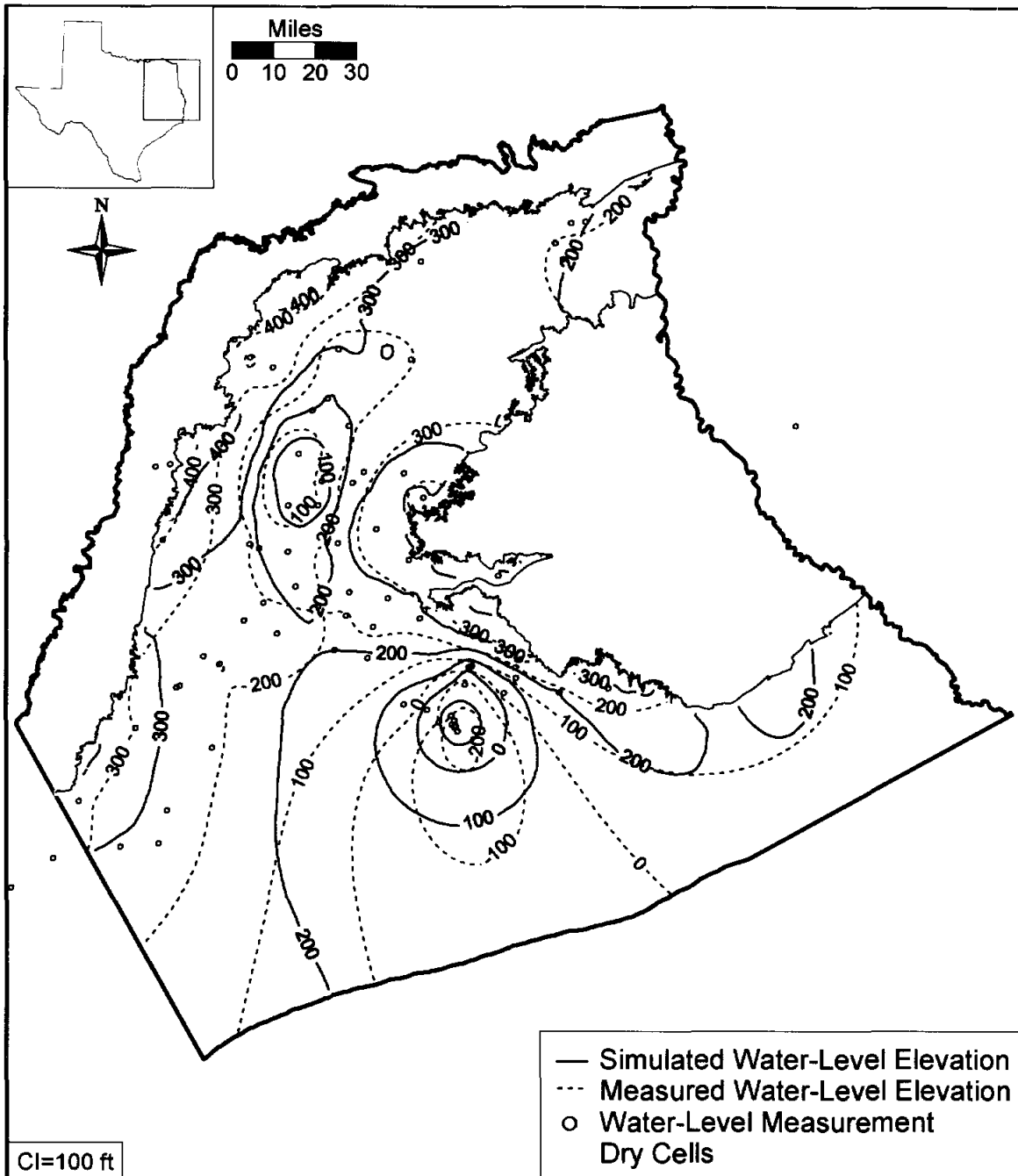


Figure 9.2.12 Simulated and measured hydraulic head distribution for Layer 3 (Carrizo) at the end of the transient model verification (December 1999).

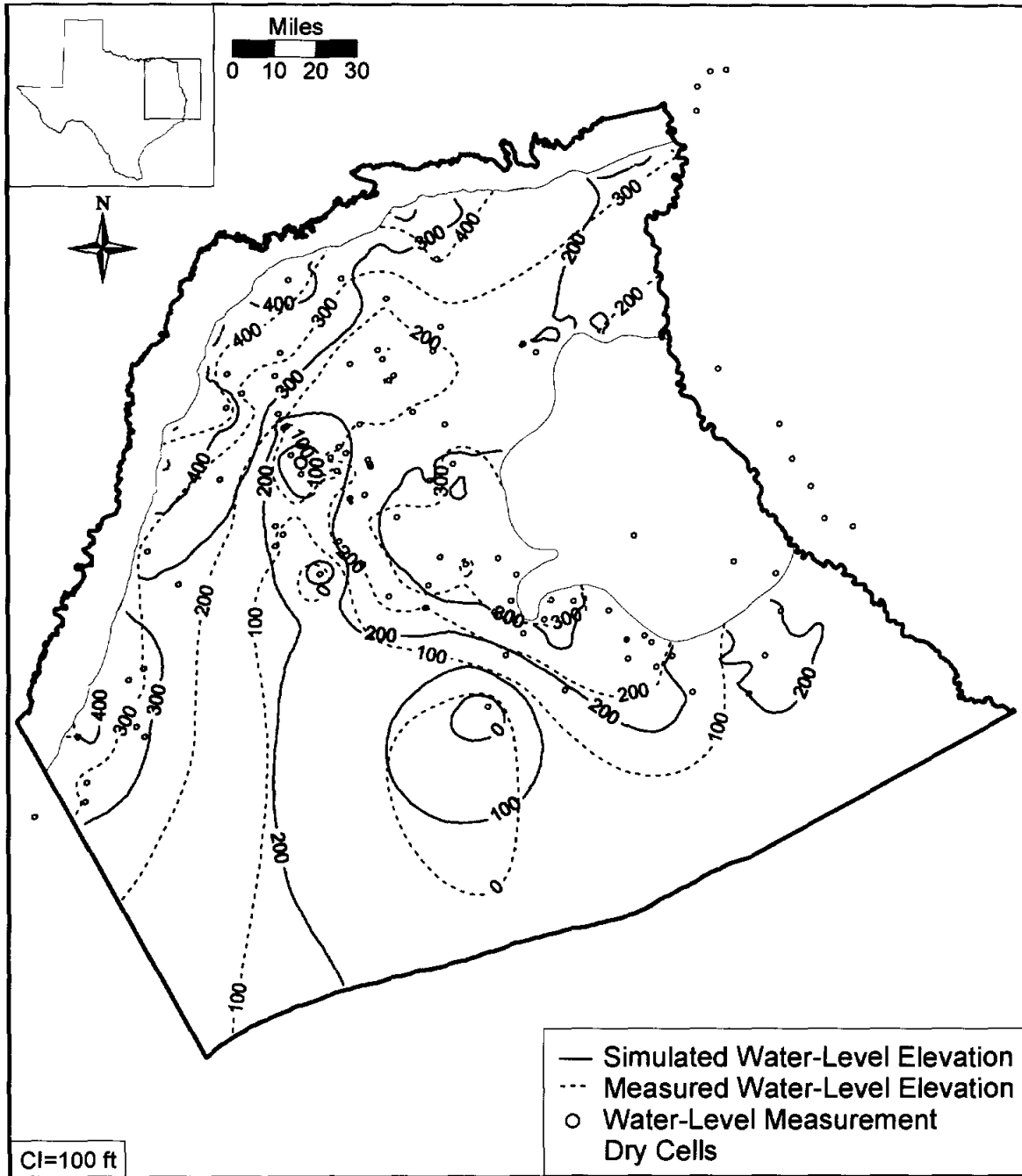


Figure 9.2.13 Simulated and measured hydraulic head distribution for Layer 4 (upper Wilcox) at the end of the transient model verification (December 1999).

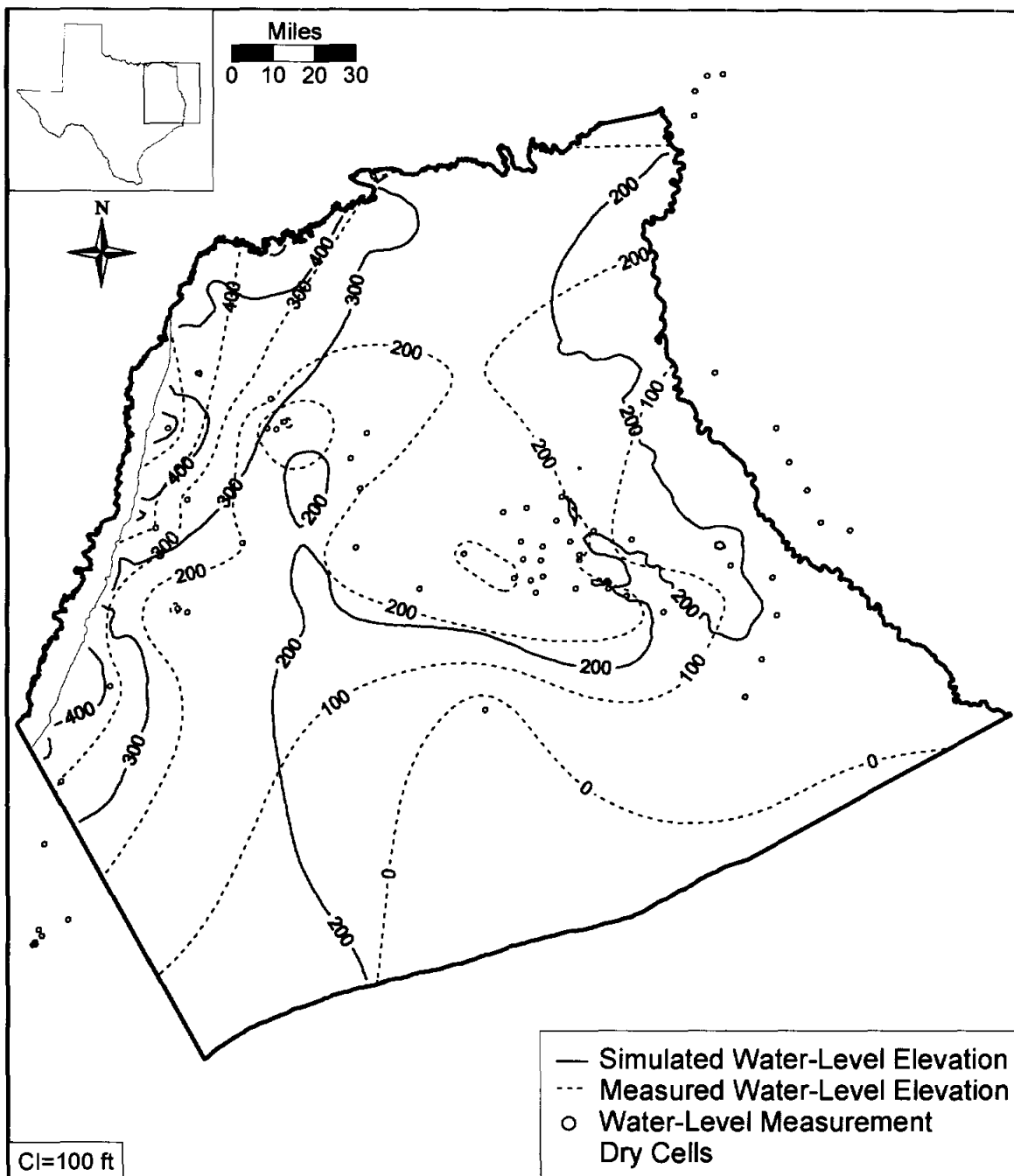


Figure 9.2.14 Simulated and measured hydraulic head distribution for Layer 5 (middle Wilcox) at the end of the transient model verification (December 1999).

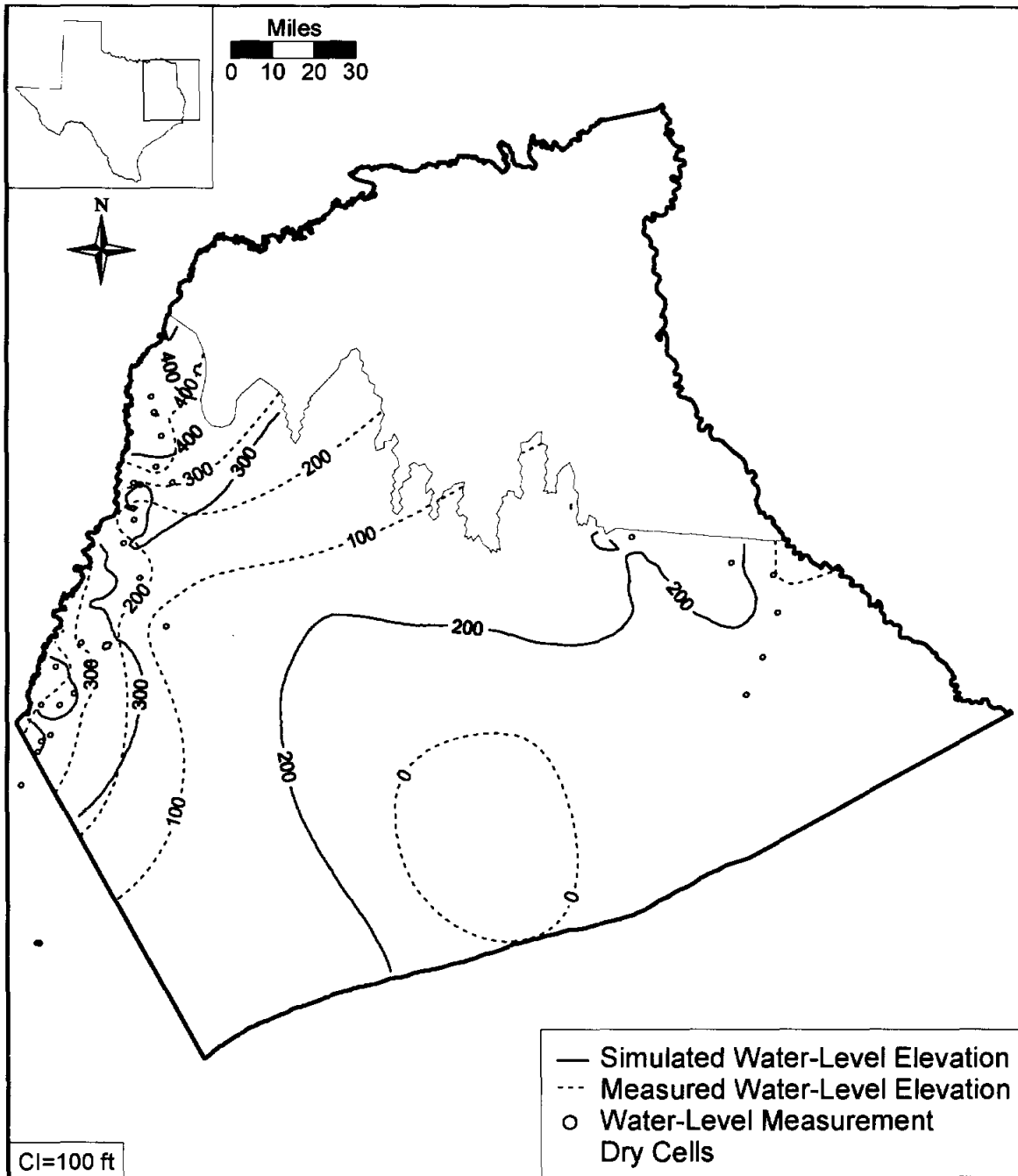


Figure 9.2.15 Simulated and measured hydraulic head distribution for Layer 6 (lower Wilcox) at the end of the transient model verification (December 1999).

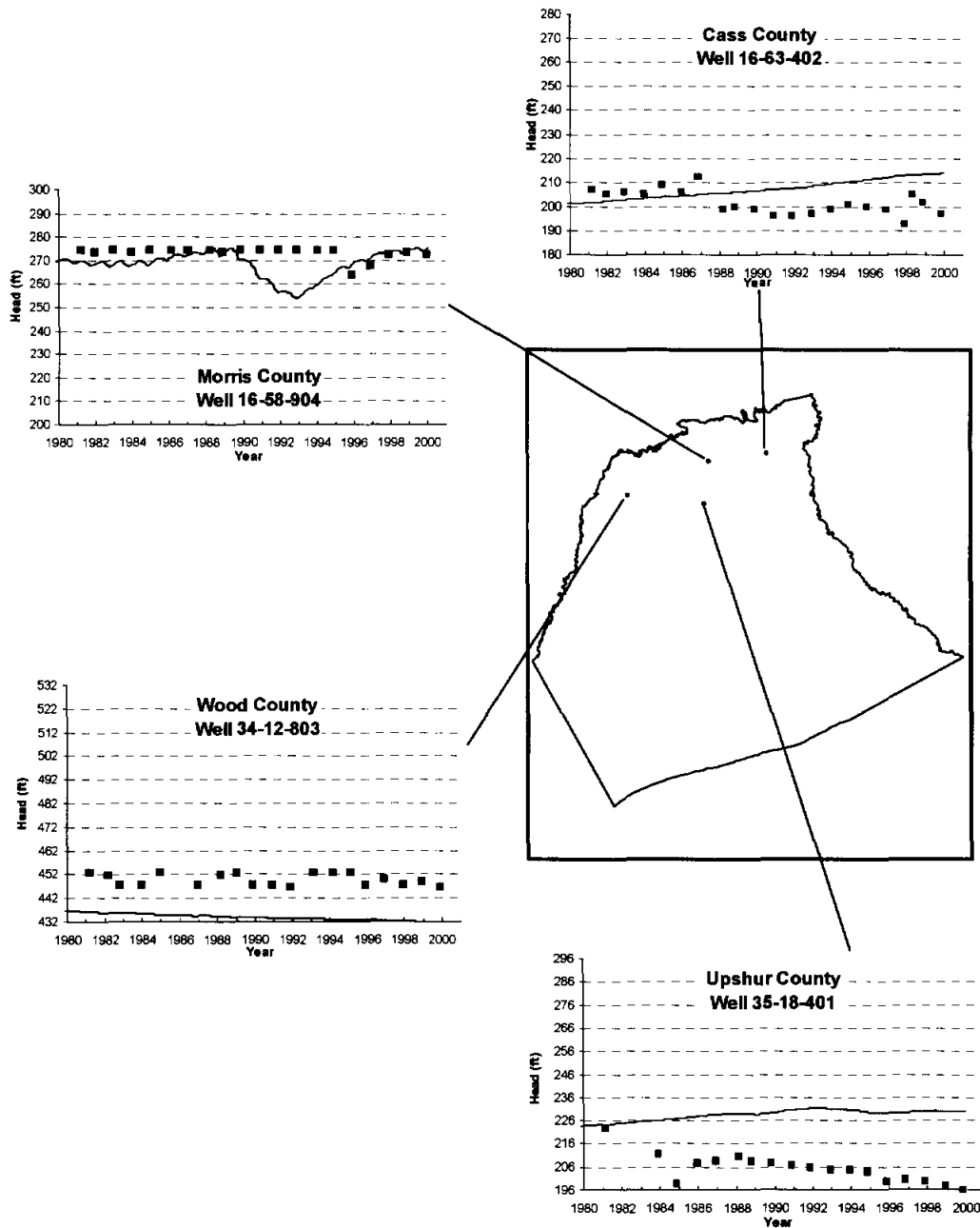


Figure 9.2.16a Selected hydrographs of simulated (lines) and measured (points) hydraulic heads in the northern part for Layer 3 (Carrizo).

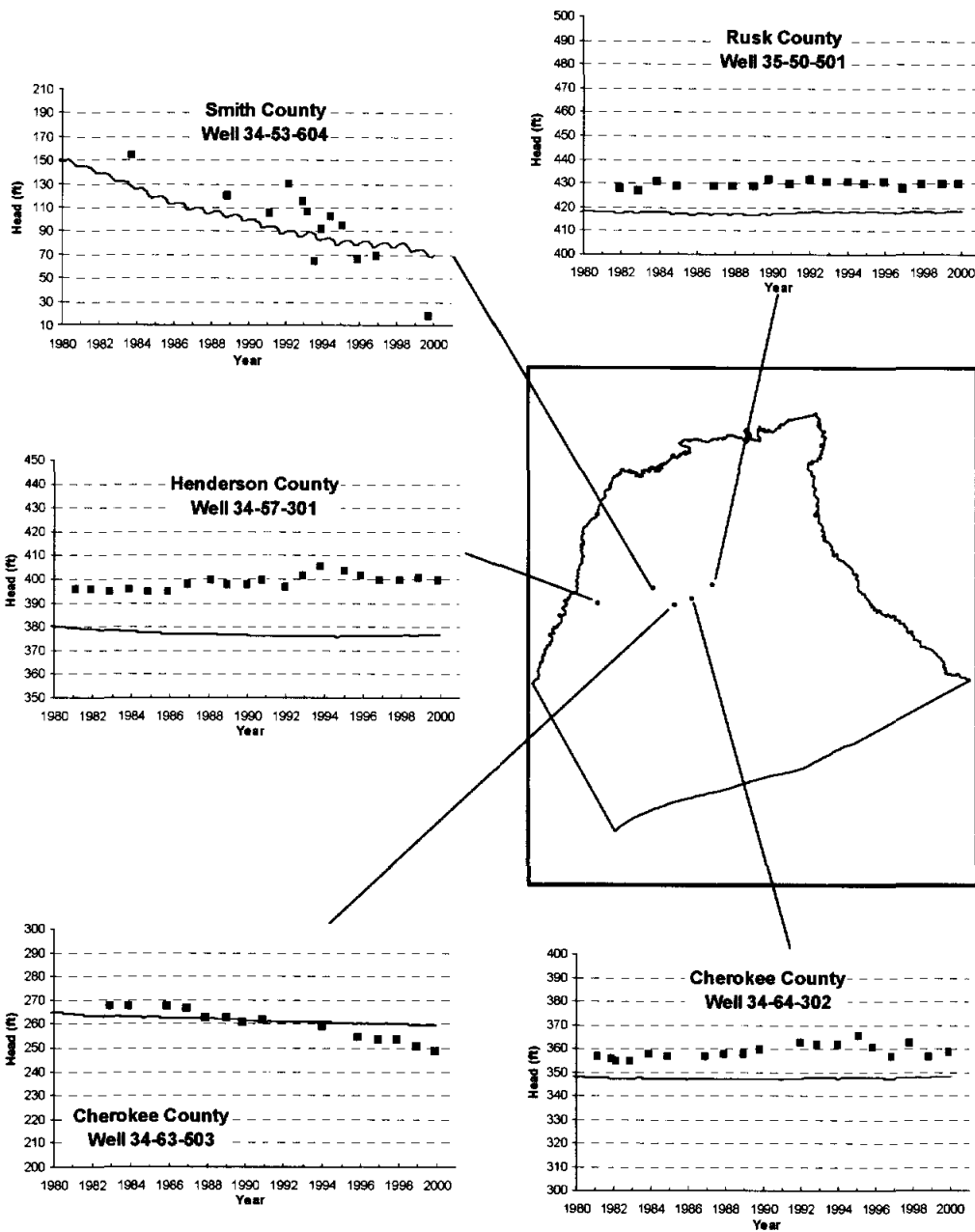


Figure 9.2.16b Selected hydrographs of simulated (lines) and measured (points) hydraulic heads in the central part for Layer 3 (Carrizo).

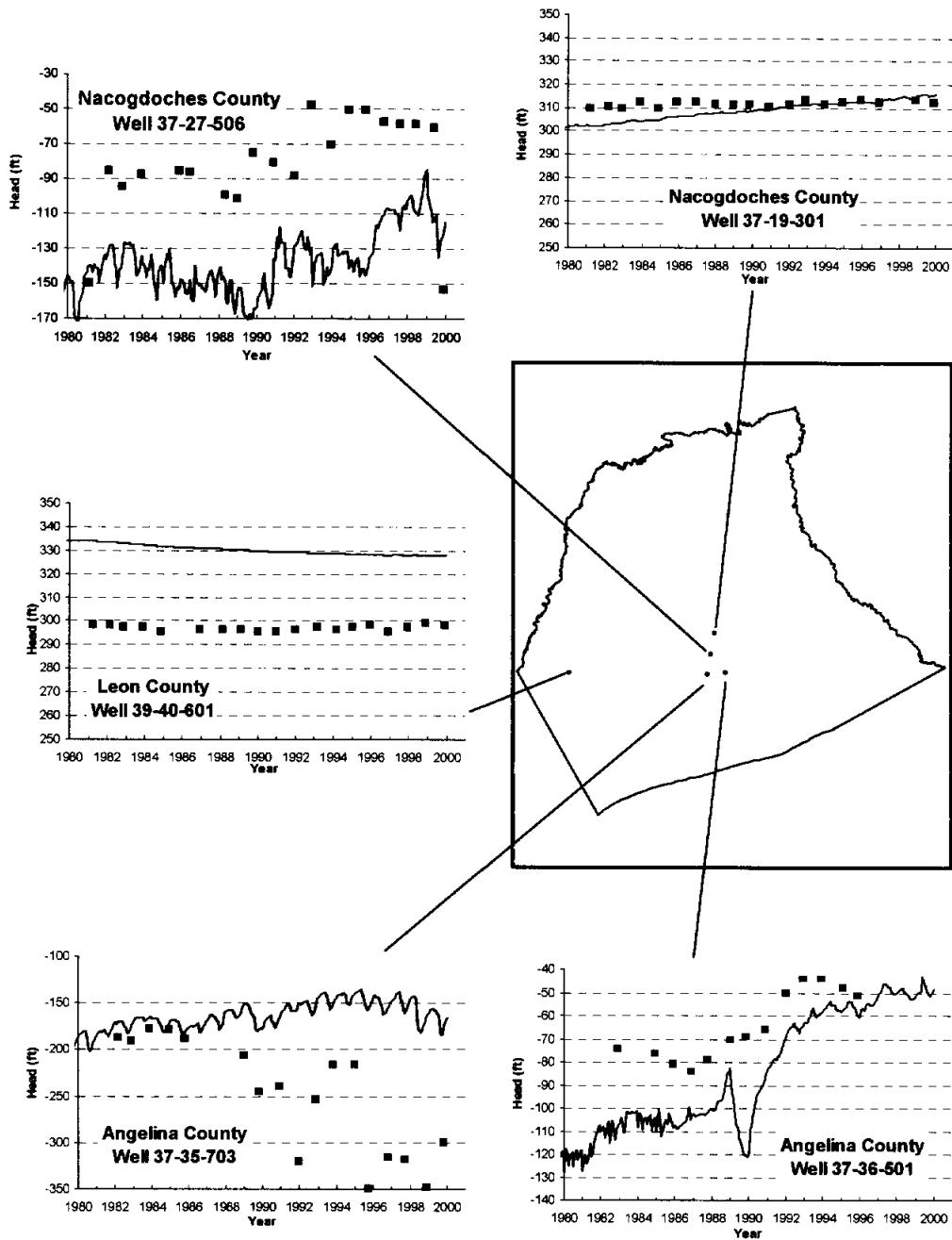


Figure 9.2.16c Selected hydrographs of simulated (lines) and measured (points) hydraulic heads in the southern part for Layer 3 (Carrizo).

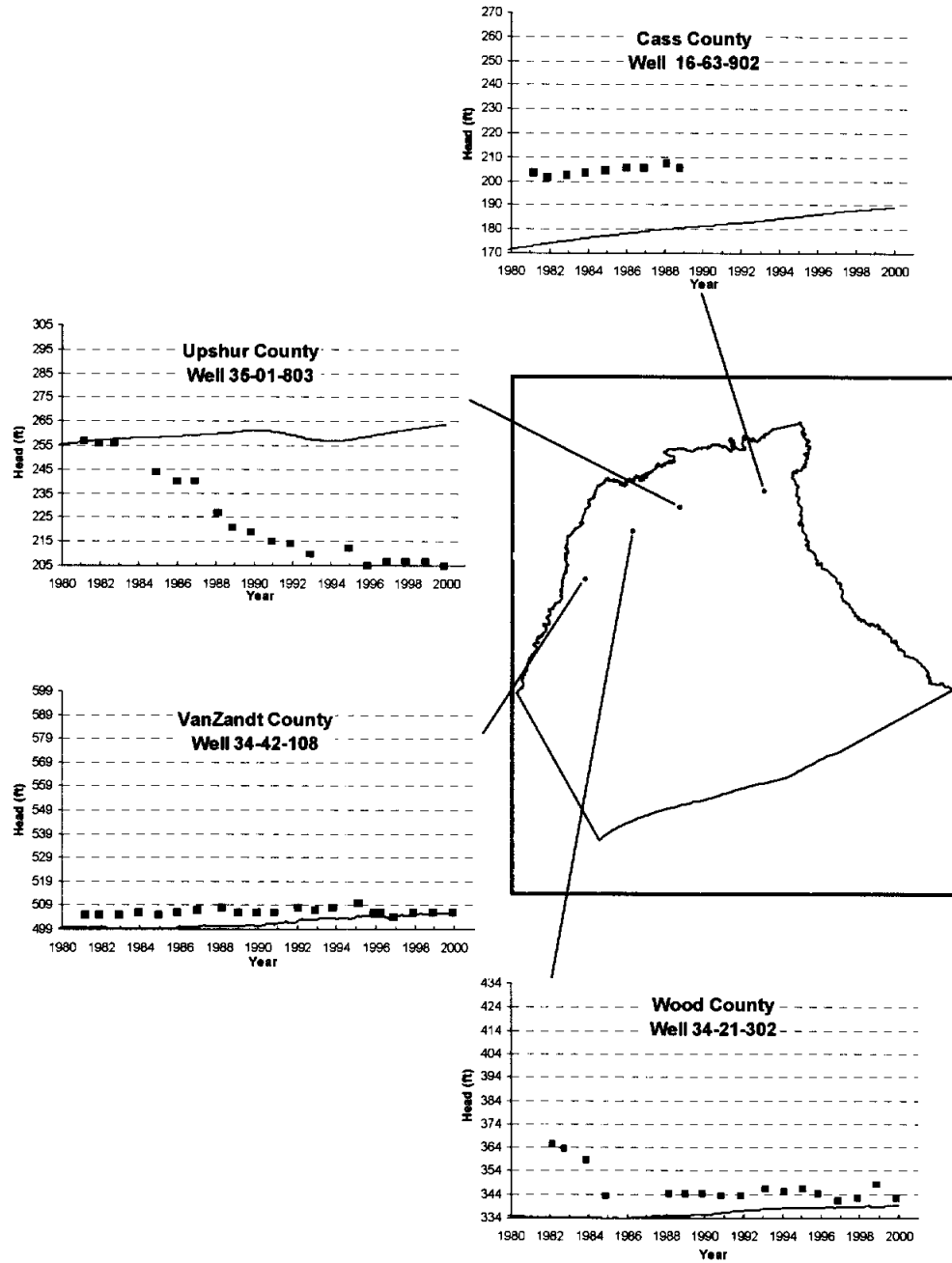


Figure 9.2.17a Selected hydrographs of simulated (lines) and measured (points) hydraulic heads in the northern part for Layer 4 (upper Wilcox).

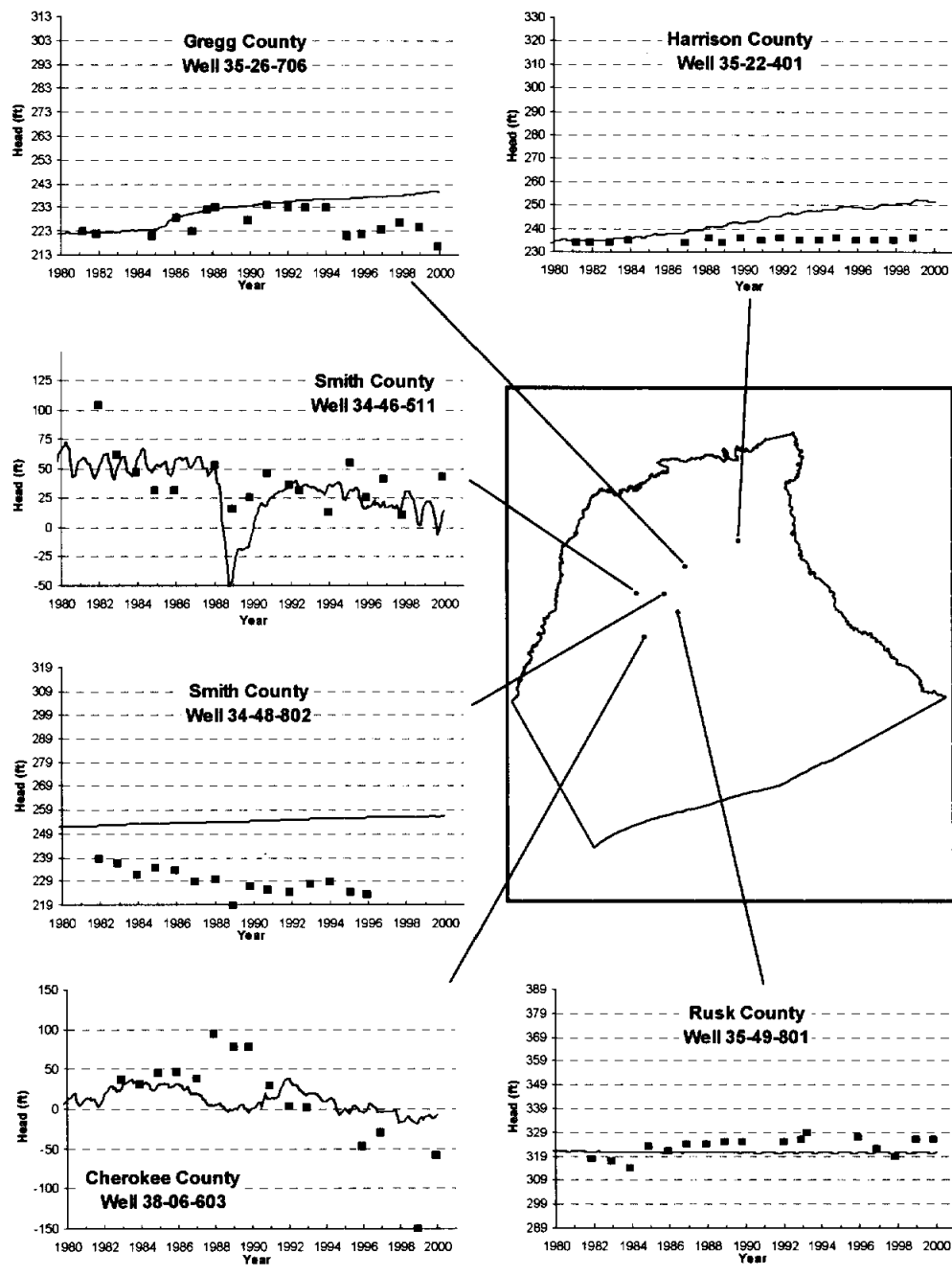


Figure 9.2.17b Selected hydrographs of simulated (lines) and measured (points) hydraulic heads in the central part for Layer 4 (upper Wilcox).

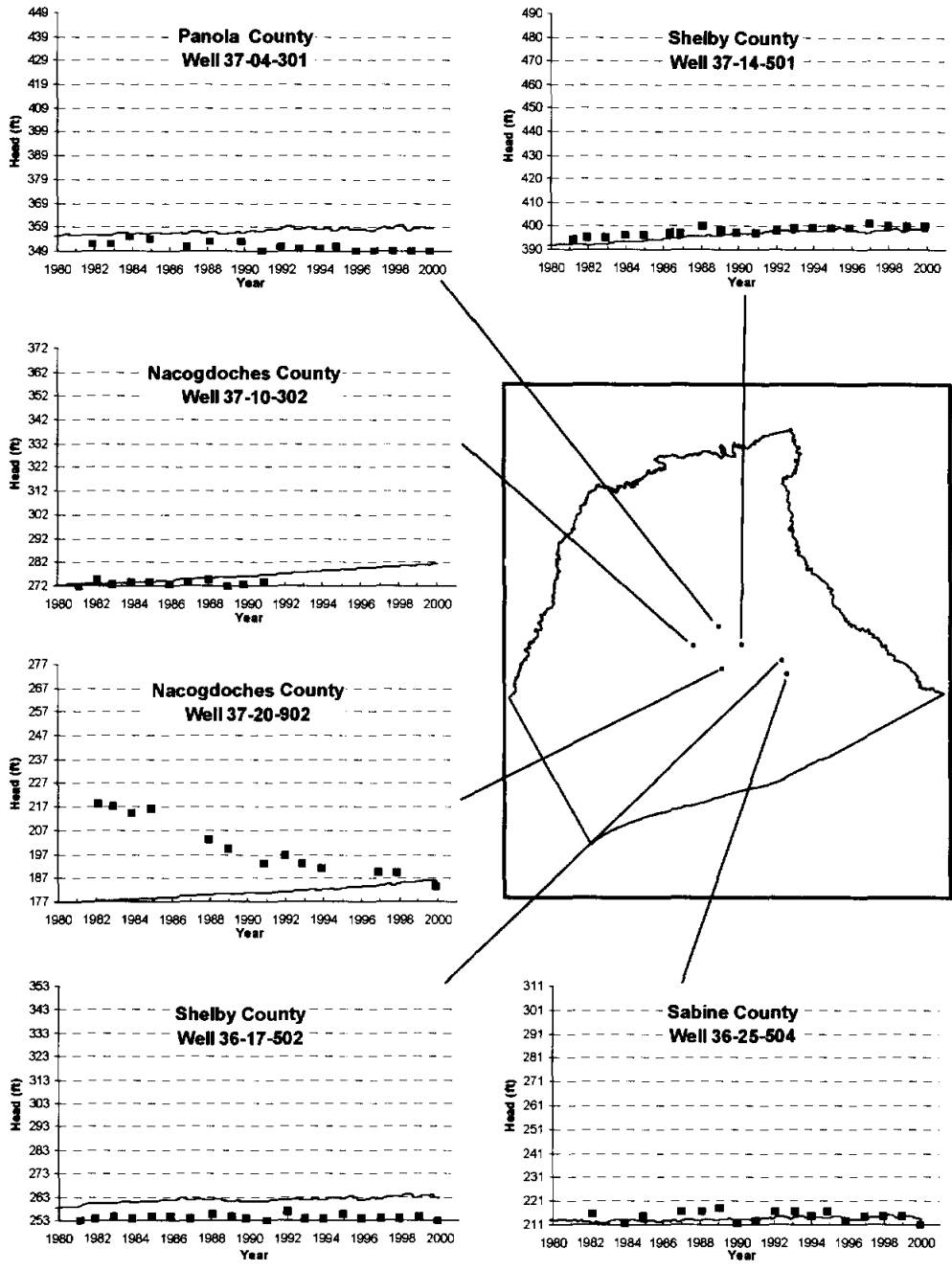


Figure 9.2.17c Selected hydrographs of simulated (lines) and measured (points) hydraulic heads in the southern part for Layer 4 (upper Wilcox).

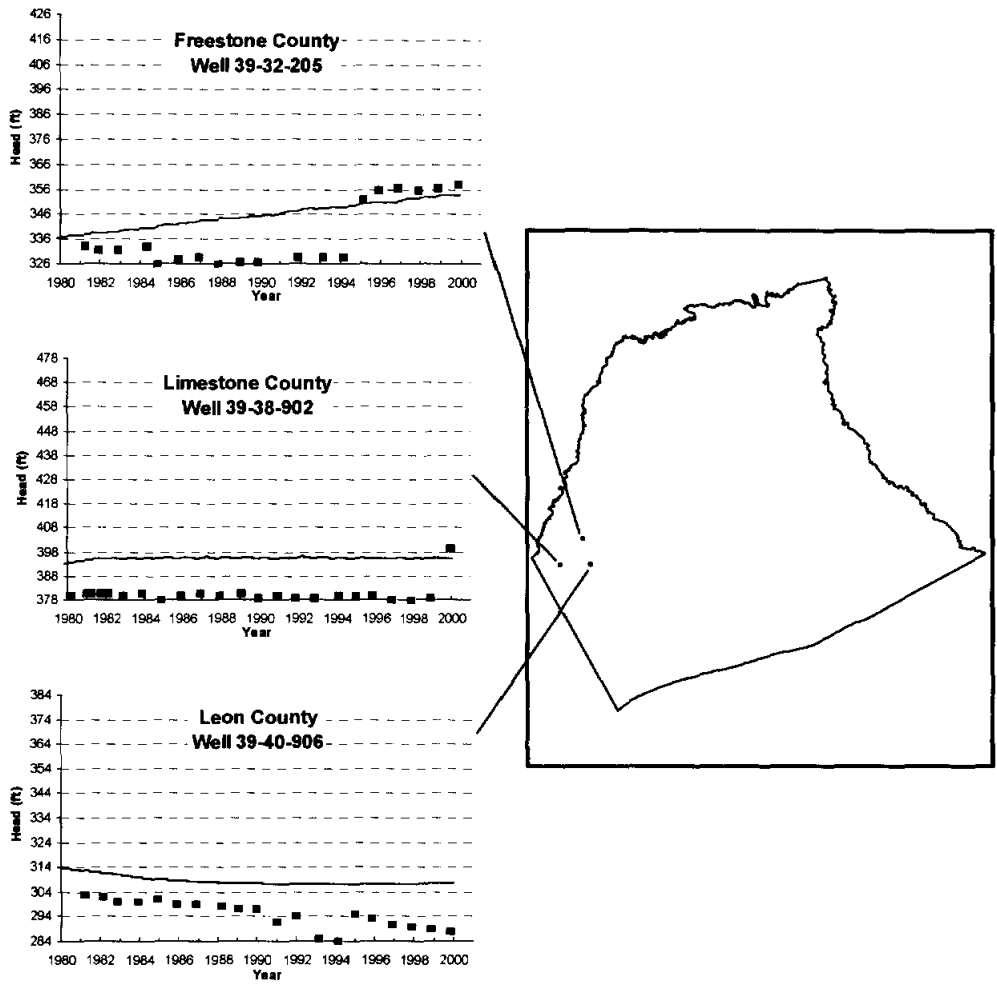


Figure 9.2.17d Selected hydrographs of simulated (lines) and measured (points) hydraulic heads in the western part for Layer 4 (upper Wilcox).

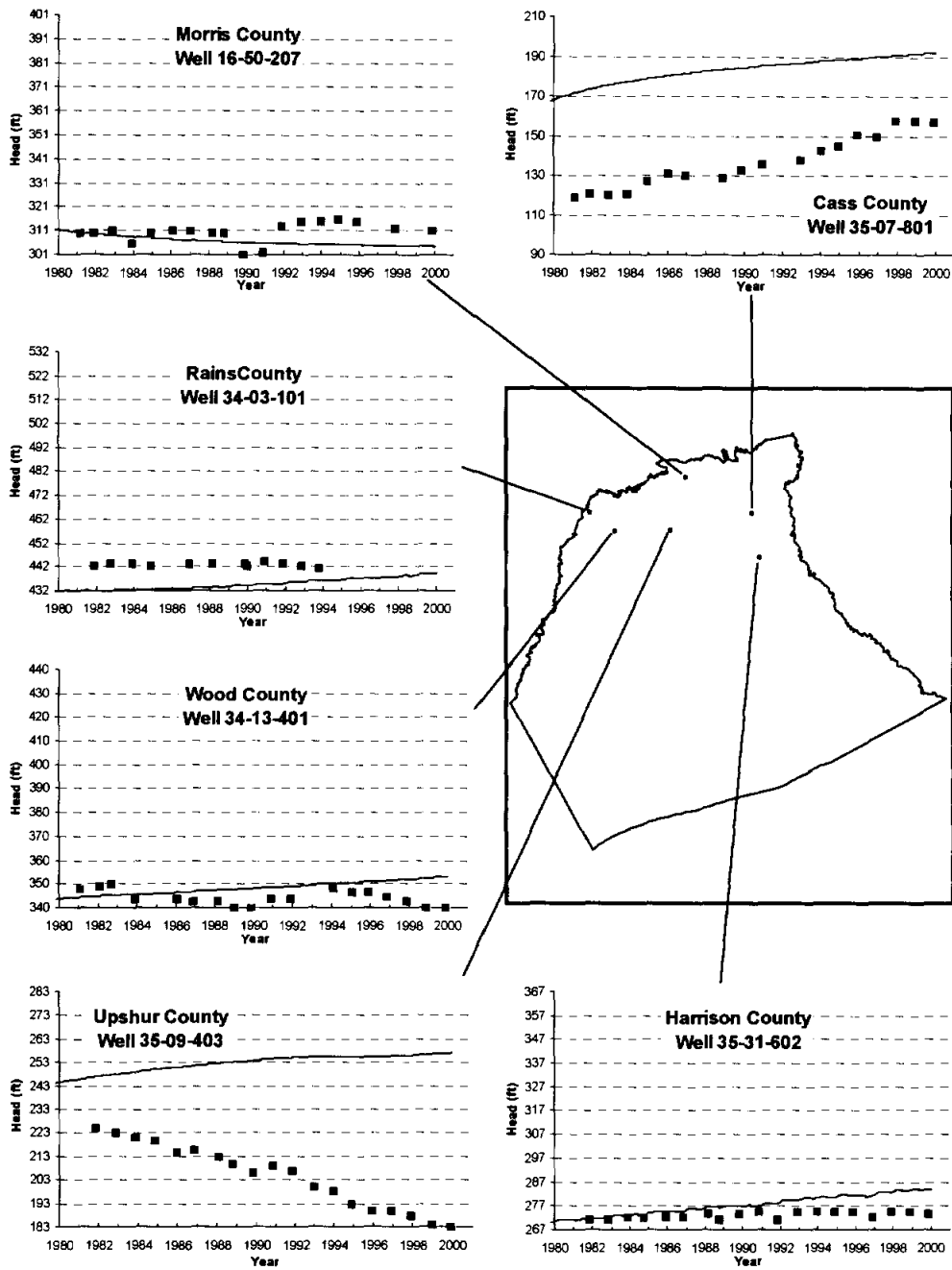


Figure 9.2.18a Selected hydrographs of simulated (lines) and measured (points) hydraulic heads in the northern part for Layer 5 (middle Wilcox).

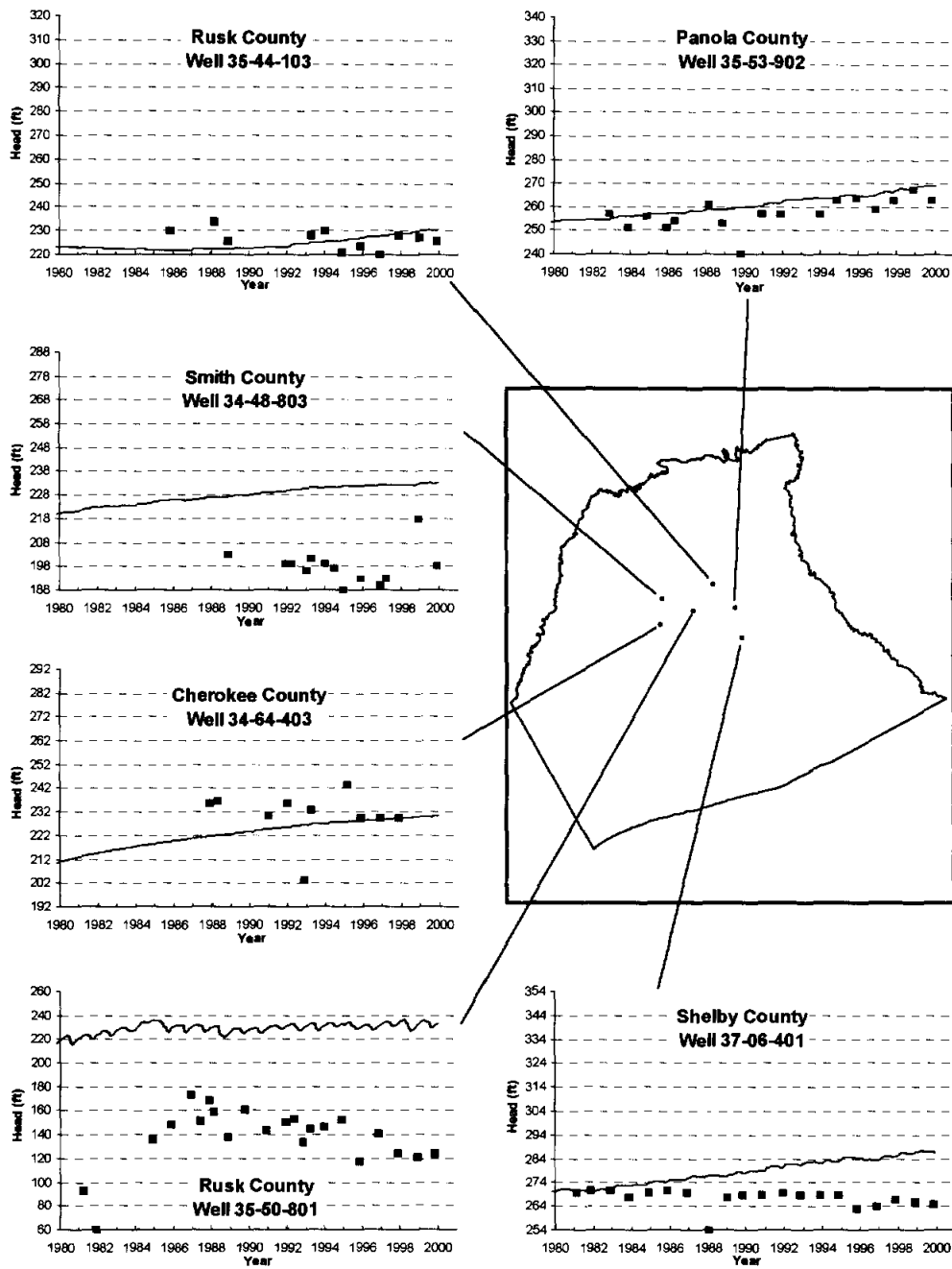


Figure 9.2.18b Selected hydrographs of simulated (lines) and measured (points) hydraulic heads in the central part for Layer 5 (middle Wilcox).

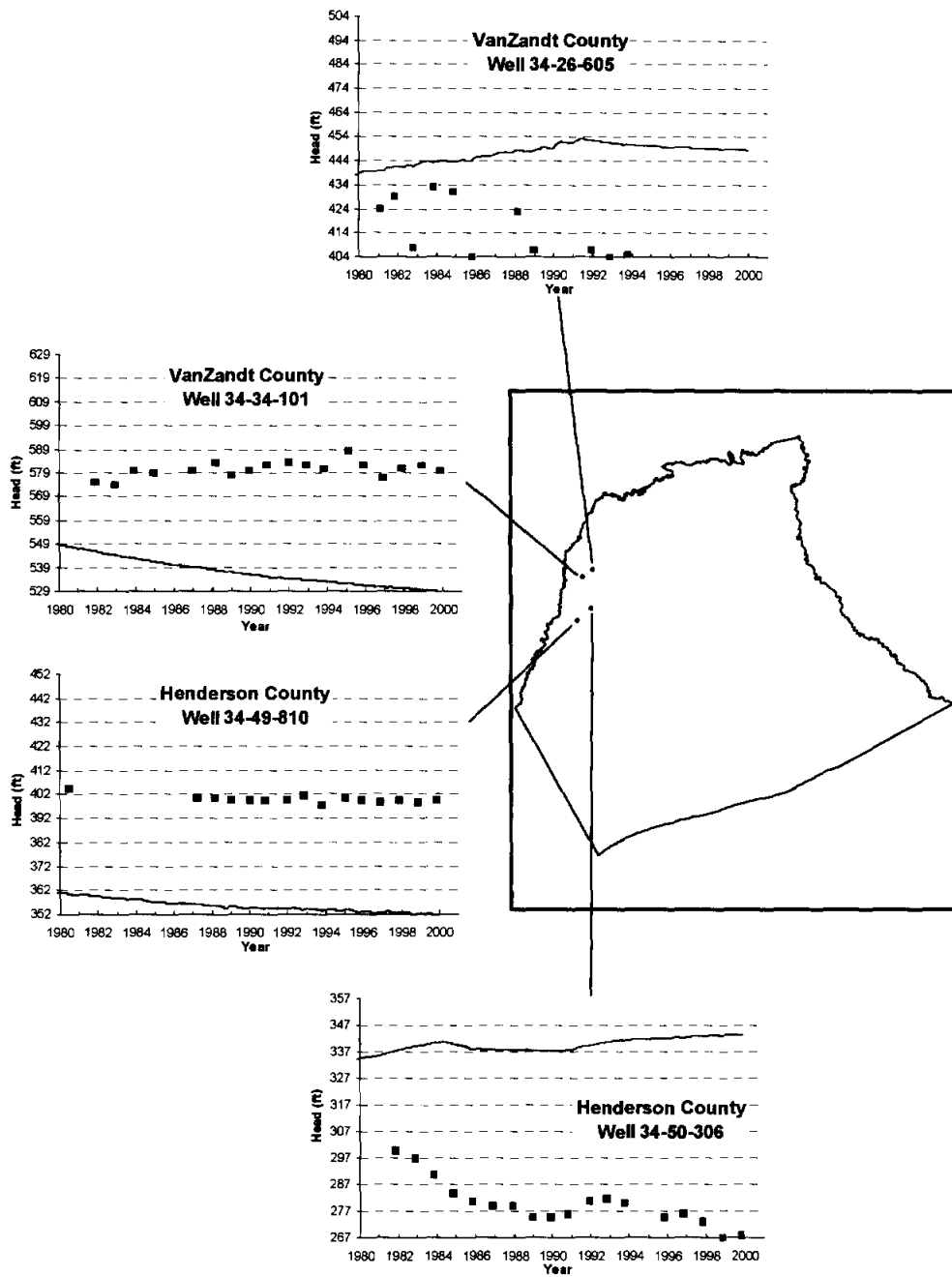


Figure 9.2.18c Selected hydrographs of simulated (lines) and measured (points) hydraulic heads in the western part for Layer 5 (middle Wilcox).

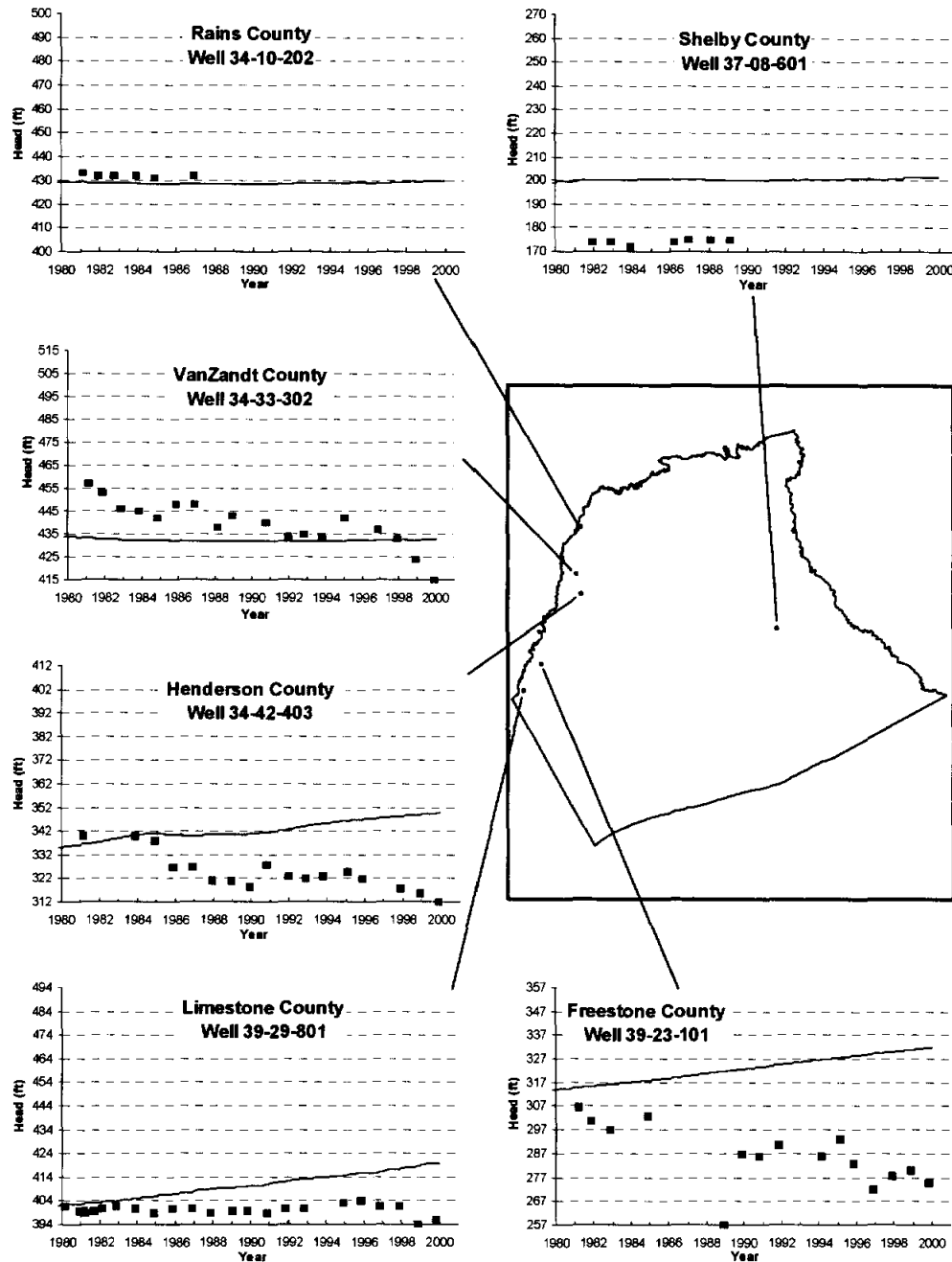


Figure 9.2.19 Selected hydrographs of simulated (lines) and measured (points) hydraulic heads in Layer 6 (lower Wilcox).

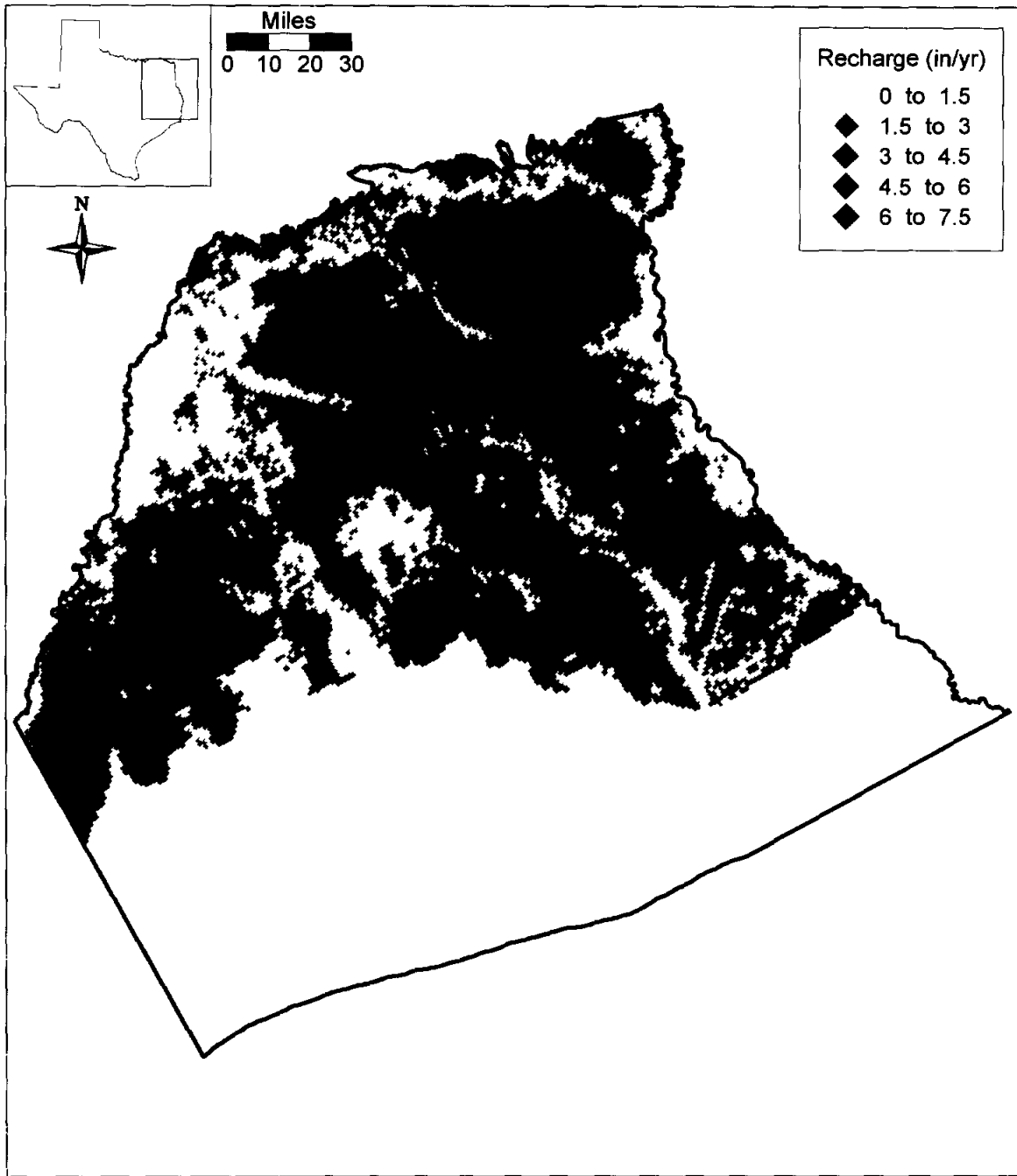


Figure 9.2.20 Average recharge for the transient simulation period (1980-1999).

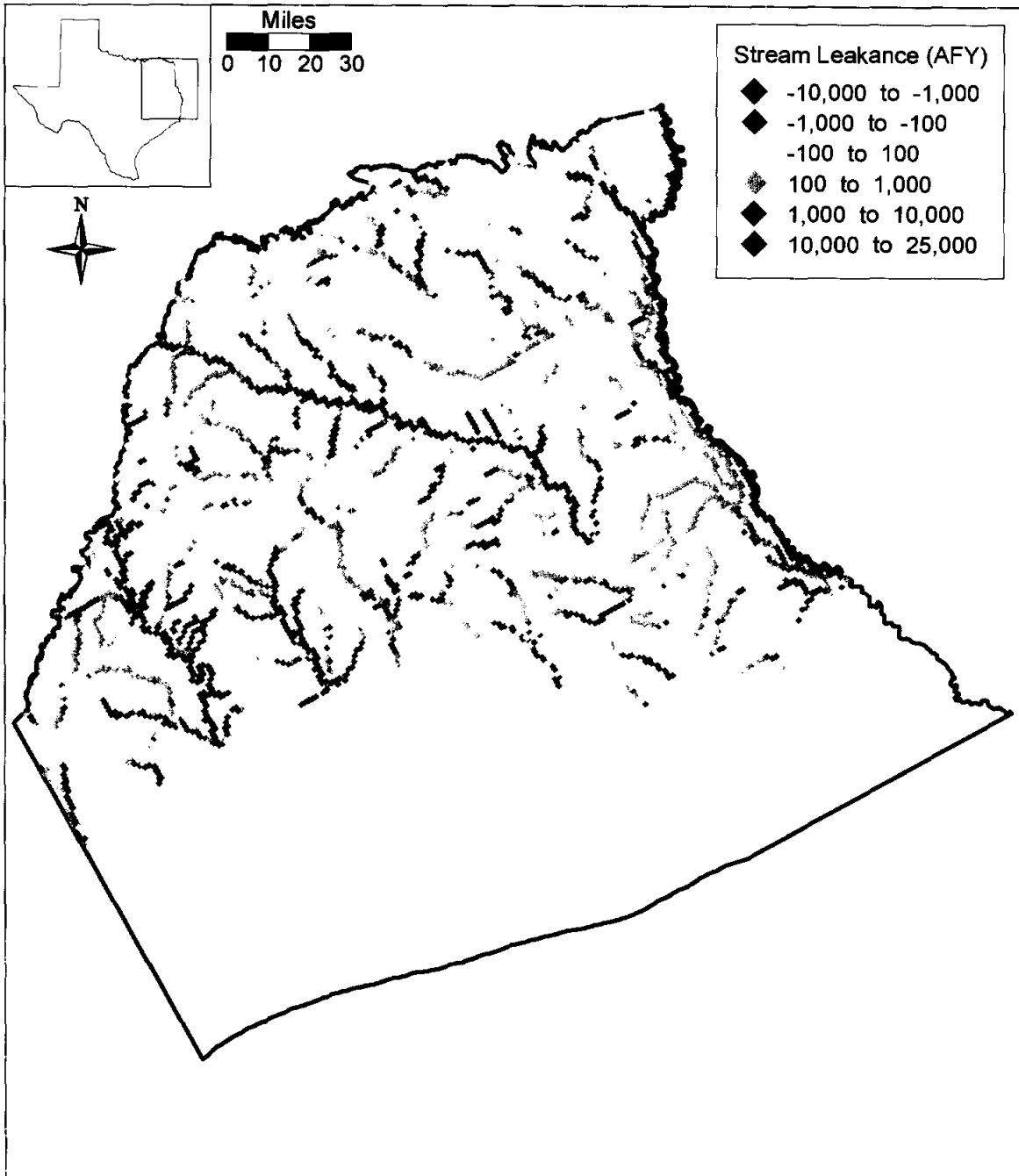


Figure 9.2.21 Simulated stream gain/loss for May 1989.

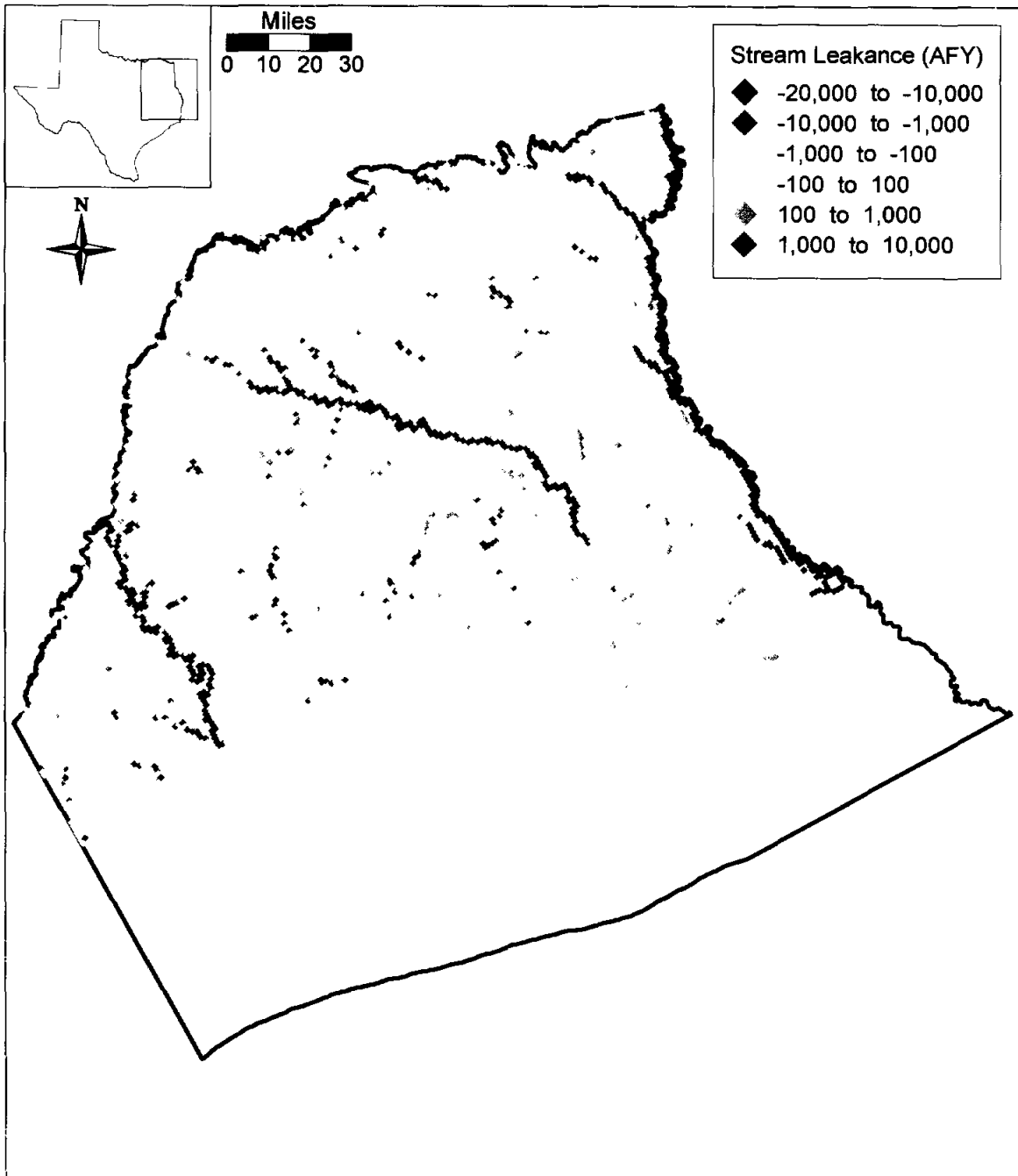


Figure 9.2.22 Simulated stream gain/loss for November 1989.

Comparison of Neches River Gauge 8032000 to Model Predicted Streamflow

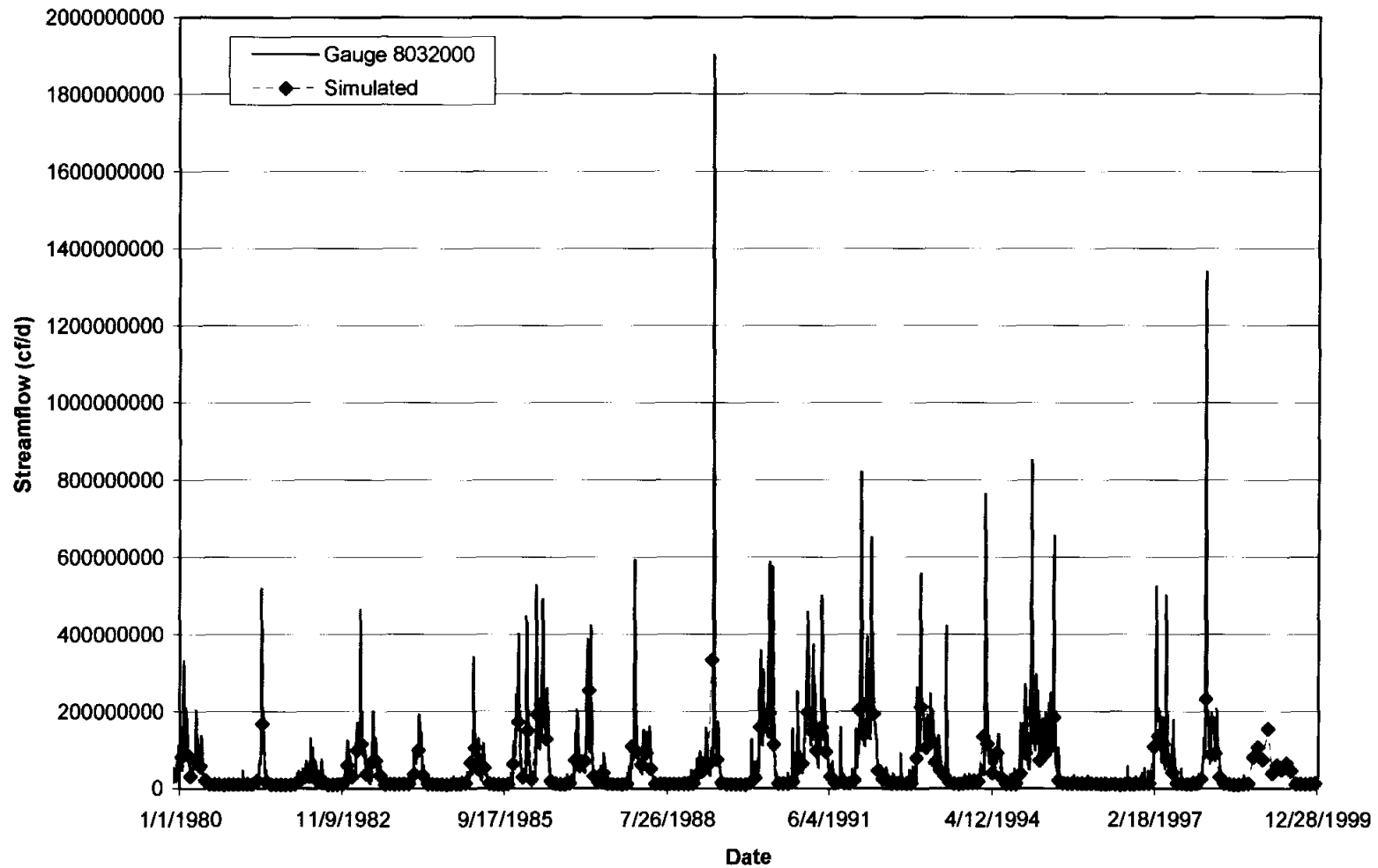


Figure 9.2.23a Simulated and measured stream flow at gauging station 8032000 on the Neches River.

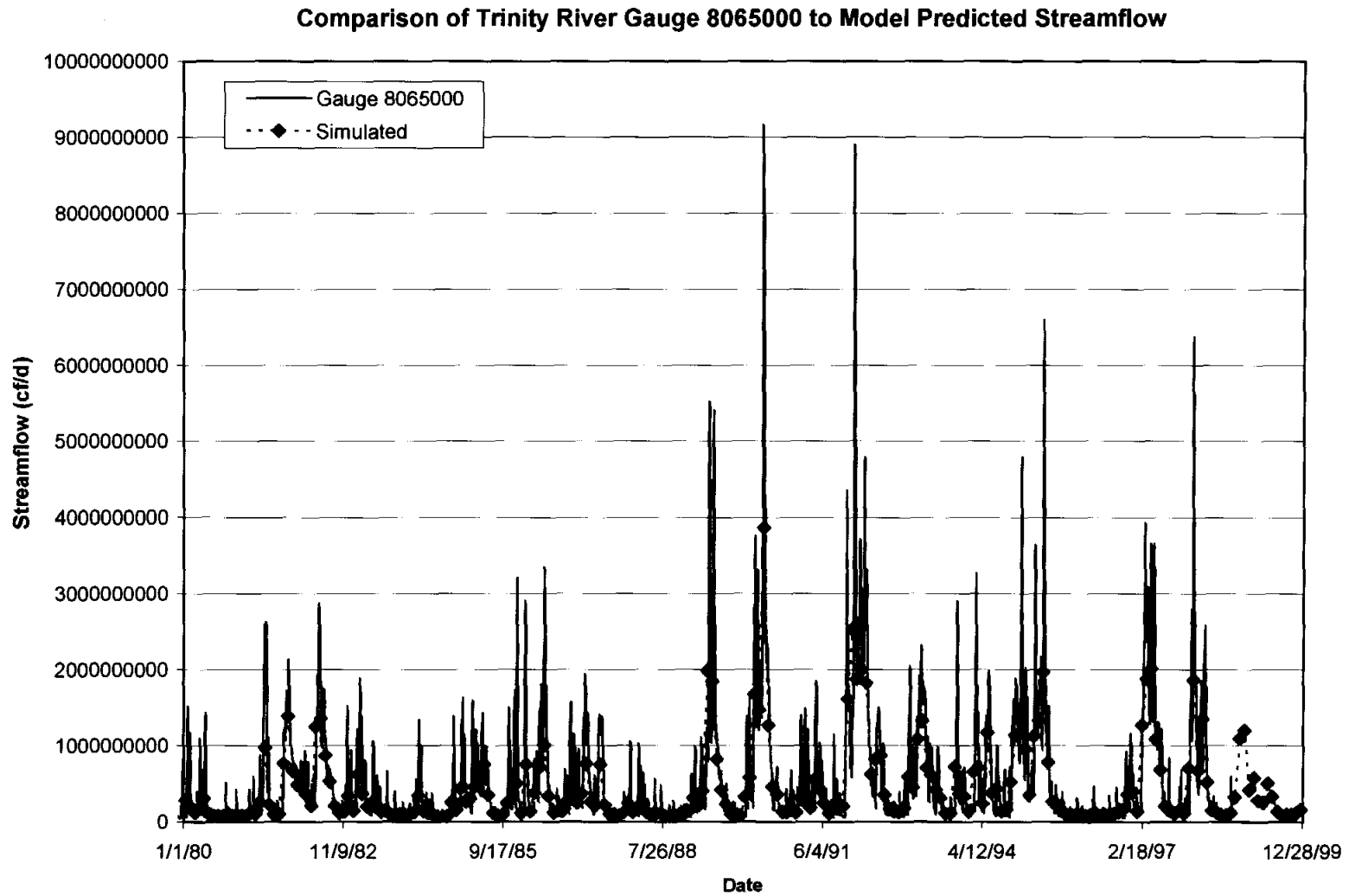
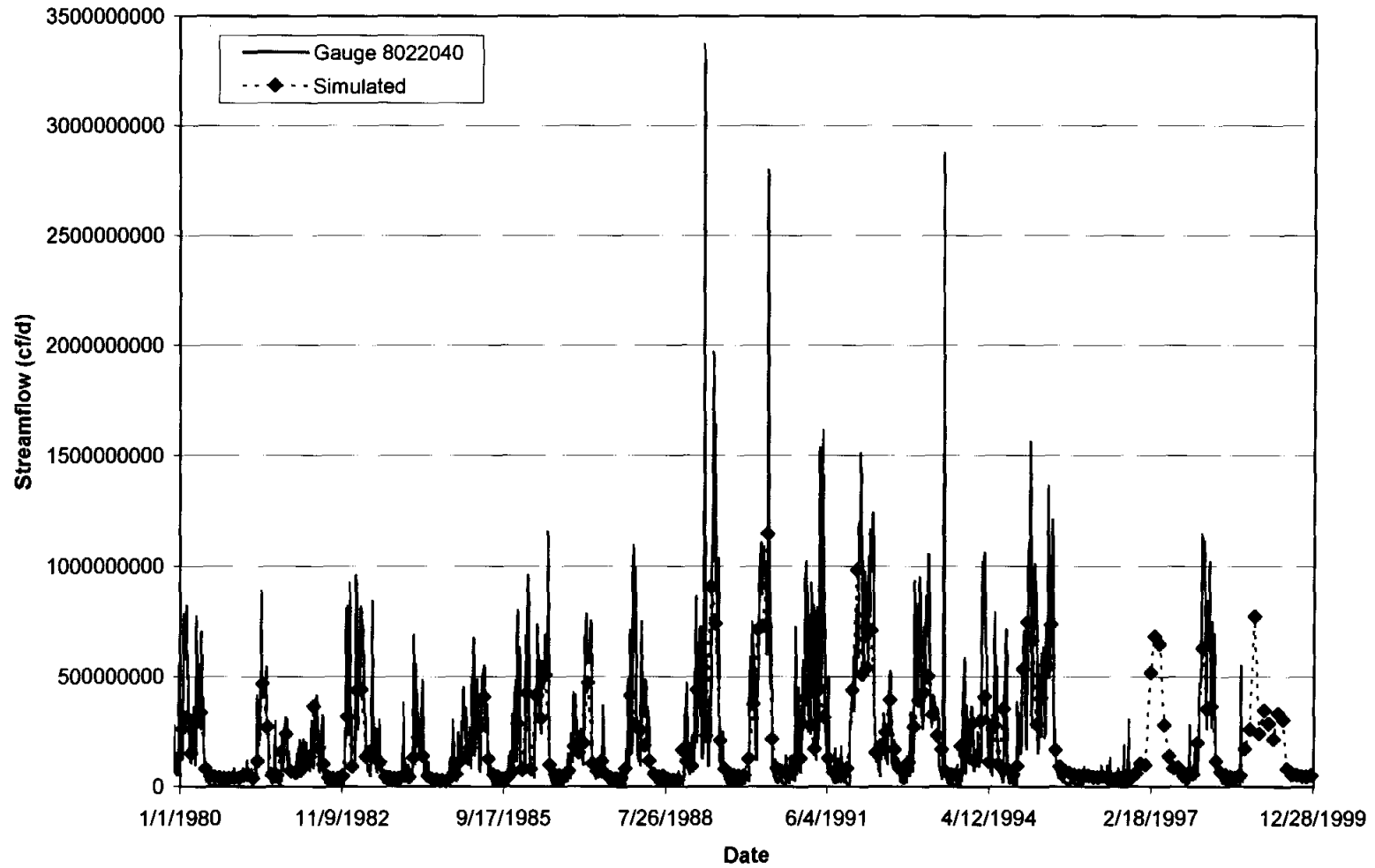


Figure 9.2.23b Simulated and measured stream flow at gauging station 8065000 on the Trinity River.

Comparison of Sabine River Gauge 8022040 to Model Predicted Streamflow



c.

Figure 9.2.23c Simulated and measured stream flow at gauging station 8022040 on the Sabine River.

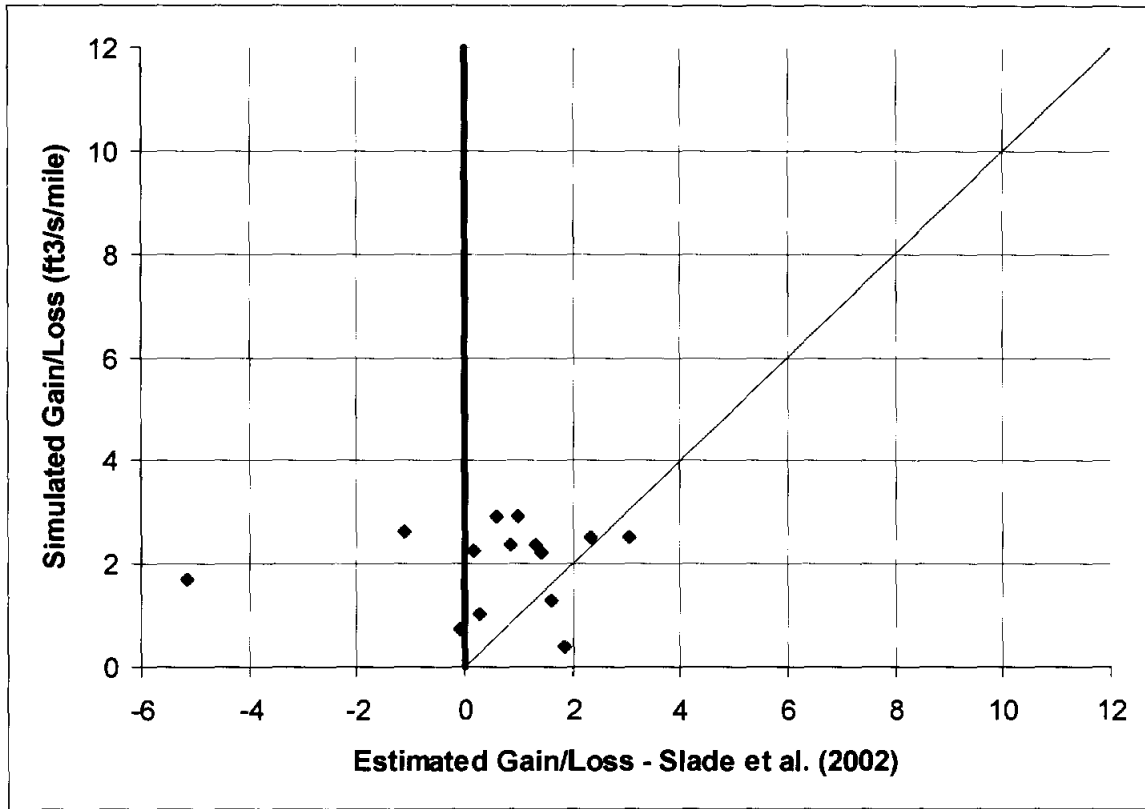
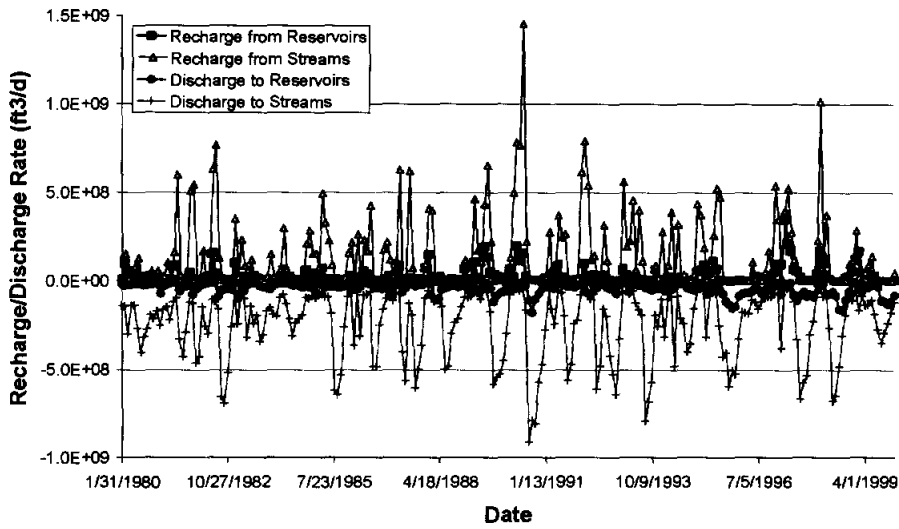
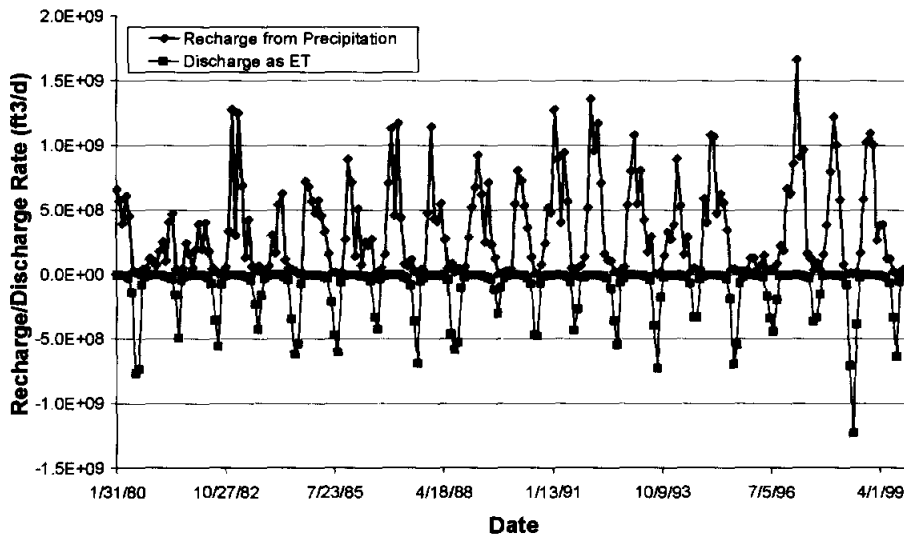


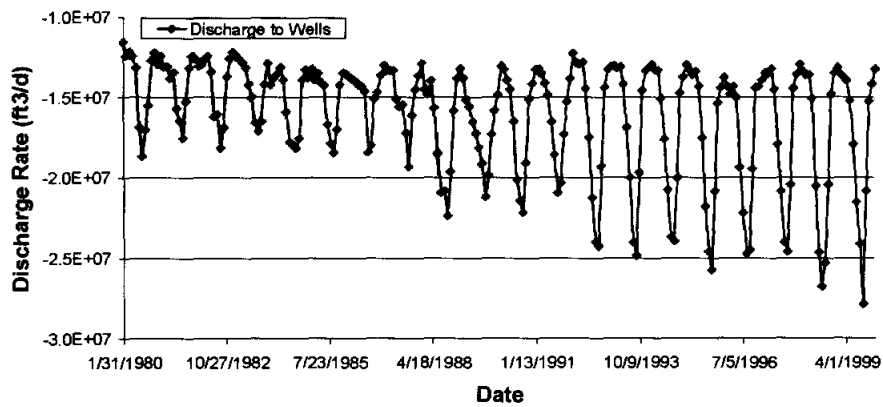
Figure 9.2.24 Simulated stream gain/loss compared to measurements compiled by Slade et al. (2002) for selected stream segments.



a.



b.



c.

Figure 9.2.25 Time history of water budgets for (a) streams and reservoirs, (b) recharge and ET, and (c) pumpage.

9.3 Sensitivity Analysis

Section 8.3 discussed the approach for sensitivity analyses for the steady-state model. The analyses were similar for the transient model, with the addition of several sensitivities. For the transient analysis, we completed 10 parameter sensitivities:

1. Horizontal hydraulic conductivity, Layer 3 (K_h -Carrizo)
2. Horizontal hydraulic conductivity, Layers 4 - 6 (K_h -Wilcox)
3. Vertical hydraulic conductivity in Layer 2 (K_v -Reklaw) (leakance between Layers 2 and 3)
4. Vertical hydraulic conductivity in Layers 4 - 6 (K_v -Wilcox) (leakance between layers 3 - 4, 4 - 5, and 5 - 6)
5. Recharge, model-wide
6. Streambed conductance, model-wide (K-stream)
7. GHB conductance, model-wide (K-GHB)
8. Storativity in Layer 3 (storage-Carrizo)
9. Storativity in Layers 4 - 6 (storage-Wilcox)
10. Pumping rate
11. Reservoir conductivity (K-reservoir)
12. Specific yield, model-wide

Equation 8.3.1 (varying linearly) for parameter variation was used for sensitivities 5, 10, and 12, and Equation 8.3.2 was used for the rest of the sensitivities listed above.

As with the steady-state model, we checked the mean difference between the base simulated head and the sensitivity in simulated head by applying Equation 8.3.3 at all gridblocks and also only at gridblocks where targets were present. Figure 9.3.1 shows the transient sensitivity results for Layer 3 (Carrizo) calculated for the target gridblocks and Figure 9.3.2 shows the transient sensitivity results for Layer 3 calculated at all gridblocks. As with the steady-state model, the order of the first four most important sensitivities is the same between both methods, even though the magnitude of the mean head differences (MD) is significantly different. This is to be expected as the target cells are concentrated in areas of groundwater decline. This indicates an adequate target coverage in this layer.

Figure 9.3.2 shows that the most positively correlated parameter for the Carrizo is horizontal hydraulic conductivity. The most negatively correlated parameter for the Carrizo is pumping. This is an important result, because these parameters were changed very little during calibration (Section 9.1). The third most important parameter is the vertical hydraulic conductivity of the Reklaw. This parameter was adjusted significantly during calibration. In comparison, in the steady-state model recharge was the dominant parameter followed by the horizontal hydraulic conductivity of Layers 4 - 6 (Wilcox), the vertical hydraulic conductivity of Layer 2 (Reklaw), and the horizontal hydraulic conductivity of Layer 3 (Carrizo) having significantly lower sensitivities. In the transient model, heads become more sensitive to the horizontal hydraulic conductivity of Layer 3 (Carrizo), followed by the vertical hydraulic conductivity of Layer 2 (Reklaw), and then by the horizontal hydraulic conductivity of Layers 4 - 6 (Wilcox). This difference is another indication of the importance of calibrating two hydrologic scenarios to improve the uniqueness of the calibrated parameter values.

Figures 9.3.3 through 9.3.7 show the transient sensitivity results for Layers 1, 2, 4, 5, and 6. The results for the Layer 1 (Figure 9.3.3) indicates that recharge and the GHB conductance show the greatest MDs, due to the fact that the Queen City crops out over the northern section and is confined in the southern part overlain by younger sediments, which are represented by a GHB boundary. As one expects, the greatest sensitivity for Layer 2 is the vertical hydraulic conductivity of the Reklaw (Figure 9.3.4.). Layers 4 – 6 show similar sensitivity patterns, except that for Layer 4 the horizontal hydraulic conductivity of the Wilcox shows the greatest MD values (Figure 9.3.5), whereas for Layer 5 and Layer 6, the highest positively correlated MDs are for the vertical hydraulic conductivity of the Wilcox layers followed by the Wilcox horizontal hydraulic conductivity (Figures 9.3.6 and 9.3.7). Note that, for the negatively correlated parameters, the most sensitive parameter is pumpage for Layer 4, whereas for Layers 5 and 6 the most sensitive parameter is the Wilcox storativity followed by pumpage.

Figure 9.3.8 shows the sensitivity results for all layers, where the vertical hydraulic conductivity of the Reklaw is varied. The layer with the greatest MD is Layer 2 followed by Layer 3, indicating that the Carrizo is most hydrologically affected by vertical flow across the Reklaw. Figure 9.3.9 shows the sensitivity results for all layers for variations in recharge. As indicated above, recharge is most important for Layer 1 (Queen City) followed by Layer 5

(middle Wilcox), because of the relatively large outcrop areas, respectively. Note that the maximum mean difference for both of these sensitivities is less than 1 ft. These figures indicate that recharge and specific yield, which should be most important in the outcrop, do not have a large overall effect on the heads in the model. Figure 9.3.10 shows the sensitivities to the Wilcox horizontal hydraulic conductivity on hydraulic heads in the different layers. The results show that Layer 4 (upper Wilcox) shows the greatest MDs followed by Layer 3 (Carrizo). That is, changes in horizontal hydraulic conductivity of the Wilcox layers significantly affect hydraulic heads in the overlying Carrizo.

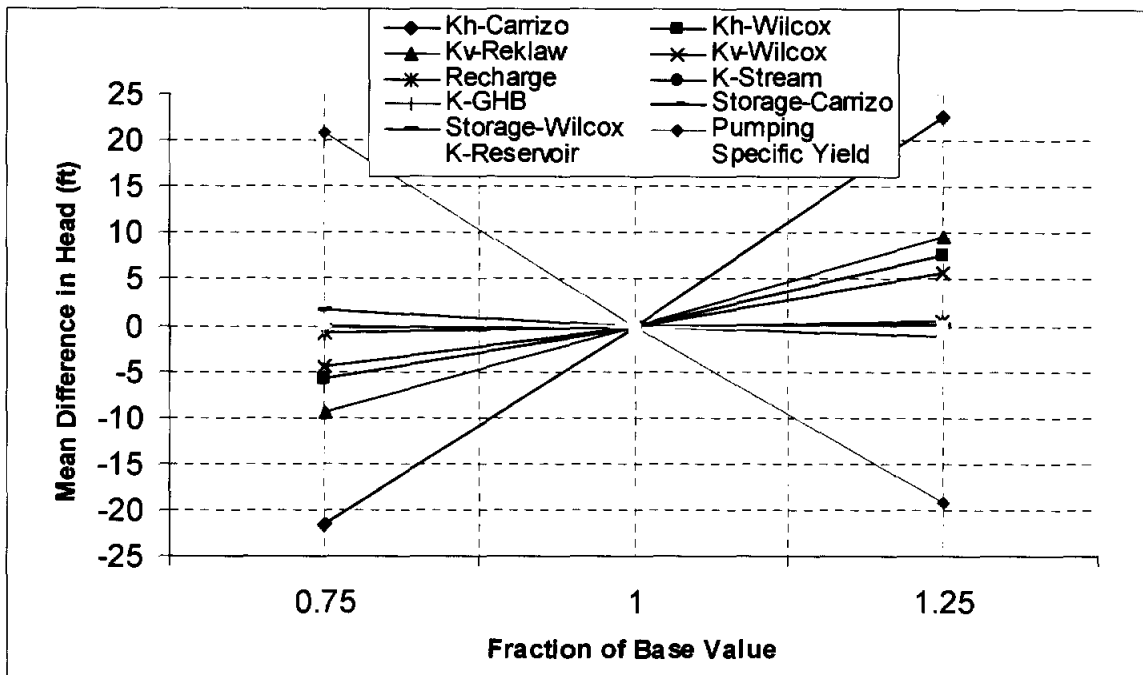


Figure 9.3.1 Transient sensitivity results for Layer 3 (Carrizo) using target locations.

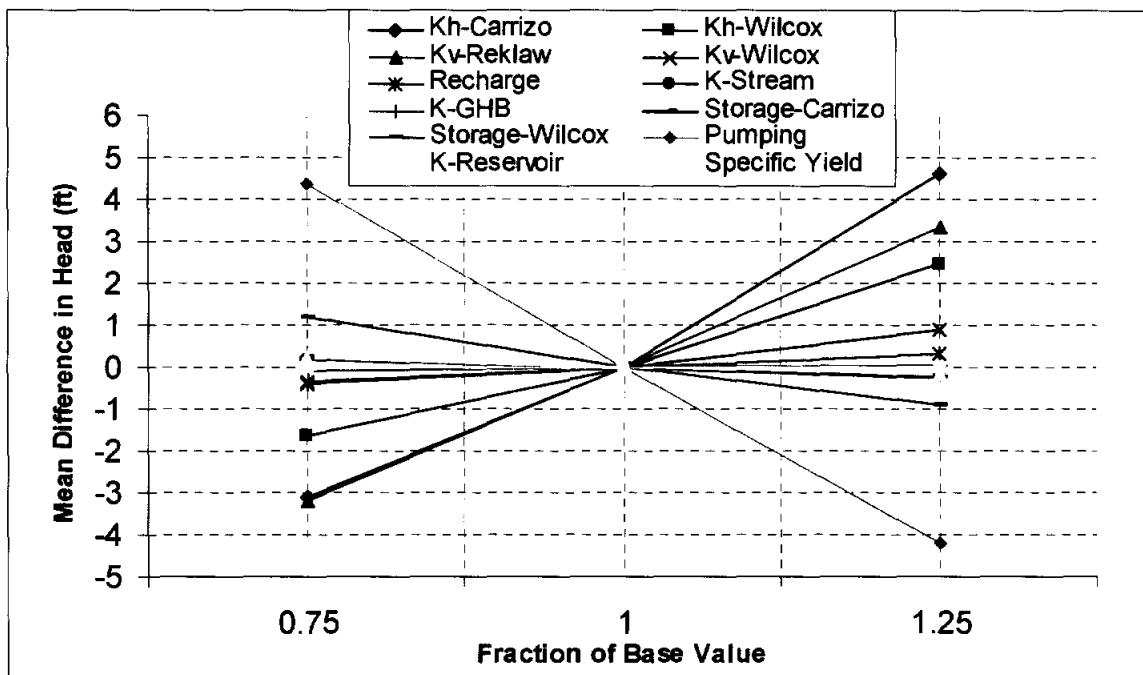


Figure 9.3.2 Transient sensitivity results for Layer 3 (Carrizo) using all active gridblocks.

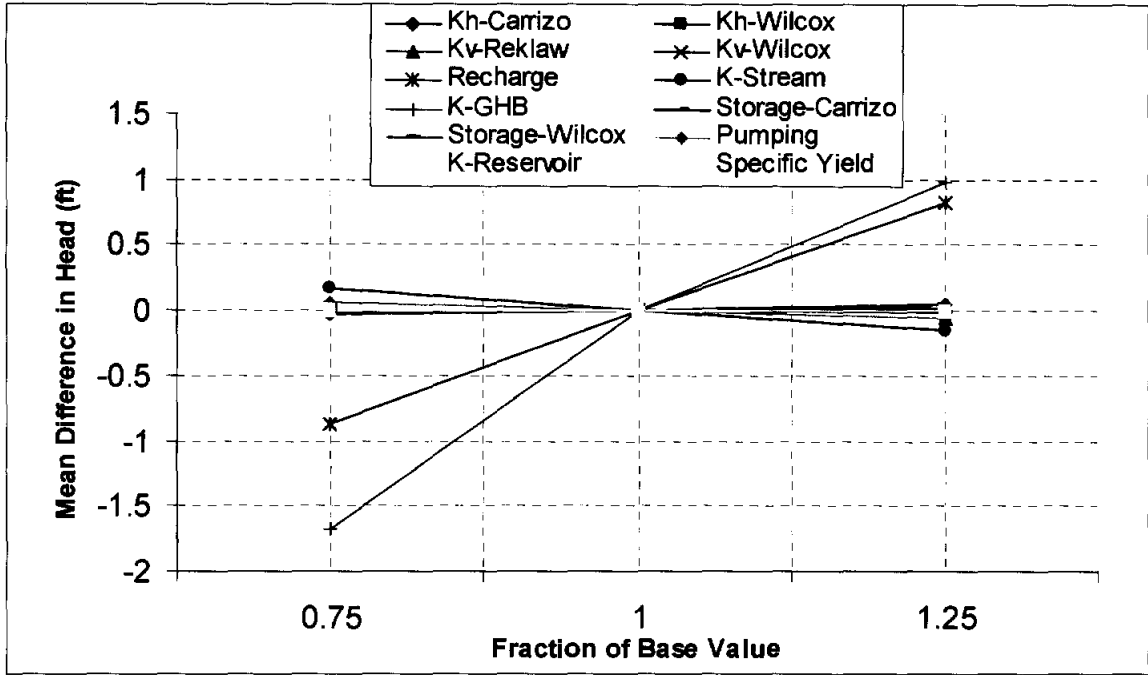


Figure 9.3.3 Transient sensitivity results for Layer 1 (Queen City) using all active gridblocks.

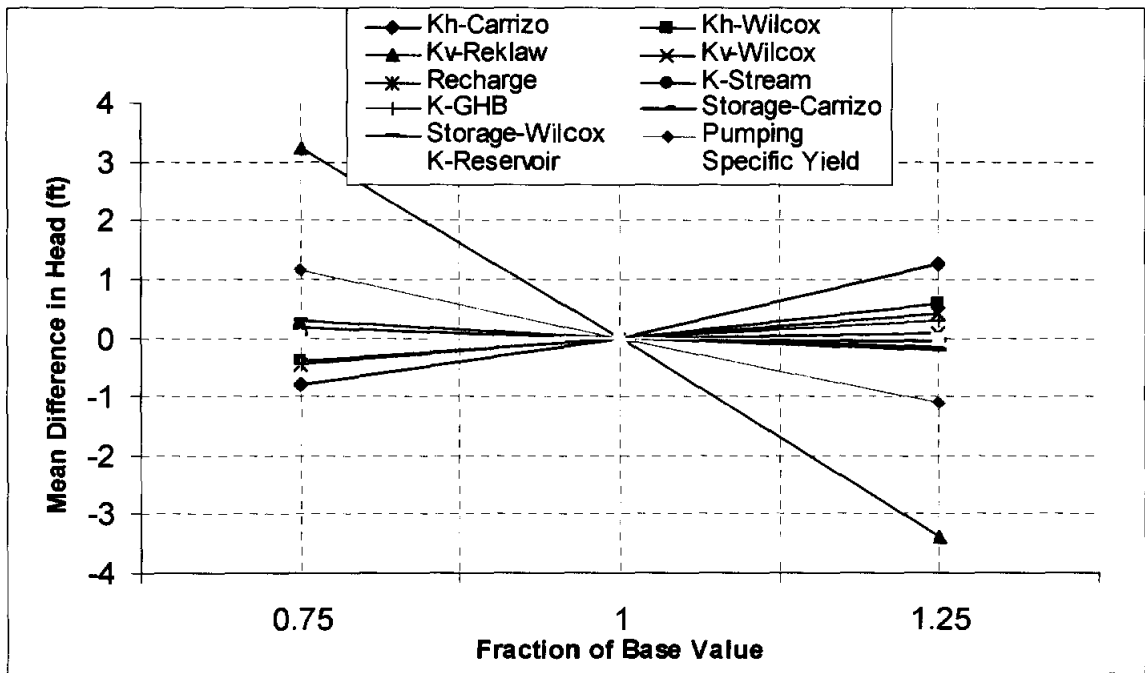


Figure 9.3.4 Transient sensitivity results for Layer 2 (Reklaw) using all active gridblocks.

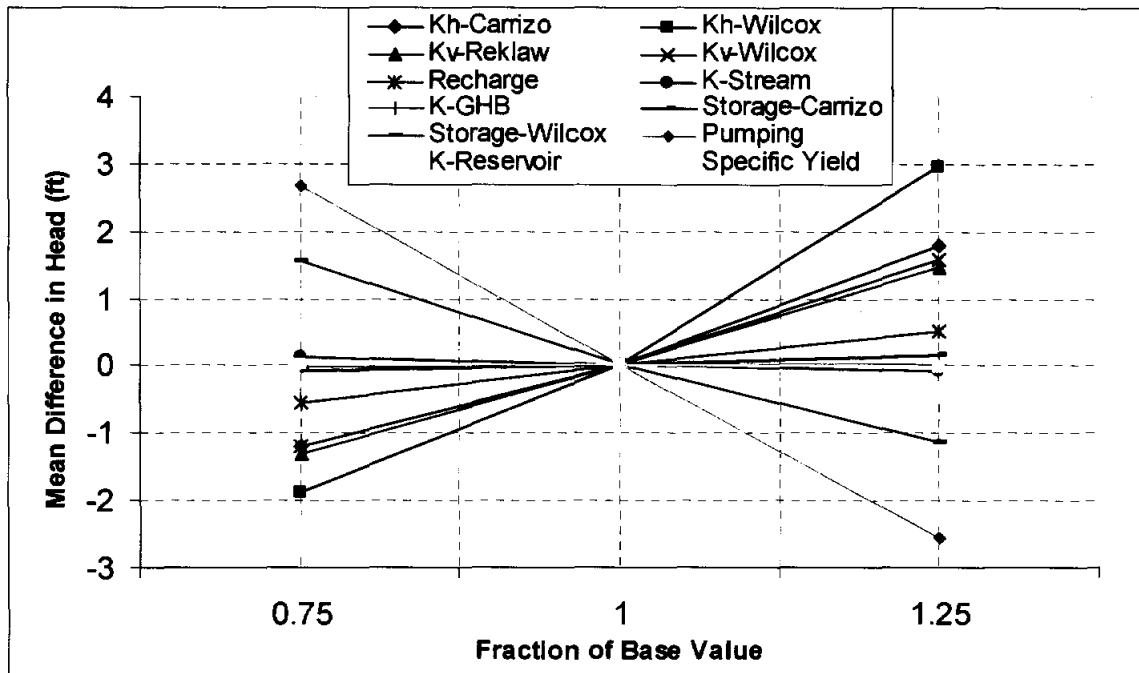


Figure 9.3.5 Transient sensitivity results for Layer 4 (upper Wilcox) using all active gridblocks.

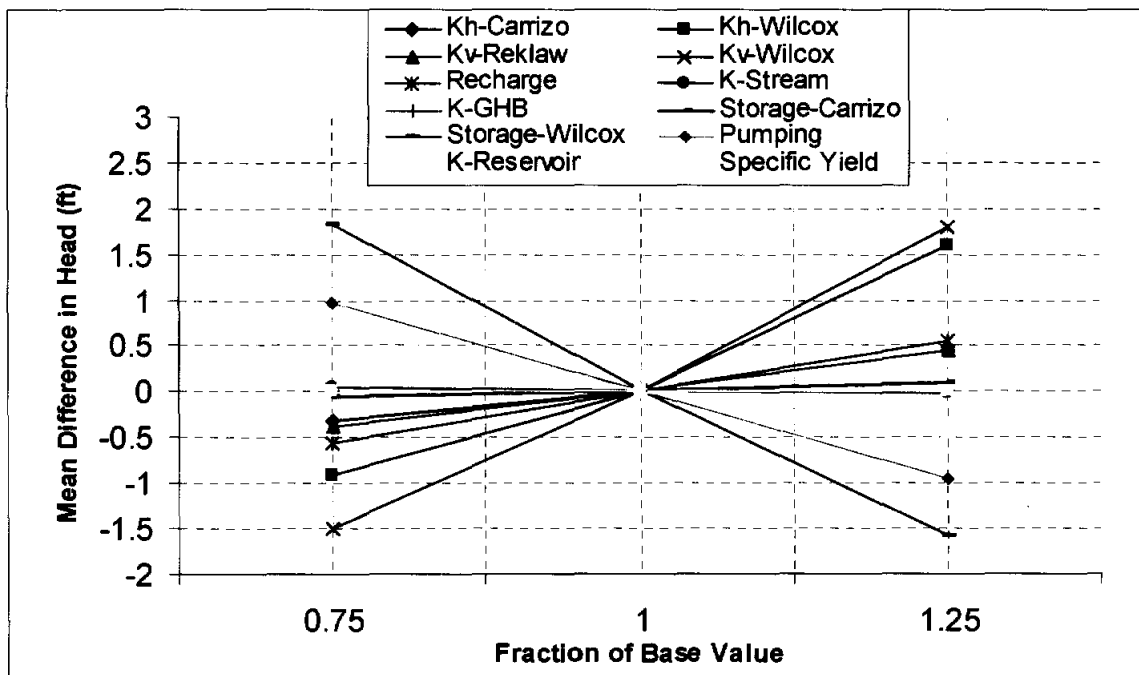


Figure 9.3.6 Transient sensitivity results for Layer 5 (middle Wilcox) using all active gridblocks.

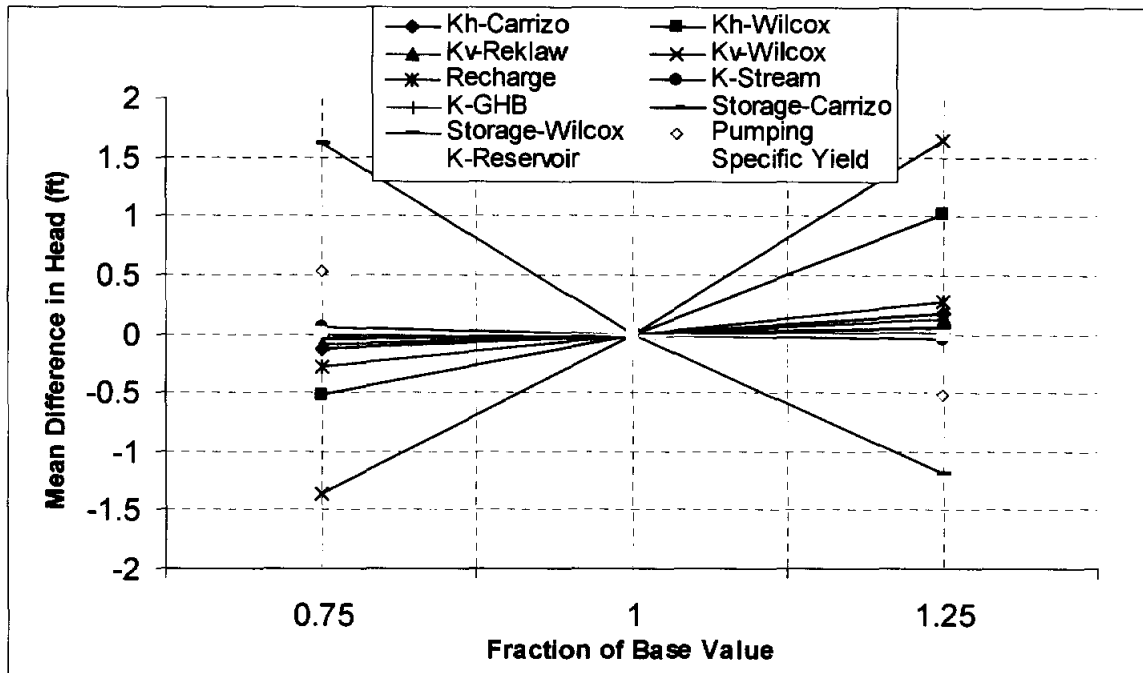


Figure 9.3.7 Transient sensitivity results for Layer 6 (lower Wilcox) using all active gridblocks.

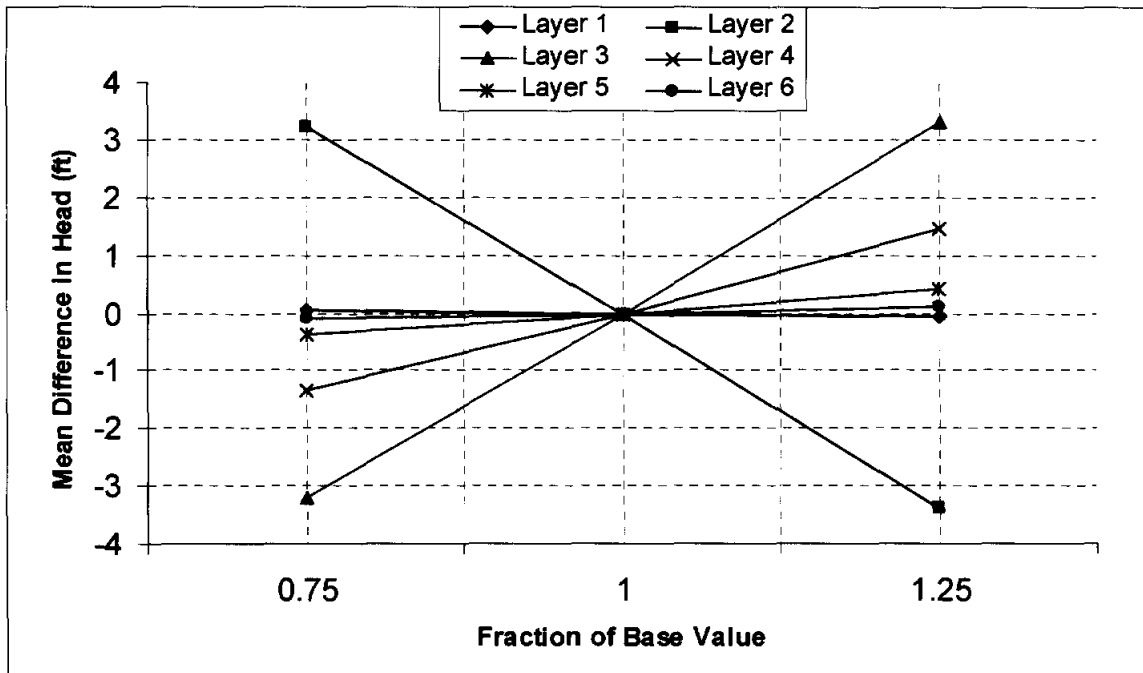


Figure 9.3.8 Transient sensitivity results where the vertical hydraulic conductivity of Layer 2 (Reklaw) is varied.

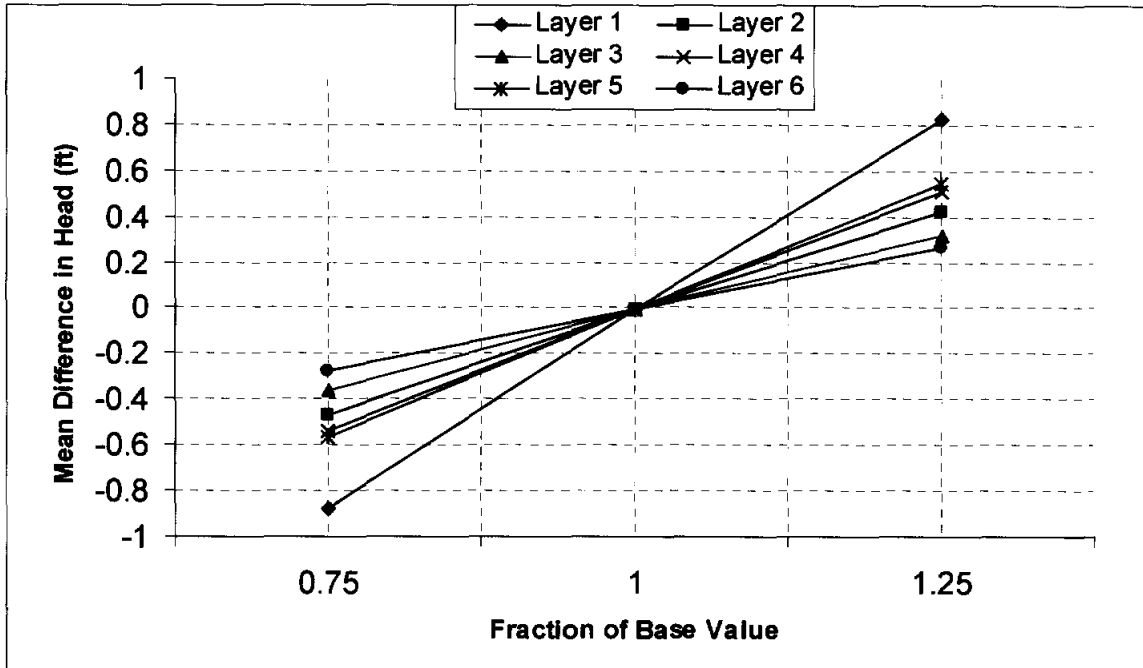


Figure 9.3.9 Transient sensitivity results where recharge is varied.

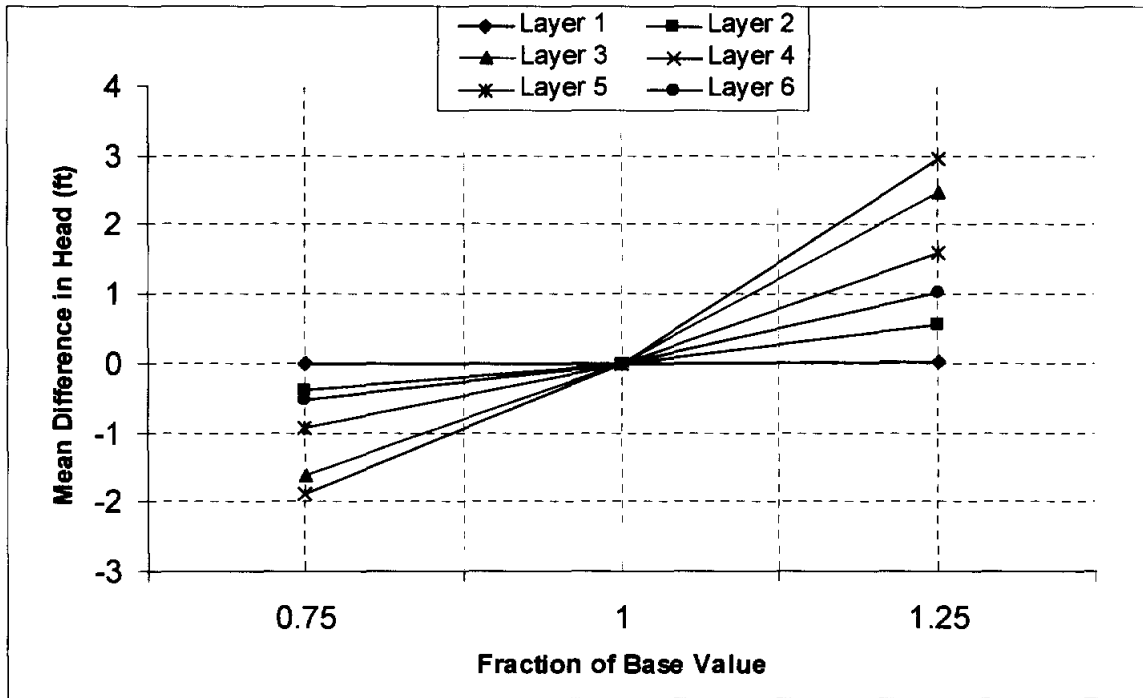


Figure 9.3.10 Transient sensitivity results where the horizontal hydraulic conductivity of the Wilcox is varied.

10.0 MODEL PREDICTIVE SIMULATIONS

The purpose of the GAM is to assess groundwater availability within the modeled northern Carrizo-Wilcox region over a 50-year planning period (2000-2050) using RWPG water-demand projections under drought-of-record (DOR) conditions. The GAM will be used to predict changes in regional groundwater water levels (heads) and fluxes related to baseflow to major streams and rivers, springs, and cross-formational flow. The two most important stresses to be considered in the future predictive modeling period are the same two stresses imposed during the calibration and verification periods; recharge and pumping.

Predictive pumping demands from the RWPGs are used in the predictive mode simulations assuming that the pumping distribution (as determined in Appendix D) for 1999 applies in the future (2000-2050). Predictive simulations assume average recharge conditions for the duration of the prediction ending with DOR conditions. For purposes of this report, average recharge is defined as the average recharge rate applied in the transiently calibrated model from 1975 through 1999.

Six basic predictive model runs are presented and documented: (1) average recharge through 2050, (2) average recharge ending with the DOR in 2010, (3) average recharge ending with the DOR in 2020, (4) average recharge ending with the DOR in 2030, (5) average recharge ending with the DOR in 2040, and (6) average recharge ending with the DOR in 2050.

Development of the predictive model datasets requires determination of the DOR and development of the predictive pumping datasets. The procedure for determining the predictive pumping demands is described in Appendix D. Similar to the model implementation of the historical pumpage data, it was assumed that the predicted pumpage from the Reklaw (Layer 2) is actually from the Carrizo (Layer 3). However, for the model predictive simulations, pumpage from the Queen City was not reallocated to the Carrizo, as was done in the transient model (Chapter 9). The following will discuss the development of the DOR.

10.1 Drought of Record

GAM specifications require that the DOR used for model predictions be representative for the past 100 years and be defined by severity and duration. Drought is considered a normal, recurring climatic event. It is conceptually defined by the National Drought Mitigation Center as

a protracted period of deficient precipitation resulting in extensive damage to crops with loss of yield. Operational definitions of drought are typically used to define the beginning, end, and severity of a drought over a given historical period. Operational definitions typically quantify the departure of precipitation, or some other climatic variable, from average conditions over a defined time window (typically 30 years).

Drought indices are quantitative measures that assimilate raw data into a single value that defines how precipitation has varied from a specific norm. As discussed above, drought is a phenomenon related directly to available moisture from precipitation. Precipitation is the primary variable controlling recharge in the model region. Accordingly, we used precipitation data as the raw data for defining the DOR in the Northern Carrizo-Wilcox GAM region.

In the Northern Carrizo-Wilcox GAM model region, historical precipitation data are available for approximately 250 stations from 1930 to 2000 (Figure 2.10). From Figure 2.10, it is evident that the spatial distribution of precipitation data is relatively dense in the model domain. However, most stations possess incomplete records across the 100-year time frame of interest. Most gages began recording precipitation in the late 1930s through the 1960s. The earliest monthly precipitation records in the area extend as far back as 1930. Approximately 25 precipitation gages have records in 1931 as opposed to only one in 1930.

There are many drought indices available to measure the degree that precipitation has deviated from historical norms. The typical measure is “percent of normal”, calculated by dividing the actual precipitation depth by the normal precipitation depth and multiplying by 100. This calculation could be performed over a range of time scales but is typically annualized. The normal precipitation depth is usually a long-term arithmetic mean. The available precipitation records within the model domain were analyzed to calculate the percent of normal as an indicator of drought. Figure 2.12 shows a select set of long-term annual precipitation records in the model region. Inspection of these time series shows particularly dry periods in 1936, 1948, 1954 through 1956, 1963 through 1964, 1980, and 1988. The two most severe droughts occurred in 1954 through 1956 and 1963 through 1964.

The 1950’s represents a period of historical drought in Texas including the region being modeled. The drought peaked in 1954 and continued through 1956. In 1956, 13 of 75 gages (17%) recorded their period of record low annual precipitation depths. In 1963, 23 of 81 gages

(28%) recorded their period of record low annual precipitation depths. In 1988, 16 of 88 available gages (18%) recorded their period of record low annual precipitation depths. From this analysis, we concluded that the 1963-1964 drought might be the DOR. However, when the average deficit across the model area was considered, it became evident that the DOR was in the 1950s. The average precipitation, as measured in percent of normal averaged across all available gages in the model area, was equal to 84% from 1950 through 1956. The same metric calculated for the drought peak years from 1954 through 1956 was 73% of normal.

The secondary drought index we used to quantify the DOR is the Standardized Precipitation Index (SPI). This index was developed to define precipitation deficits over multiple time scales (McKee et al., 1993). The SPI is calculated based upon the precipitation record for a given location. The long-term precipitation record is fitted to a general probability distribution (typically the Gamma distribution). This distribution is then normally transformed and standardized so that the mean SPI for that location over the time period of interest is equal to zero. When the SPI is equal to zero, it signifies median precipitation conditions for that location based upon the time integration window specified (Edwards and McKee, 1997). Because the index is normalized, comparison of SPI values between locations (i.e., across our model domain), is simplified in that an SPI of -1 represents a similar magnitude deficit for all stations. Monthly precipitation averages are used as the raw data for the SPI calculation. A one-month SPI would represent normalized precipitation data without temporal averaging. The SPI is backward-averaged over some user-specified duration, typically between six months and three years. By lengthening this time integration window, one effectively looks at longer term precipitation trends less subject to short-term variations. Short-term deficit conditions or anomalies are of less concern for predicting groundwater conditions; for this reason, the SPI was calculated for long time periods (1 year, 2 year, and 3 year windows). Figure 10.1.1 shows the SPI for precipitation gage 415424 in Angelina County calculated using one-year, two-year, and three-year averaging windows. Current SPI index maps are available online for the State of Texas for multiple time averaging periods from one month through three years at the following URL: <http://www.txwin.net/Monitoring/Meteorological/Drought/spi.htm>

McKee et al. (1993) defined a classification system for defining drought conditions using the SPI. This classification is taken from (Hayes, 2001) and presented in the table below.